

Semiconductor Nanocrystals as Building Blocks for Organized Superstructures

A dissertation
submitted to the University of Hamburg for the degree
of
Doctor of Natural Sciences

Alexey Shavel
from Vitebsk (Belarus)

December 2005

The work described in this thesis was carried out in the Institute of Physical Chemistry, University of Hamburg in the group of Prof. Dr. H. Weller.

1. Referee: Prof. Dr. H. Weller
2. Referee: Prof. Dr. A. Eychmüller

Acknowledgements

I want to thank *Prof. Dr. Horst Weller and Prof. Dr. Alexander Eychmüller* for the invitation to join their working group, for a very interesting research topic, for providing excellent experimental facilities and for many useful discussions. Additional gratitude is expressed for a friendly group atmosphere.

I want to specially thank *Prof. Dr. Alexander Eychmüller* for supervising my investigations and for stimulating discussions and especially for writing and correcting our manuscripts.

My special thanks go to my adviser and friend *Dr. Nikolai Gaponik* for his help and for useful discussions. His insight and advises were always valuable and appreciated. Without him, I would not be writing this thesis in this place today. Additional thanks for prompt and perfect corrections of our manuscripts.

I want to thank my friends and colleagues *Dr. Dimitri V. Talapin* and *Dr. Elena V. Schevchenko* for very stimulating discussions and help.

I am indebted to *Dr. Kathrin Hoppe*, to *Dr. Stephen G. Hickey* and to *Marija Nolic* for thorough reading of this thesis, multiple corrections and valuable comments.

I am very thankful to *Thomas Franzl*, *Dr. Thomas A. Klar*, *Dr. Andrey L. Rogach* and *Prof. Dr. Jochen Feldmann* (Ludwig-Maximilians-Universität München) for their help and for the successful collaboration in the FRET investigation.

I am very thankful to *Dr. Sergey Poznyak* and *Dr. Nikolai P. Osipovich* (Physico-Chemical Research Institute, Belarussian State University) for performing the successful electrochemical investigations on the CdTe and ZnSe nanocrystals.

I want to thank *Prof. Dr. Jordi Martorell*, *Dr. Albert Molinos* and *Marc Maymo* for successful collaboration in preparation of composite materials for photonic application.

I want to thank *Dipl.-Ing. Andreas Kornowski* and *Sylvia Bartholdi-Nawrath* for excellent TEM and HRTEM images. *Almut Barck* is acknowledged for the powder XRD measurements and *Frank Bürl* and *Lothar Ruth* for technical support.

I am also very thankful to *Rosemarie Pakula* for her willingness to help us in all bureaucratic affairs.

The work described in this thesis was carried out in the Institute of Physical Chemistry, University of Hamburg, from September 2002 to April 2005, and was supported by the DFG SP 1072, EU project FUNLIGHT, EU Network of Excellence “PHOREMOST” and by the NATO Scientific and Environmental Affairs Division (PST.CLG 979631).

I want to thank everyone in the nanochemistry group and in particular *Vesna, Marija, Kathrin, Stephen, Dirk, Nadja, Mona,* and *Jan* for making the lab an enjoyable and productive place to work, for fruitful discussions and for pleasant ways of spending time together.

Content

Titel	i
Acknowledgements	iii
Content	v
Notations	vi
1. Introduction.	1
2. Synthesis of thiol-stabilized nanocrystals.	5
2.1 Introduction	5
2.2 Synthesis of aqueous ZnSe NCs	7
2.3 Synthesis of aqueous CdTe NCs. Optimization of the initial condition of synthesis of CdTe nanocrystals	10
2.4 Conclusions	19
2.5 References	20
3. Post preparative treatment of semiconducting NCs.	24
3.1 Introduction	24
3.2 Efficient UV-blue photoluminescing thiol-stabilized water soluble alloyed ZnSe(S) nanocrystals.	26
3.3 Post preparative improvement of luminescence efficiency of CdTe NCs.	31
3.4 Conclusions	36
3.5 References	37
4. Electrochemical properties of aqueous nanocrystals.	40
4.1 Introduction	40
4.2. Size dependent electrochemical properties of CdTe nanocrystals.	41
4.3 <i>In situ</i> electrochemical observation of photo induced formation of alloyed ZnSe(S) nanocrystals	47
4.4 Conclusions	51
4.5 References	52
5. The Assembling of Semiconductor Nanocrystals.	54
5.1 Introduction	54
5.2 Layer-by-layer assembly of semiconductor nanocrystals.	55
5.3 Electrostatic assembly of semiconductor nanocrystals	58
5.4 Covalent coupling of SC NCs	60
5.4.1 <i>Covalent linking of CdTe NCs to flat surfaces</i>	60
5.4.2 <i>Covalent linking of CdTe NCs to silica and glass beads</i>	62
5.4.3 <i>Covalent linking of CdTe NCs to the functionalized Latex beads</i>	64
5.5 Rapid Förster energy transfer	66
5.5.1 <i>Förster energy transfer in the close-packed structures.</i>	68
5.6 Conclusions	70
5.7 References	71
6. Summary	74
7. Appendix 1. Calculation of concentration cadmium ions in solution.	77
Appendix 1a. Estimation of the calculation validity.	87
9. Appendix 2. Experimental section	89
10. Appendix 3. Safety precaution information on the used chemicals	93

Notations

3APTES	3-(aminopropyl)-triethoxysilane
AFM	Atomic Force Microscopy
CV	cyclic voltammetry
DDA	Dodecylamine
DIC	N,N'-diisopropylcarbodiimide
DMAP	4-dimethylaminopyridine
DMF	<i>N,N</i> -Dimethylformamide
EDC	1-Ethyl-3-[3-(dimethylamino)propyl]carbodiimide hydrochloride
EDX	Energy Dispersive X-ray analysis
HDA	Hexadecylamine
HRSEM	High Resolution Scanning Electron Microscopy
HRTEM	High Resolution Transmission Microscopy
ITO	Indium Tin Oxides
MA	2-mercaptoethylamine
MES buffer	(2-(<i>N</i> -morpholino)ethanesulfonic acid 0,1 mM
MHS	<i>N</i> -Hydroxysuccinimide
MPA	Mercaptopropionic acid
NCs	Nanocrystals
OA	Oleic Acid
PEI	poly(ethyleneimine)
PDDA	poly(diallyldimethylammonium chloride)
PL	photoluminescence
QD	Quantum dots
QE	Quantum efficiency
QY	Quantum yield
SAXS	Small Angle X-Ray Scattering
SEM	Scanning Electron Microscopy
TDPA	Tetradecylphosphonic Acid
TEM	Transmission Electron Microscopy
TG	Thioglycerol
TGA	Thioglycolic acid
TOP	Tri- <i>n</i> -octylphosphine
TOPO	Tri- <i>n</i> -octylphosphine Oxide
vol.	Volume
wt.	Weight
XRD	X-Ray Diffraction
XRD-size	Nanoparticle size calculated by Debye-Sherrer equation
UV	Ultraviolet light

Chapter 1

Introduction.

The unique size-dependent optical properties of colloidal semiconductor nanocrystals (NCs) have been the subject of considerable interest in the past two decades [1, 2]. Strongly luminescing II-VI semiconductor NCs have found potential applications in biological imaging and labeling [3-6], photovoltaics [7], electroluminescence devices [8-11], optical sensors [12] etc. Structural [13], photophysical, [1, 13, 14] photochemical [15, 16] and photoelectrochemical [17-19] properties of the semiconductor NCs have been intensively studied. Among the II-VI semiconductor the nanocrystals synthesized in organic media are most intensively studied. The nanocrystals synthesized in this way have a high QY (up to 80%), high photostability but relatively low stability against water and oxygen. By comparison the nanocrystals synthesized in water are stable against oxidation and biological surroundings (biological buffers), but have relatively low quantum yield and do not cover all spectral regions. Thus, the improvement of the QY of thiol-stabilized NCs as well as synthesis of the new NCs' types is an important task.



True color image of the various samples of the aqueous thiol-capped CdTe and ZnSe nanocrystals.

There are two general possibilities for improving the quantum efficiency: i) improving the synthesis itself (changing conditions, precursors etc) and ii) post-preparative treatment of the nanocrystals (shell growth, phototreatment, etching etc).

Chapter 2 is devoted to the first successful synthesis of high quality ZnSe nanocrystals as well as to the improvement of the well known aqueous synthesis of the CdTe NCs. In order to understand the influence of the synthetic conditions on the quantum yield of CdTe nanocrystals the distribution of the cadmium complexes in the synthetic solution have been simulated. The details of the simulation procedure and their correlation with the experimental conditions are described in chapter 2.3 and in appendix 1.

Chapter 3 describes the improving of the quantum yield of aqueous, thiol-stabilized ZnSe and CdTe nanocrystals. The photoassisted “switching on” of the ZnSe nanocrystals and possible explanation of the mechanism of the switching-on processes are described in chapter 3.2. Chapter 3.3 is mainly focused on the photo-assisted shell formation. The photo-assisted quantum yield improvement (up to 50-60%) will be demonstrated.

Chapter 4 focused on the electrochemical investigation semiconductor nanocrystals preadsorbed on the gold electrodes. The aqueous thiol-capped CdTe and ZnSe nanocrystals have demonstrated several distinct oxidation and reduction peaks in the voltammograms. The peak positions are dependent on the nanocrystals’ size and on the post preparative treatment. The sensitivity of electrochemical methods to the surface state will be demonstrated. The clear correlation between peak position (i.e. presence of surface state) and PL quantum yield of ZnSe NCs will be shown.

Chapter 5 is mainly focused on the Layer-by-Layer techniques (LbL) [20] as well as linking of the nanocrystals to functionalized substrates [21]. In this chapter the efforts in the building of organizing superstructure via LbL techniques will be demonstrated. The building up of the superstructure, constructed from alternating layers of differently sized and charged aqueous nanocrystals, will be demonstrated. The possibility of producing an electrostatic assembly of nanocrystals (a kind of LbL without using intermediate polyelectrolyte layers) will also be demonstrated. The direct linking of the thio-acid stabilized nanocrystals to the substrate functionalized with amino-groups is also the issue of chapter 5. Carbodiimide chemistry was used for the preparation of monolayer structures on flat and spherical substrates.

Great interest attract last time the Förster energy transfer in organized superstructures [22, 23]. The chapter 5.5 is devoted to the study of rapid FRET in such systems. The higher FRET rate (near the theoretical limit) in the electrostatic assembly of nanocrystals is demonstrated in this chapter.

References

1. Gaponenko, S.V., *Optical Properties of Semiconductor Nanocrystals*. 1998: Cambridge Univ Press, Cambridge, UK. 240 pp.
2. Alivisatos, A.P., *Perspectives on the physical chemistry of semiconductor nanocrystals*. J. Phys. Chem., 1996. **100**(31): p. 13226-13239.
3. Dubertret, B., P. Skourides, D.J. Norris, V. Noireaux, A.H. Brivanlou and A. Libchaber, *In Vivo Imaging of Quantum Dots Encapsulated in Phospholipid Micelles*. Science, 2002. **298**(5599): p. 1759-1762.
4. Alivisatos, P., *The use of nanocrystals in biological detection*. Nature Biotechnology, 2004. **22**(1): p. 47-52.
5. Jaiswal, J.K., H. Mattoussi, J.M. Mauro and S.M. Simon, *Long-term multiple color imaging of live cells using quantum dot bioconjugates*. Nature Biotechnology, 2003. **21**(1): p. 47-51.
6. Han, M., X. Gao, J.Z. Su and S. Nie, *Quantum-dot-tagged microbeads for multiplexed optical coding of biomolecules*. Nature biotechnology. **19**(7): p. 631-635.
7. Huynh Wendy, U., J. Dittmer Janke and A.P. Alivisatos, *Hybrid nanorod-polymer solar cells*. Science. **295**(5564): p. 2425-2427.
8. Schlamp, M.C., X. Peng and A.P. Alivisatos, *Improved efficiencies in light emitting diodes made with CdSe(CdS) core/shell type nanocrystals and a semiconducting polymer*. J. Appl. Phys., 1997. **82**(11): p. 5837-5842.
9. Mattoussi, H., L.H. Radzilowski, B.O. Dabbousi, E.L. Thomas, M.G. Bawendi and M.F. Rubner, *Electroluminescence from heterostructures of poly(phenylene vinylene) and inorganic CdSe nanocrystals*. J. Appl. Phys., 1998. **83**(12): p. 7965-7974.
10. Gao, M.Y., C. Lesser, S. Kirstein, H. Mohwald, A.L. Rogach and H. Weller, *Electroluminescence of different colors from polycation/CdTe nanocrystal self-assembled films*. J. Appl. Phys., 2000. **87**(5): p. 2297-2302.
11. Steckel, J.S., S. Coe-sullivan, V. Bulovic and M.G. Bawendi, *1.3 mm to 1.55 mm tunable electroluminescence from PbSe quantum dots embedded within an organic device*. Adv. Mater., 2003. **15**(21): p. 1862-1866.

12. Nazzal, A.Y., L. Qu, X. Peng and M. Xiao, *Photoactivated CdSe Nanocrystals as Nanosensors for Gases*. Nano Lett., 2003. **3**(6): p. 819-822.
13. Eychmueller, A., *Structure and Photophysics of Semiconductor Nanocrystals*. J. Phys. Chem. B, 2000. **104**(28): p. 6514-6528.
14. Lifshitz, E., A. Glozman, I.D. Litvin and H. Porteanu, *Optically detected magnetic resonance studies of the surface/interface properties of II-VI semiconductor quantum dots*. J. Phys. Chem. B, 2000. **104**(45): p. 10449-10461.
15. Jones, M., J. Nedeljkovic, R.J. Ellingson, A.J. Nozik and G. Rumbles, *Photoenhancement of Luminescence in Colloidal CdSe Quantum Dot Solutions*. J. Phys. Chem. B, 2003. **107**(41): p. 11346-11352.
16. Aldana, J., Y.A. Wang and X. Peng, *Photochemical Instability of CdSe Nanocrystals Coated by Hydrophilic Thiols*. J. Am. Chem. Soc., 2001. **123**(36): p. 8844-8850.
17. Ogawa, S., K. Hu, F.-R.F. Fan and A.J. Bard, *Photoelectrochemistry of films of quantum size lead sulfide particles incorporated in self-assembled monolayers on gold*. J. Phys. Chem. B, 1997. **101**(29): p. 5707-5711.
18. Hickey, S.G., D.J. Riley and E.J. Tull, *Photoelectrochemical studies of CdS nanoparticle modified electrodes: Absorption and photocurrent investigations*. J. Phys. Chem. B, 2000. **104**(32): p. 7623-7626.
19. Torimoto, T., N. Tsumura, H. Nakamura, S. Kuwabata, T. Sakata, H. Mori and H. Yoneyama, *Photoelectrochemical properties of size-quantized semiconductor photoelectrodes prepared by two-dimensional cross-linking of monodisperse CdS nanoparticles*. Electrochim. Acta, 2000. **45**(20): p. 3269-3276.
20. Decher, G., *Fuzzy nanoassemblies: toward layered polymeric multicomposites*. Science, 1997. **277**(5330): p. 1232-1237.
21. Shipway, A.N., E. Katz and I. Willner, *Nanoparticle arrays on surfaces for electronic, optical, and sensor applications*. ChemPhysChem, 2000. **1**(1): p. 18-52.
22. Kagan, C.R., C.B. Murray, M. Nirmal and M.G. Bawendi, *Electronic energy transfer in CdSe quantum dot solids*. Phys. Rev. Lett., 1996. **76**(9): p. 1517-1520.
23. Kagan, C.R., C.B. Murray and M.G. Bawendi, *Long-range resonance transfer of electronic excitations in close-packed CdSe quantum-dot solids*. Physical Review B: Condensed Matter, 1996. **54**(12): p. 8633-8643.

Chapter 2

Synthesis of thiol-stabilized nanocrystals.

The aqueous synthesis of thiol-stabilized II-VI semiconductor (CdTe, ZnSe) colloidal nanocrystals has been studied. The optimal condition of synthesis of the high quality ZnSe NCs has been found. The influence of the initial conditions of synthesis (structure and concentration of the Cd-Thiol complexes) on the quality of the CdTe nanocrystals has been revealed. The numerical simulation undertaken has shown clear correlation between the concentration of CdL (where L is $(SCH_2COO)^{2-}$) in the initial solution and the photoluminescence quantum yield of CdTe nanocrystals.

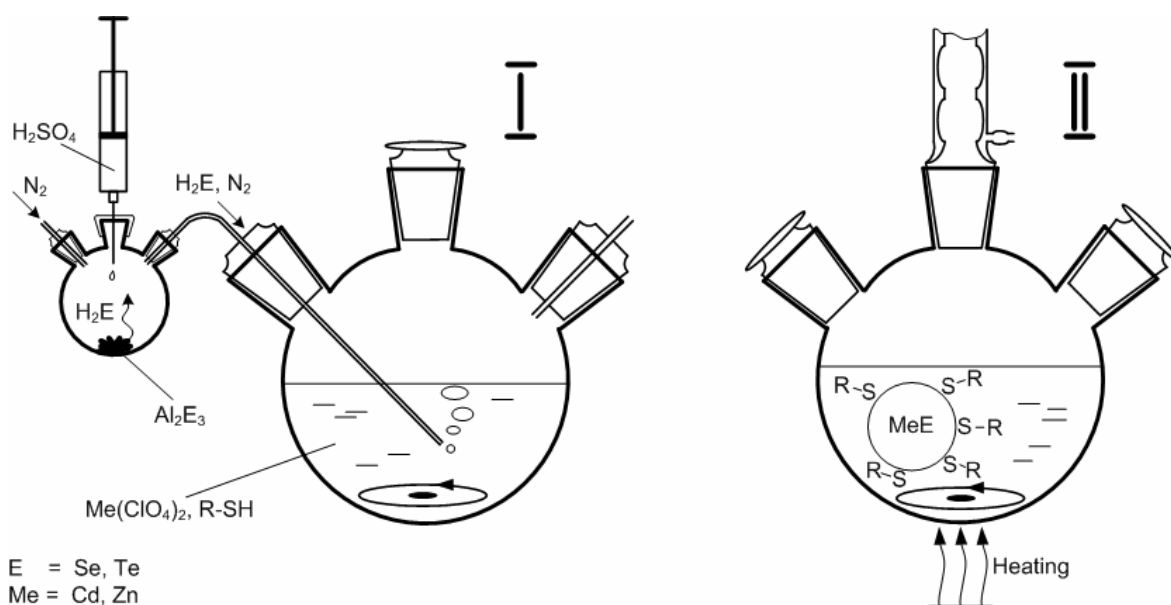
2.1. Introduction

Chemically synthesized semiconductor nanocrystals (or colloidal quantum dots (QDs)) have attracted considerable interest during the last decades. Narrow and intensive emission spectra, continuous absorption bands, high chemical and photobleaching stability, processability and surface functionality are among the most attractive properties of these materials. The properties of the QDs depend strongly on the type of nanocrystals, the size (quantum-confinement) and the capping agent, thus they can be tuned by a proper choice of the synthetic conditions.

There is a wide range of very efficient light emitting QDs which can be synthesized by wet chemical approach. Worthy of mention are ZnSe [1], ZnSe/ZnS [2] and CdS [3, 4] (UV-blue spectral region), CdSe [5-7], InP [8, 9], CdTe [10-12] (visible region), PbSe [13, 14], HgTe [15], and InAs [16] (near-infrared region). The majority of successful syntheses were done in organic media. However, the potential applications of such particles are restricted by their incompatibility with water and/or air. This kind of compatibility is especially important in the field of bio-applications. Worthy of mention is that the phase transfer of NCs from organics to aqueous solution is a time consuming procedure involving capping-agent exchange [17], encapsulation in phospholipid micelles [18], silanization of the individual QDs [19] and preparation of polymeric or dendrimer shells around the

particles [20]. Beside the complicity, the main drawbacks of these procedures are limited stability, low PL quantum yield, large increase of the actual size (critical in the case of conjugation with single bio-molecules or penetration markers through membrane).

At the same time the direct aqueous synthesis of NCs can be a good alternative to the organometallic approach, especially when possible applications demand stability in aqueous media. The simplicity and use of relatively soft conditions, as well as less dangerous materials in comparison with organometallic approach have made aqueous synthesis attractive for researches during the last two decades. For example, IR-emitting HgTe [15] and CdHgTe [21] as well as blue-emitting CdSe [22] are now available. Aqueous CdTe NCs have been successfully synthesized using the traditional procedure [23, 24] as well as in a microwave irradiated sell [25]. Thus, the possibilities to synthesize a wide range of aqueous II-VI semiconductor colloidal nanocrystals have been revealed. **Scheme** presents an example of a general procedure for the aqueous synthesis of thiol-capped NCs [10].



Scheme for the synthesis of aqueous semiconducting nanocrystals.

It is worth to mention that aqueous nanocrystals which may efficiently emit light in the UV-blue spectral region (below 500 nm) are rare. Among them mainly CdS (PL QE up to 10%) [3] and ZnSe (PL QE below 1%) [26, 27] QDs can be mentioned. In the case of

CdTe the aqueous synthesis allows to produce CdTe NCs with a quantum efficiency of about 5-10% for “as prepared” particles and up to 40% after post-preparative treatment [10]. At the same time the organometallic approach to the synthesis of CdTe NCs leads to nanocrystals with a QE of up to 65% [11, 12].

Thus, there are two main disadvantages of the aqueous synthesis of NCs: i) relatively low QY (2-10 times lower than in the case of the organometallic approach) and ii) PL of the existing aqueous NCs does not cover all spectral regions. Thus, the search for new aqueous synthetic approaches as well as improvements of the known procedures is now of special interest.

Here the first successful aqueous synthesis of ZnSe(S) nanocrystals [28] and the sufficient improvement of the synthesis of CdTe nanocrystals [10] is reported. Worth to mention that after our publication [28] a number of the papers devoted to the improving of the quality of the ZnSe NCs have been published [29-31].

2.2. Synthesis of aqueous ZnSe NCs.

The synthesis of ZnSe NCs was developed on the basis of a well known synthetic procedure [10]. In a typical synthesis 0.875 g (2.35 mmol) of $\text{Zn}(\text{ClO}_4)_2 \times 6\text{H}_2\text{O}$ was dissolved in 125 mL of water, and 5.7 mmol of the thiol stabilizer (thioglycerol (TG), thioglycolic acid (TGA), thiomalic acid or 3-mercaptopropionic acid (MPA)) were added under stirring, followed by adjusting the pH by dropwise addition of a 1 M solution of NaOH to 6.5 in the case of TGA or MPA capping, or to 11.2-11.8 in the case of TG. The above mentioned pH values were found experimentally to be optimal for the synthesis of stable colloids. The solution was placed in a three-necked flask fitted with a septum and valves and was deaerated by N_2 bubbling for 1 hour. Under stirring, H_2Se gas (generated by the reaction of 0.134 g (0.46 mmol) of Al_2Se_3 lumps with an excess amount of 1 N H_2SO_4 under N_2 atmosphere) was passed through the solution together with a slow nitrogen flow for nearly 20 min. ZnSe precursors were formed at this stage. The further nucleation and growth of the nanocrystals proceeded on refluxing at 100°C under open-air conditions (with a condenser attached). To follow the evolution of the NC ensemble, aliquots of the colloidal solution were taken for spectroscopic characterization after different times of reflux. A typical temporal evolution of the absorption spectra of the ZnSe QDs is shown in **Figure 2.2.1A**.

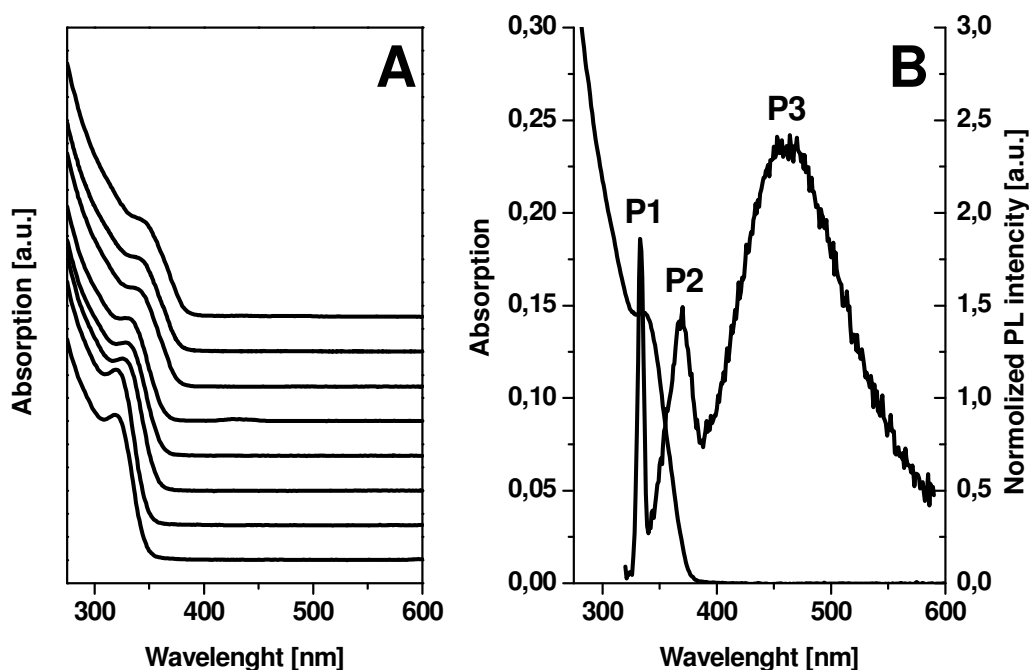


Figure 2.2.1 Evolution of the absorption spectra of a crude solution of ZnSe NCs during the synthesis (A). Absorption and luminescence spectra of the crude solution of the ZnSe NCs (B). The peaks in the PL spectrum correspond to water Raman signal (P1), band-gap emission (P2) and trap-emission (P3).

A growth of the NCs during reflux is indicated by a low-energy shift of the absorption edge. The PL of the crude solutions (**Figure 2.2.1B**) is negligible and shows mainly a broad trap emission band (Peak P3, 400-600 nm). An additional very weak band-edge emission (Peak P2) appears only after long times of reflux. It is observed that among the capping agents used a relatively stronger trap-emission is found to be characteristic for TG-capped ZnSe QDs. The synthesis and characterization of this type of “whitish – blue” emitting QDs with PL QE being below 1% was reported recently [26].

In order to improve the quality of the nanoparticles, a size selective precipitation procedure has been applied to the crude solution of ZnSe NCs [32]. Briefly, the ZnSe QDs were concentrated 3-5 times with the rotor-evaporator and precipitated from the concentrated crude solution by portion-wise addition of a non-solvent (2-propanol) and subsequent centrifugation. The precipitates were separated from the supernatant and were redissolved in pure water giving stable colloidal solutions. The absorption spectra of

different size selected fractions of ZnSe NCs are shown in **Figure 2.2.2A**. The fractions of ZnSe NCs possess a narrow size distribution and well pronounced first excitonic transition (especially for the smallest particles). The selected fractions of the smallest and largest particles possess no luminescence properties (only the water Raman signal (P1) is detectable in the PL spectra). At the same time the fraction in the middle shows weak broad PL similar to the crude solution (see **Figure 2.2.1B**, peak P3).

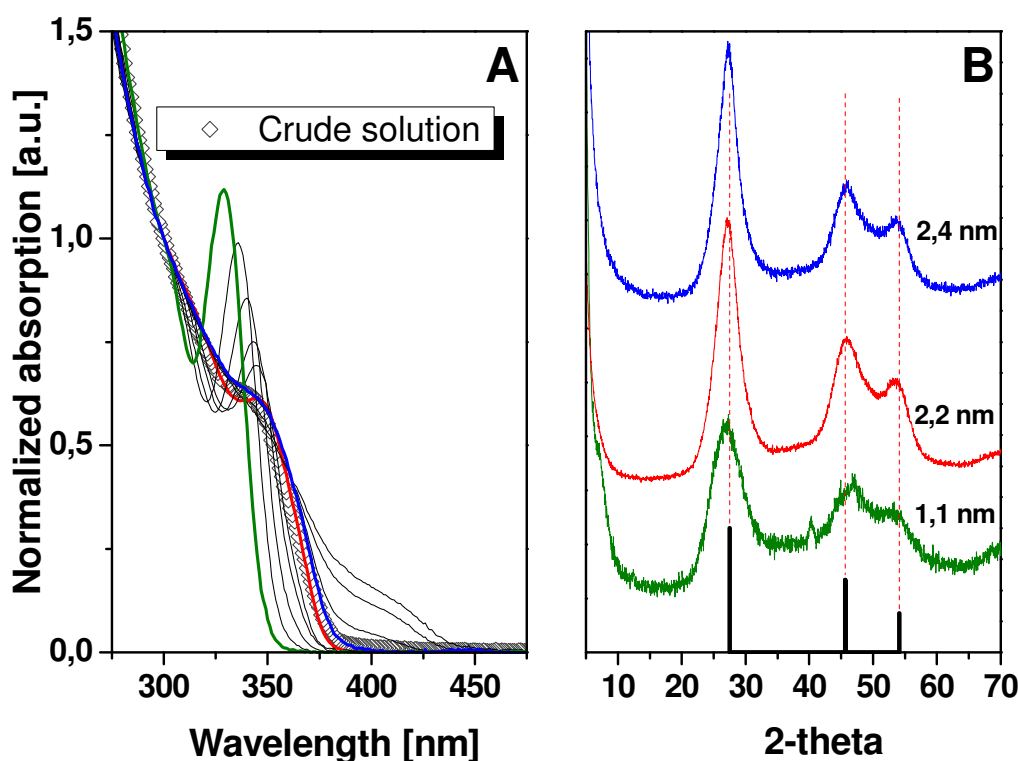


Figure 2.2.2. Absorption spectra of size selected fractions of ZnSe. Gray rhombs show the absorption spectrum of “as prepared” ZnSe nanocrystals. The right panel presents the XRD patterns of three different size selected fractions of ZnSe NCs. The lines, corresponding to the absorption spectra and XRD patterns of the same samples have the same colors in the panels A and B.

Figure 2.2.2B shows the XRD patterns of three fractions of size selected ZnSe NCs. Reflexes of the ZnSe NCs correspond to the cubic ZnSe structure. The sizes

(diameters) of the ZnSe NCs in the **Figure 2.2.2B** are calculated from the broadening of the XRD reflexes.

In order to improve the PL properties of ZnSe NCs a post preparative phototreatment has been applied to the solution of nanocrystals. Briefly, irradiation by “white light” leads to the creation of an inorganic alloyed ZnSeS shell on the surface of the nanocrystals which provide a high QY (25-30%) from the NCs. The source of materials for the shell formation are molecules of TGA (sulfur) and Zn ions (see **Chapter 3** for details). This finding may explain the very weak band gap emission which appears after a long time of refluxing (see **Figure 2.2.1B**, peak P3). The emission can be as a result of the illumination of an unprotected flask in the day light (the reaction mixture contains zinc ions and molecules of TGA).

The absence of luminescence from “as prepared” ZnSe nanoparticles may be explained through the existence of Se traps on the surface of the NCs. Presence of the Se traps on the NC’s surface was proven by electrochemical methods (see **Chapter 4** for details).

2.3. Synthesis of aqueous CdTe NCs. Optimization of the initial conditions of synthesis of CdTe nanocrystals.

It is known that changing of the type and amount of stabilizer strongly influences the PL properties of nanocrystals synthesized both in organic [33, 34] and aqueous media [10]. The pH of the solution is another important factor which may influence the PL of thiol-capped aqueous nanocrystals [35, 36]. The pH dependence of the PL appears due to the formation of thiolates under basic conditions which may play a role in hole trapping [36]. Thus, changing the amount of stabilizer and pH of the solution may lead to an improvement in the PL of the NCs. Moreover, changing of the initial conditions of the synthesis (before injection of H₂Te) may lead to an improvement in the quality of aqueous nanocrystals in the same way.

The improvement of the synthesis of the aqueous CdTe nanocrystals was based on the optimization of the well known experimental procedure [10, 37]. According to the ref [10] the optimum pH value is strongly dependent on the nature of the stabilizer and the recommended value for thioglycolic acid and 3-mercaptopropionic acid is 11.2-11.8. The proposed value for the TGA/Cd ratio is 2.45. In order to investigate the influence of the

initial conditions on the optical properties and quantum efficiency the initial conditions of synthesis (pH and Cd/thiol ratio) were systematically changed.

Briefly, CdTe nanocrystals were prepared as follows ed [10]. In a typical synthesis 0.985 g (2.35 mmol) of $\text{Cd}(\text{ClO}_4)_2 \cdot 6\text{H}_2\text{O}$ (Alfa Aesar) was dissolved in 125 mL of water, and 5.7 mmol of the thiol stabilizer were added under stirring, followed by adjusting the pH by dropwise addition of a 1 M solution of NaOH. The solution was placed in a three-necked flask fitted with a septum and valves and was deaerated by N_2 bubbling for 1 hour. Under stirring, H_2Te gas (generated by the reaction of 0.2 g (0.46 mmol) of Al_2Te_3 lumps with an excess amount of 1 N H_2SO_4 under N_2 atmosphere) was passed through the solution together with a slow nitrogen flow for nearly 20 min. CdTe precursors were formed at this stage. The further nucleation and growth of the nanocrystals proceeded on refluxing at 100°C under open-air conditions (with a condenser attached). The typical evolution of the absorption and luminescence spectra during the synthesis has been shown in **Figure 2.3.1**.

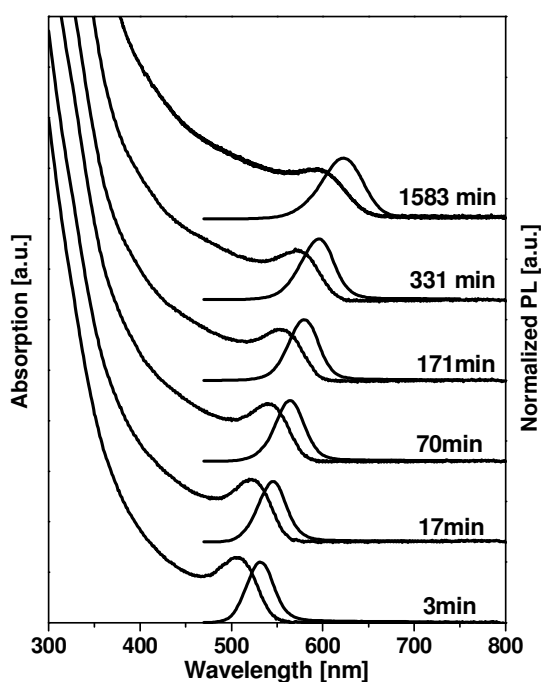


Figure 2.3.1. Typical evolution of the absorption and luminescence spectra of a crude solution of CdTe NCs during the synthesis. Experimental condition: pH 11.5, TGA/Cd ratio 1/1.3.

It is possible to determine three main steps in the aqueous synthesis: i) formation of the Cd-thiolate complexes in solution of the cadmium salt and stabilizer, ii) injection of the chalcogen precursors (for example H_2Se or H_2Te) into the reaction solution and, iii) growing nanocrystals at the temperature of boiling water.

Here, the optimization of the synthesis of CdTe by changing the conditions at the initial stage of synthesis of CdTe NCs namely the pH and TGA/Cd ratio, by maintaining the initial cadmium ion concentration constant. TGA/Cd ratios between 2.45 and 1.1 were used. The experimental data show that decreasing the TGA/Cd ratio leads to a drastic increase of the quantum yield of the CdTe NCs. See **Figure 2.3.2**.

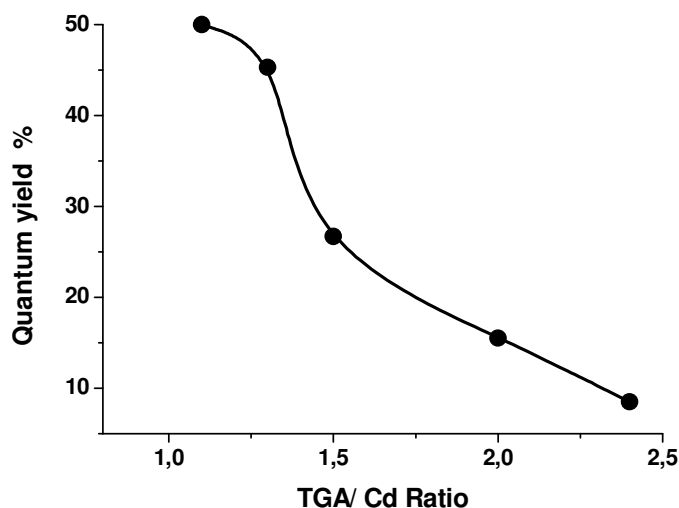


Figure 2.3.2. The relationship between TGA/Cd ratio in the initial reaction mixture and quantum yield of a crude solution of CdTe NCs. Experimental conditions: 20 hrs of synthesis, pH 11.5.

In order to understand the influence of the initial conditions of the synthesis on the properties of the NCs, the experimental data were compared with the results of the numerical simulation of the solution composition. Unfortunately, there are only a few reports on the stability constant of cadmium complexes with thiols: thioglycolic acid [38-40], 3-mercaptopropionic acid [39, 41], 2-mercaptopropionic acid [42, 43] and mercapto- and dimercaptosuccinic acid [44]. The most complete data devoted to the study of the cadmium complexes of thioglycolic acid (TGA) over a wide range of pH values were

provided by ref [38]. This data together with the earliest results [39, 40] and together with information about the stability constants of the hydroxy- complexes of cadmium [45], provided us with the complete information about the composition of the cadmium complexes with thioglycolic acid. It is worth to mention that the stability constants of cadmium complexes with thioglycolic acid are much higher than the stability constants of hydroxy- complexes (few orders of magnitude) and as a result hydroxy- complexes play an important role only at very high pH. See **Appendix A1** for details of calculations.

Briefly, the calculation of concentration and composition of cadmium complexes was carried out as shown below:

Taking into account the total concentration of the cadmium ions and TGA:

$$C_{TGA} = [L^{2-}] + [HL^-] + [H_2L] + 3[CdL_3^{4-}] + 2[CdL_2^{2-}] + [CdL] + [CdH_1L_1^{1+}] + 2[CdH_1L_2^{1-}] + 3[CdH_1L_3^{3-}] + 2[CdH_2L_2] + 3[CdH_2L_3^{2-}] \quad (1)$$

$$C_{Cd} = [Cd^{2+}] + [CdL_3^{4-}] + [CdL_2^{2-}] + [CdL] + [CdH_1L_1^{1+}] + [CdH_1L_2^{1-}] + [CdH_1L_3^{3-}] + [CdH_2L_2] + [CdH_2L_3^{2-}] + [Cd(OH)_1^{1+}] + [Cd(OH)_2] + [Cd(OH)_3^{1-}] + [Cd(OH)_4^{2-}] \quad (2)$$

where L represent the TGA²⁻ ions

Using the expression for the protonation constants of mercaptoacetate ion:

$$\beta_i = \frac{[(H_iL)^{i-2}]}{[L^{2-}][H^+]^i} \quad (3)$$

and for the stability complexes:

$$\beta_{1ij} = \frac{[Cd(H)_i(L)_j^{2+i-2j}]}{[Cd^{2+}][H^+][L^{2-}]^j} \quad (4)$$

the final equations for the equilibrium concentration of cadmium and TGA ions in solution depending only on pH and the total concentration of cadmium and TGA have been obtained:

$$C_{Cd} = [Cd^{2+}] (1 + B_3[L^{2-}]^3 + B_2[L^{2-}]^2 + B_1[L^{2-}] + K) \quad (5)$$

$$C_{TGA} = B_0[L^{2-}] + [Cd^{2+}](3B_3 [L^{2-}]^3 + 2B_2 [L^{2-}]^2 + B_1 [L^{2-}]) \quad (6)$$

where B_0 , B_1 , B_2 , B_3 , B_4 and K are parameters, which depend only on pH and stability constants:

$$\begin{aligned} B_0 &= \beta_2[\text{H}^+]^2 + \beta_1[\text{H}^+] + 1 \\ B_1 &= \beta_{111}[\text{H}^+] + \beta_{101} \\ B_2 &= \beta_{122}[\text{H}^+]^2 + \beta_{112}[\text{H}^+] + \beta_{102} \\ B_3 &= \beta_{123}[\text{H}^+]^2 + \beta_{113}[\text{H}^+] + \beta_{103} \\ K &= \beta_{10}[\text{OH}^-] + \beta_{20}[\text{OH}^-]^2 + \beta_{30}[\text{OH}^-]^3 + \beta_{40}[\text{OH}^-]^4 \end{aligned}$$

Numerical simulation of **Eqs 5** and **6** should allow the determination of the equilibrium concentration of cadmium ions and TGA ions and finally the concentration of all complexes in solution.

In this calculation a several presumptions which can reduce the validity of our calculation are used. The most important source of deviation is using the concentration of the ions for calculation instead of the activity. A second source of deviation is the low solubility of the uncharged complexes of cadmium (for example CdL). The precipitation of the uncharged species leads to the shifting of the equilibrium and further production of these substances. Thus, precipitation leads to the underestimation of the overall amount of the insoluble complex. It is assumed here that the deviation induced by all of our presumptions is within 10 % (see appendix **A1.1** for details).

The calculation has shown that only three complexes play an important role at high pH: CdL_3^{4-} , CdL_2^{2-} and CdL. **Figure 2.3.3** depict the calculated concentration of important complexes in solution together with the QY of CdTe NCs depending on the TGA/Cd ratio at pH 12. As seen from the figure, changing the TGA/Cd ratio between 5 and 0.85 is followed by a decrease in the concentration of CdL_3^{4-} complex and an increase in the concentration of the CdL complex. At the same time the concentration of the complex CdL_2^{2-} goes through a maximum at a TGA/Cd ratio of approximately 2. Simultaneously, **Figure 2.3.3** shows that the evolution of the quantum yield of CdTe NCs is in good correlation with the concentration of the CdL complex at the initial stage of the synthesis.

In other words the increase of the quantum yield of CdTe with the decrease in the TGA concentration can be attributed to the increase in the concentration of the CdL complex. The following deceleration of the growth of the QY of the nanocrystals at very low values of Cd/TGA ratio (near 1) can be explained by an insufficient amount of stabilizer in the system. In fact the thioglycolic acid plays the role of stabilizer, source of sulfur, surfactant in the system, and is also necessary for the formation of cadmium

complexes in the solution. Actually, there is a competition of factors during the synthesis: i) improving the quality of the nanocrystals with the increase in the concentration of CdL complex (by means of decreasing the concentration of TGA) and ii) the necessity for sufficient amount of stabilizer to provide stability and surface passivation of growing particles to be present in solution. As a result of this competition the optimum concentration of the TGA (TGA/Cd ratio) can exist only under certain conditions in the initial solution.

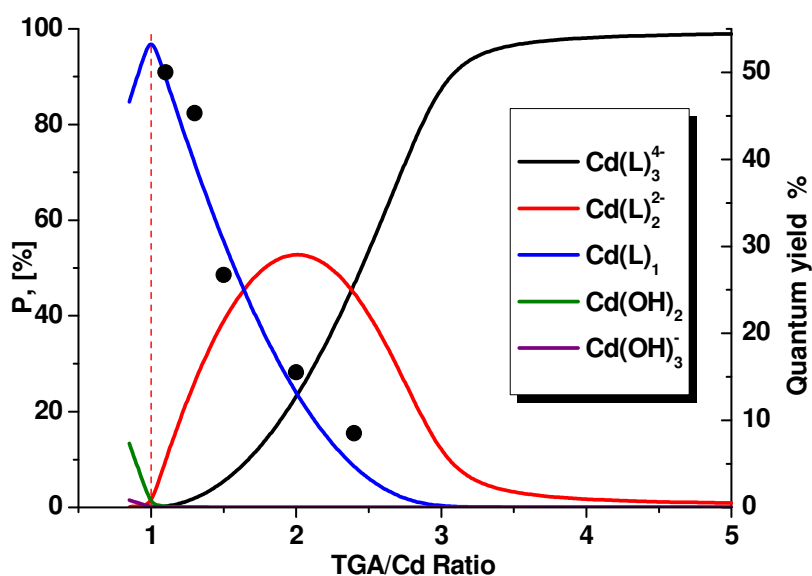


Figure 2.3.3. Distribution of cadmium complexes in solution and QY of CdTe NCs after 20hrs of synthesis (black dots) depending on the TGA/Cd ratio in initial reaction mixture.

It should be noted that the solution of Cd-precursor at low TGA/Cd ratios is turbid. This fact is additional indirect evidence of the domination of the uncharged, low soluble CdL complex. This observation also means that the CdL concentration has been underestimated as was mentioned above. The turbidity of the solution does not disappear during reflux and the precipitate can be easily removed from the solution of NCs by filtration. The precipitate of CdL plays an additional role as a source of cadmium. Gradual dissolution of the CdL complex during the particle growth could provide a constant rate of transport of Cd ions to the particles. A slow flux of the cadmium precursor provides the possibility to grow the particles under diffusion control which, as has been theoretically

predicted [46], is preferable for narrowing of the size distribution. It's should be mentioned that precipitation of the CdL complex shifts the equilibrium in the solution towards this complex. Thus, the real amount of this complex is even higher than shown by numerical simulation.

The simulation also shows that the changing of the pH does not really influence the distribution of the cadmium complexes in the solution. As is seen from **figure 2.3.4** the distribution of the complexes in solution is stable in a pH range of between 10.5 and 12.5. At the same time the situation in the “real” solution changes. The pH in the initial solution was adjusted by the addition of a certain amount of the 1M NaOH solution. Therefore a different pH means a different volume of the NaOH solution added and as a result different ionic strength. The deviation is about 6% for pH 12 and TGA/Cd ratio 1.3 (about 7.3 mL of 1.0 M NaOH). Thus, it is may be assumed that different ionic strengths could influence the kinetics of nanocrystal growth.

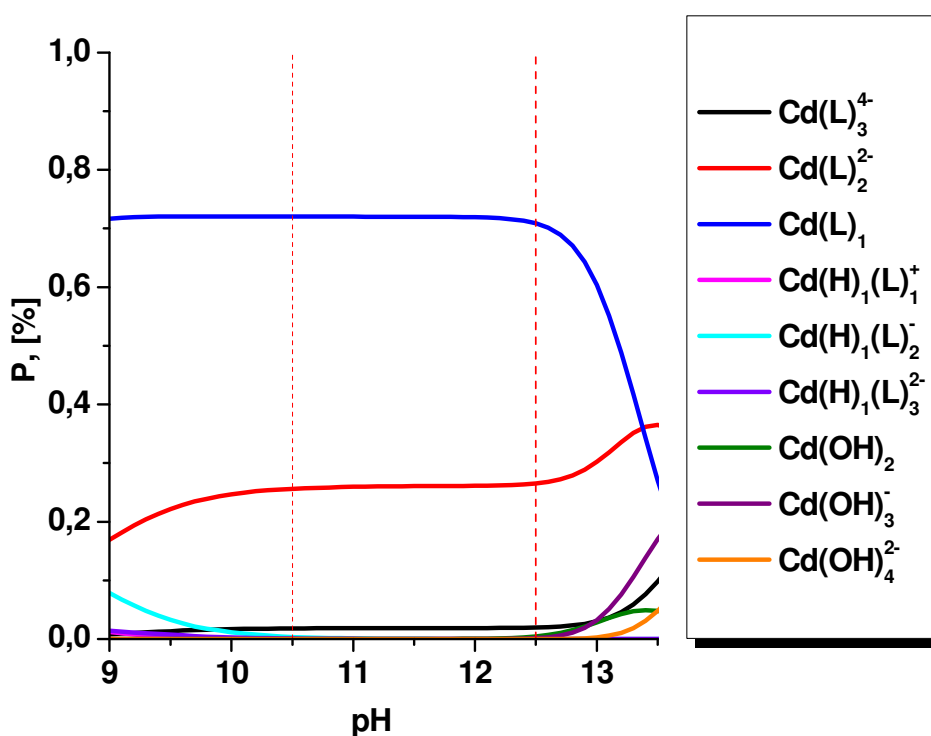


Figure 2.3.4. . Distribution of cadmium complexes in solution as a function of the pH in the initial reaction mixture.

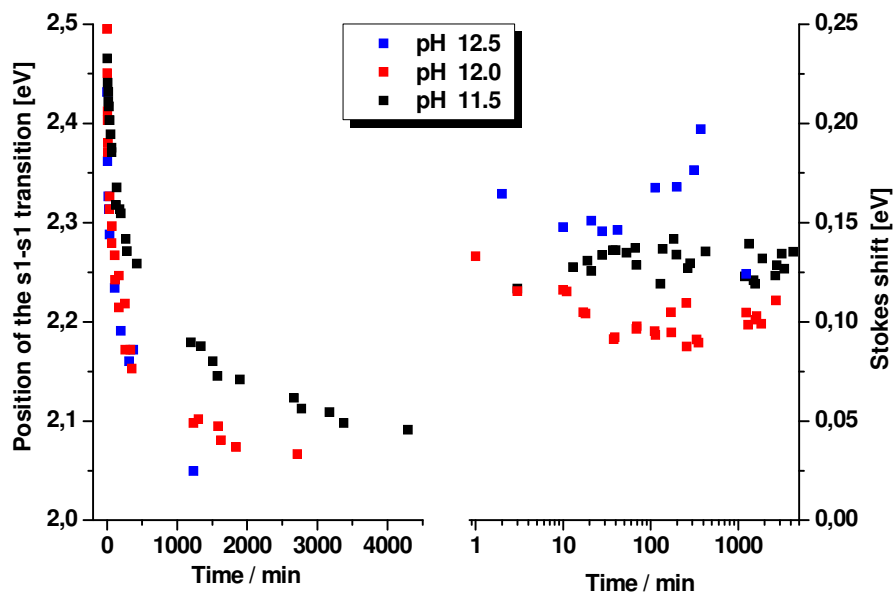


Figure 2.3.5. Evolution of the positions of the s1-s1 transition in absorption spectra (left) and Stokes shift (right) during the synthesis at pH 11.5 (Black), pH 12.0 (Red) and pH 12.5 (Blue).

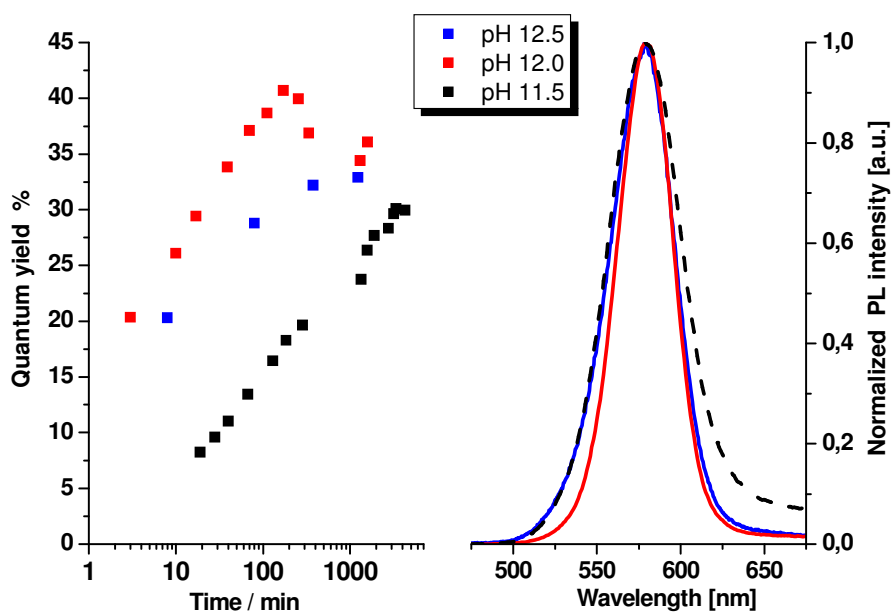


Figure 2.3.6. Evolution of the QY of CdTe NCs during the syntheses at different pH values (left) and PL spectra of CdTe NCs with the same position of PL maxima (Right). The PL spectra were taken after: 285 min of synthesis (Black), 171 min of synthesis (Red) and 42 min of synthesis (Blue). The same colors in the panels correspond the same pH of synthesis.

The experimental data shows an increase of the pH of the initial solution followed by the acceleration of the rate of the nanocrystal growth (**figure 2.3.5 left**). At the same time, particles synthesized at pH 12.0 have the smallest Stokes' shift (near 0.1 eV) (**figure 2.3.5 right**) and narrower size distribution - a smaller FWHM of the PL spectra (**figure 2.3.6 right**). The evolution of QY during the synthesis is shown on the **figure 2.3.6 left**. The largest quantum efficiency was also obtained at pH 12. Thus, pH 12 is found to be an optimum for the synthesis of aqueous TGA stabilized CdTe nanocrystals.

Another important factor which may have an influence on the quality of the thiol stabilized aqueous nanoparticles is the sulfur content. The sulfur content in a typical synthesis is quite high due to thermo hydrolysis of the TGA at high pH and incorporation of the sulfur into the CdTe nanocrystals which is followed by the formation of a mixed phase [10, 47]. **Figure 2.3.7C** shows the relative shift of the XRD reflexes during the synthesis of nanocrystals. The process of nanocrystal growth (boiling of the nanoparticle solution) followed by the continuous shift of XRD reflexes toward a position corresponding to cubic CdS.

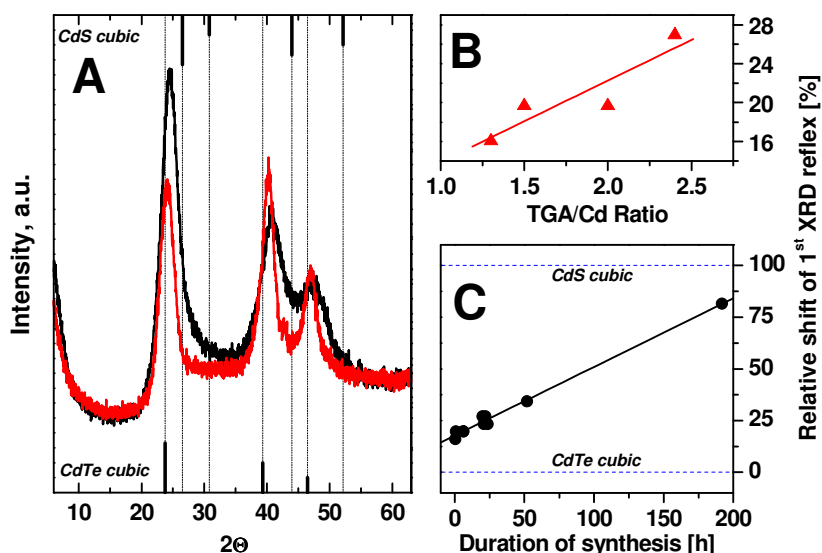


Figure 2.3.7. XRD patterns of the CdTe NCs synthesized with a TGA/Cd ratio of 1.3 (Red) and 2.45 (black) after 20hrs of synthesis (A). Panel B shows the influence of the TGA/Cd ratio on the relative positions of the XRD reflexes of the CdTe NCs. Panel C presents the evolution of the relative shift of the XRD reflexes of the CdTe NCs during the synthesis.

It should be noted, that reduction of the amount of the stabilizer used for synthesis leads to the reduction of the sulfur content in the nanoparticles. XRD patterns of the CdTe NCs show that reduction of the TGA/Cd ratio results in a smaller shift of the reflexes toward the position corresponding to cubic CdS (see **figure 2.3.7 A and B**). This finding can be explained by the fact that decreasing the amount of stabilizer in solution during particle preparation and acceleration of the particles growth leads to a decreasing probability of TGA hydrolysis and, as a result, to a lower sulfur content. Thus, increasing the duration of the synthesis as well as the TGA/Cd ratio leads to an increasing of the sulfur content in the CdTe nanoparticles. Thus, changing the pH of the initial solution allows to regulate the rate of particle growth and as a result the amount of sulfur in the CdTe NCs.

2.4. Conclusions

The aqueous synthesis of thiol-stabilized II-VI semiconductor colloidal nanocrystals has been studied. The optimal conditions of synthesis of the ZnSe NCs have been found. The aqueous ZnSe NCs possess narrow size distributions but poor luminescence properties. The influence of the initial conditions of synthesis (structure and concentration of the Cd-Thiol complexes) on the quality of the CdTe nanocrystals has been revealed. The distribution of the complexes of cadmium with TGA has been across a wide range of pH value and concentration of the cadmium ions. Only the CdL_3^{4-} , CdL_2^{2-} and CdL (where L is $(\text{SCH}_2\text{COO})^{2-}$) complexes play an important role at the across synthetic condition (pH 9.0-12.5). The numerical simulation shows a clear correlation between the concentration of CdL in the initial solution and the photoluminescence quantum yield of the CdTe NCs. Improvement of the QY of CdTe NCs was achieved through decreasing of the TGA/Cd ratio which is preferable for increasing of the concentration of the CdL complex. Reduction of the TGA/Cd ratio allowed preparation of highly luminescent (PL QY up to 50% for the crude solution) CdTe NCs. Thus, the optimum conditions of synthesis for the CdTe NCs is a pH 12 and low TGA/Cd ratio (the best ratio is 1.3). The existence of optimal conditions can be explained by the growing of CdTe particles at an optimum rate. Quick particle

growth leads to an insufficient quality: low crystallinity and a high amount of defects and surface states. Conversely too slow rate leads to incorporation of a large amount of sulfur and the formation of a mixed phase. Decreasing the amount of stabilizer also leads to a decrease in the sulfur content. Thus, judicious choice of the initial conditions of the synthesis can lead to the synthesis of high quality aqueous CdTe nanocrystals.

2.5. References

1. Hines, M.A. and P. Guyot-Sionnest, *Bright UV-blue luminescent colloidal ZnSe nanocrystals*. J. Phys. Chem. B, 1998. **102**(19): p. 3655-3657.
2. Lomascolo, M., A. Creti, G. Leo, L. Vasanelli and L. Manna, *Exciton relaxation processes in colloidal core/shell ZnSe/ZnS nanocrystals*. Appl. Phys. Lett., 2003. **82**(3): p. 418-420.
3. Spanhel, L., M. Haase, H. Weller and A. Henglein, *Photochemistry of colloidal semiconductors. 20. Surface modification and stability of strong luminescing CdS particles*. J. Am. Chem. Soc., 1987. **109**(19): p. 5649-5655.
4. Cao, Y.C. and J. Wang, *One-Pot Synthesis of High-Quality Zinc-Blende CdS Nanocrystals*. J. Am. Chem. Soc., 2004. **126**(44): p. 14336-14337.
5. Alivisatos, A.P., *Perspectives on the physical chemistry of semiconductor nanocrystals*. J. Phys. Chem., 1996. **100**(31): p. 13226-13239.
6. Murray, C.B., D.J. Norris and M.G. Bawendi, *Synthesis and characterization of nearly monodisperse CdE (E = sulfur, selenium, tellurium) semiconductor nanocrystallites*. J. Am. Chem. Soc., 1993. **115**(19): p. 8706-8715.
7. Talapin, D.V., A.L. Rogach, A. Kornowski, M. Haase and H. Weller, *Highly Luminescent Monodisperse CdSe and CdSe/ZnS Nanocrystals Synthesized in a Hexadecylamine-Trioctylphosphine Oxide-Trioctylphosphine Mixture*. Nano Lett., 2001. **1**(14): p. 207-211.
8. Micic, O.I., J. Sprague, Z. Lu and A.J. Nozik, *Highly efficient band-edge emission from InP quantum dots*. Appl. Phys. Lett., 1996. **68**(22): p. 3150-3152.
9. Talapin, D.V., N. Gaponik, H. Borchert, A.L. Rogach, M. Haase and H. Weller, *Etching of Colloidal InP Nanocrystals with Fluorides: Photochemical Nature of the Process Resulting in High Photoluminescence Efficiency*. J. Phys. Chem. B, 2002. **106**(49): p. 12659-12663.

10. Gaponik, N., D.V. Talapin, A.L. Rogach, K. Hoppe, E.V. Shevchenko, A. Kornowski, A. Eychmüller and H. Weller, *Thiol-capping of CdTe nanocrystals: An alternative to organometallic synthetic routes*. J. Phys. Chem. B, 2002. **106**(29): p. 7177-7185.
11. Talapin, D.V., S. Haubold, A.L. Rogach, A. Kornowski, M. Haase and H. Weller, *A novel organometallic synthesis of highly luminescent CdTe nanocrystals*. J. Phys. Chem. B, 2001. **105**(12): p. 2260-2263.
12. Wuister, S.F., I. Swart, F. van Driel, S.G. Hickey and C.d.M. Donega, *Highly Luminescent Water-Soluble CdTe Quantum Dots*. Nano Lett., 2003. **3**(4): p. 503-507.
13. Wehrenberg, B.L., C. Wang and P. Guyot-Sionnest, *Interband and Intraband Optical Studies of PbSe Colloidal Quantum Dots*. J. Phys. Chem. B, 2002. **106**(41): p. 10634-10640.
14. Du, H., C. Chen, R. Krishnan, T.D. Krauss, J.M. Harbold, F.W. Wise, M.G. Thomas and J. Silcox, *Optical Properties of Colloidal PbSe Nanocrystals*. Nano Lett., 2002. **2**(11): p. 1321-1324.
15. Rogach, A., S. Kershaw, M. Burt, M. Harrison, A. Kornowski, A. Eychmüller and H. Weller, *Colloidally prepared HgTe nanocrystals with strong room-temperature infrared luminescence*. Adv. Mater., 1999. **11**(7): p. 552-555.
16. Cao, Y. and U. Banin, *Growth and Properties of Semiconductor Core/Shell Nanocrystals with InAs Cores*. J. Am. Chem. Soc., 2000. **122**(40): p. 9692-9702.
17. Medintz, I.L., H.T. Uyeda, E.R. Goldman and H. Mattoussi, *Quantum dot bioconjugates for imaging, labelling and sensing*. Nature Materials, 2005. **4**(6): p. 435-446.
18. Dubertret, B., P. Skourides, D.J. Norris, V. Noireaux, A.H. Brivanlou and A. Libchaber, *In Vivo Imaging of Quantum Dots Encapsulated in Phospholipid Micelles*. Science, 2002. **298**(5599): p. 1759-1762.
19. Bruchez, M.J., M. Moronne, P. Gin, S. Weiss and A.P. Alivisatos, *Semiconductor Nanocrystals as Fluorescent Biological Labels*. Science, 1998. **281**(5385): p. 2013-2016.
20. Guo, W., J.J. Li, Y.A. Wang and X. Peng, *Conjugation Chemistry and Bioapplications of Semiconductor Box Nanocrystals Prepared via Dendrimer Bridging*. Chem. Mat., 2003. **15**(16): p. 3125-3133.
21. Kershaw, S.V., M. Burt, M. Harrison, A. Rogach, H. Weller and A. Eychmüller, *Colloidal CdTe/HgTe quantum dots with high photoluminescence quantum efficiency at room temperature*. Appl. Phys. Lett., 1999. **75**(12): p. 1694-1696.
22. Wang, Y., Z. Tang, M.A. Correa-Duarte, I. Pastoriza-Santos, M. Giersig, N.A. Kotov and L.M. Liz-Marzan, *Mechanism of Strong Luminescence Photoactivation of Citrate-Stabilized Water-Soluble Nanoparticles with CdSe Cores*. J. Phys. Chem. B, 2004. **108**(40): p. 15461-15469.

23. Gao, M., S. Kirstein, H. Mohwald, A.L. Rogach, A. Kornowski, A. Eychmüller and H. Weller, *Strongly photoluminescent CdTe nanocrystals by proper surface modification*. J. Phys. Chem. B, 1998. **102**(43): p. 8360-8363.
24. Li, C. and N. Murase, *Surfactant-dependent photoluminescence of CdTe nanocrystals in aqueous solution*. Chemistry Letters, 2005. **34**(1): p. 92-93.
25. Li, L., H. Qian and J. Ren, *Rapid synthesis of highly luminescent CdTe nanocrystals in the aqueous phase by microwave irradiation with controllable temperature*. Chemical Communications (Cambridge, United Kingdom), 2005(4): p. 528-530.
26. Murase, N., M.Y. Gao, N. Gaponik, T. Yazawa and J. Feldmann, *Synthesis and optical properties of water soluble ZnSe nanocrystals*. International Journal of Modern Physics B: Condensed Matter Physics, Statistical Physics, Applied Physics, 2001. **15**(28, 29 & 30): p. 3881-3884.
27. Nikesh, V.V. and S. Mahamuni, *Highly photoluminescent ZnSe/ZnS quantum dots*. Sem. Sci. Techn., 2001. **16**(8): p. 687-690.
28. Shavel, A., N. Gaponik and A. Eychmüller, *Efficient UV-Blue Photoluminescing Thiol-Stabilized Water-Soluble Alloyed ZnSe(S) Nanocrystals*. Journal of Physical Chemistry B, 2004. **108**(19): p. 5905-5908.
29. Cozzoli, P.D., L. Manna, M.L. Curri, S. Kudera, C. Giannini, M. Striccoli and A. Agostiano, *Shape and Phase Control of Colloidal ZnSe Nanocrystals*. Chemistry of Materials, 2005. **17**(6): p. 1296-1306.
30. Li, L.S., N. Pradhan, Y. Wang and X. Peng, *High Quality ZnSe and ZnS Nanocrystals Formed by Activating Zinc Carboxylate Precursors*. Nano Letters, 2004. **4**(11): p. 2261-2264.
31. Chen, H.-S., B. Lo, J.-Y. Hwang, G.-Y. Chang, C.-M. Chen, S.-J. Tasi and S.-J.J. Wang, *Colloidal ZnSe, ZnSe/ZnS, and ZnSe/ZnSeS Quantum Dots Synthesized from ZnO*. J. Phys. Chem. B, 2004. **108**(44): p. 17119-17123.
32. Talapin, D.V., A.L. Rogach, E.V. Shevchenko, A. Kornowski, M. Haase and H. Weller, *Dynamic distribution of growth rates within the ensembles of colloidal II-VI and III-V semiconductor nanocrystals as a factor governing their photoluminescence efficiency*. J. Am. Chem. Soc., 2002. **124**(20): p. 5782-5790.
33. Kalyuzhny, G. and R.W. Murray, *Ligand Effects on Optical Properties of CdSe Nanocrystals*. J. Phys. Chem. B, 2005. **109**(15): p. 7012-7021.
34. Wuister, S.F., C. De Donega and A. Meijerink, *Influence of thiol capping on the exciton luminescence and decay kinetics of CdTe and CdSe quantum dots*. J. Phys. Chem. B, 2004. **108**(45): p. 17393-17397.
35. Zhang, H., Z. Zhou, B. Yang and M. Gao, *The Influence of Carboxyl Groups on the Photoluminescence of Mercaptopropionic Acid-Stabilized CdTe Nanoparticles*. J. Phys. Chem. B, 2003. **107**(1): p. 8-13.

36. Jeong, S., M. Achermann, J. Nanda, S. Ivanov, V.I. Klimov and J.A. Hollingsworth, *Effect of the Thiol-Thiolate Equilibrium on the Photophysical Properties of Aqueous CdSe/ZnS Nanocrystal Quantum Dots*. J. Am. Chem. Soc., 2005. **127**(29): p. 10126-10127.
37. Rogach, A.L., L. Katsikas, A. Kornowski, D. Su, A. Eychmüller and H. Weller, *Synthesis and characterization of thiol-stabilized CdTe nanocrystals*. Berichte der Bunsen-Gesellschaft, 1996. **100**(11): p. 1772-1778.
38. Turyan, I. and D. Mandler, *Electrochemical study of the Cd(II)/Cd(Hg) system in 2-mercaptoacetic acid solutions*. Electrochimica Acta, 1995. **40**(9): p. 1093-1100.
39. Matsui, H. and H. Ohtaki, *A potentiometric study on complex formation of cadmium(II) ion with 2-mercaptoacetic and 2-mercaptopropionic acids*. Polyhedron, 1983. **2**(7): p. 631-633.
40. Panchal, B.R. and P.K. Bhattacharya, *Metal exchange in some p-bonded complexes. II*. Acta Chimica Academiae Scientiarum Hungaricae, 1972. **74**(4): p. 399-403.
41. Saxena, R.S. and K.C. Gupta, *Polarographic study of the b-mercaptopropionic acid complexes of cadmium*. Journal of the Indian Chemical Society, 1969. **46**(11): p. 1045-1048.
42. Aguilar, M., S. Alegret and E. Casassas, *Solubility equilibriums in the system cadmium(II)-2-mercaptopropionic acid at 25 Deg C*. Journal of Inorganic and Nuclear Chemistry, 1978. **40**(11): p. 1903-1905.
43. Aguilar, M., S. Alegret and E. Casassas, *Complex formation between cadmium(II) and 2-mercaptopropionic acid in 3.0M sodium perchlorate at 25 DegC*. Journal of Inorganic and Nuclear Chemistry, 1977. **39**(4): p. 733-737.
44. Crisponi, G., A. Diaz, V.M. Nurchi, T. Pivetta and M.J. Tapia Estevez, *Equilibrium study on Cd(II) and Zn(II) chelates of mercapto carboxylic acids*. Polyhedron, 2002. **21**(14-15): p. 1319-1327.
45. Lur'e, Y.Y., *Handbook on Analytical Chemistry. 6th Ed.* 1989. 446 pp.
46. Talapin, D.V., A.L. Rogach, M. Haase and H. Weller, *Evolution of an ensemble of nanoparticles in a colloidal solution: Theoretical study*. J. Phys. Chem. B, 2001. **105**(49): p. 12278-12285.
47. Rogach, A.L., *Nanocrystalline CdTe and CdTe(S) particles: wet chemical preparation, size-dependent optical properties and perspectives of optoelectronic applications*. Materials Science & Engineering, B: Solid-State Materials for Advanced Technology, 2000. **B69-70**: p. 435-440.

Chapter 3

Post preparative phototreatment of semiconductor nanocrystals.

The post preparative irradiation of the solution of ZnSe and CdTe nanoparticles improves their luminescence properties. In particular, illumination of the ZnSe nanocrystals leads to strong (up to 25-30% photoluminescence quantum yield) band gap UV-blue emission. The irradiation results in an incorporation of sulfur into the particles and in the formation of ZnSe(S) alloyed nanocrystals. In the case of CdTe nanocrystals illumination leads to the drastically improved PL (up to 10 times) and both photoetching and shell formation can be realized.

3.1. Introduction.

The optical properties and, in particular, the photoluminescence of as prepared colloidal QDs can be improved post-preparatively. The creation of inorganic shells in organic [1, 2] and aqueous [3, 4] media, size-selective precipitation [5, 6], photochemical etching [6-9], oxidizing of NCs surface [10, 11] are among the methods for obtaining strong-luminescing nanocrystals. Changing of solution properties (e.g. pH) [6, 12], nature of capping agent [13, 14] or solvent [15] also may lead to drastic improvement of the luminescence properties of the semiconductor nanocrystals.

Recently, photo-assisted methods of post-preparative treatment were shown to be powerful tool to improve the PL QE of the NCs. Worth to mention are the photoetching of thiol-capped CdTe NCs [6], citric acid capped water soluble CdSe NCs [7, 8], TOPO-capped CdSe/CdS/ZnS nanorods [16], peptide coated CdSe/ZnS NCs in water [17], HDA-capped CdSe NCs [18, 19], and the photochemical etching in the presence of HF of TOPO-capped InP NCs [9], and preparation of CdS shell on the surface of CdTe NCs [3]. Photoassisted PL improvement in solid layered structures is also possible [7, 18-20]. A moderate (3-10 times) improvement of the PL QE of the CdTe QDs and the nanorods as

3. Post preparative phototreatment of semiconductor nanocrystals

well as a drastic improvement in the cases of CdSe and InP (hundreds of times) were demonstrated.

The several hypothetical mechanisms have been proposed for PL enhancement: i) photoinduced surface etching [6, 9], ii) oxidation of surface (oxide shell formation) [10, 11], iii) photoinduced shell formation [3, 7, 8], iv) reversible photo assisted absorption of water [18, 21] or methanol [22] molecules.

This chapter focuses on the photo-assisted creation of inorganic shell as well as on the photoetching of water soluble semiconductor nanoparticles. **Figure 3.1.1** shows photograph of experimental setup for photoetching of the aqueous CdTe nanocrystals.

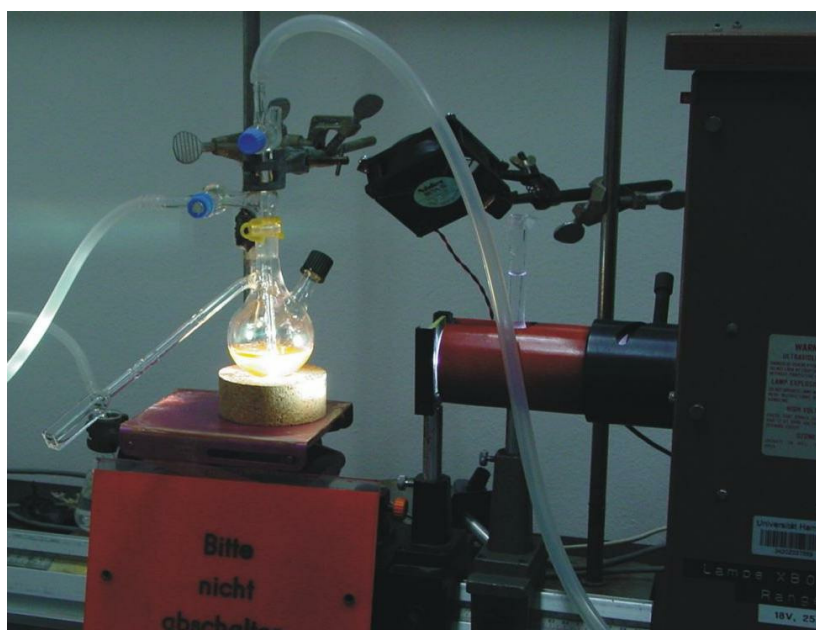


Figure 3.1.1. The picture of the experimental setup for photoetching of NCs.

3.2. Efficient UV-blue photoluminescing thiol-stabilized water soluble alloyed ZnSe(S) nanocrystals.

As it was shown in the **Chapter 2**, the PL of “as prepared” ZnSe NCs is negligible and shows mainly a whitish-blue broad trap emission band. The PL QY of this type QDs are normally below 1% [23]. An additional very weak band-edge emission appears only after long times of reflux (see, for example, **Figure2.1.1**).

The ZnSe NCs were synthesized according to slightly modified standard aqueous synthesis developed for CdTe NCs [6]. See **Chapter 2.2** and Ref [24] for details.

In order to improve the PL properties of the ZnSe NCs (enhancement of the band-edge and suppression of the trap-emission), the colloidal solutions were irradiated with the “white light” of a 100 W xenon lamp with a water filter to cut off the NIR part of the spectrum. The intensity of the light was approximately 200 mW/cm² (measured by a Powerlitemeter C5100 (Continuum) with a PowerMax PM30V2 detector). The photochemical treatment was performed as follows. The solutions were exposed to the light and aliquots were taken for spectroscopic measurements after different periods of time. The dependence of the PL properties of selected fraction of NCs on the duration of the irradiation is shown in **Figure 3.2.1**. After several hours under illumination, the PL QE increases from near zero ($\leq 0.1\%$), being characteristic for the as prepared solutions, up to 10-30% depending on the conditions used. The room-temperature PL QE of the ZnSe nanocrystals was estimated following the procedure of Ref [25] by comparison with Quinine (Fluka) in 1 N H₂SO₄ solution assuming its PL QE to be 51%. Being removed from the light, the colloids showed a reasonable stability. Several months of storage in the dark under air resulted neither in coagulation, nor in recognizable changes in the optical properties. It should be mentioned that ZnSe QDs capped with TGA, MPA or TG showed a similar increase in PL efficiency. However, for both MPA- and TG- capped QDs a pronounced increase also of the trap-emission band under irradiation is observed. Therefore, only the TGA-capped QDs were chosen for more detailed studies.

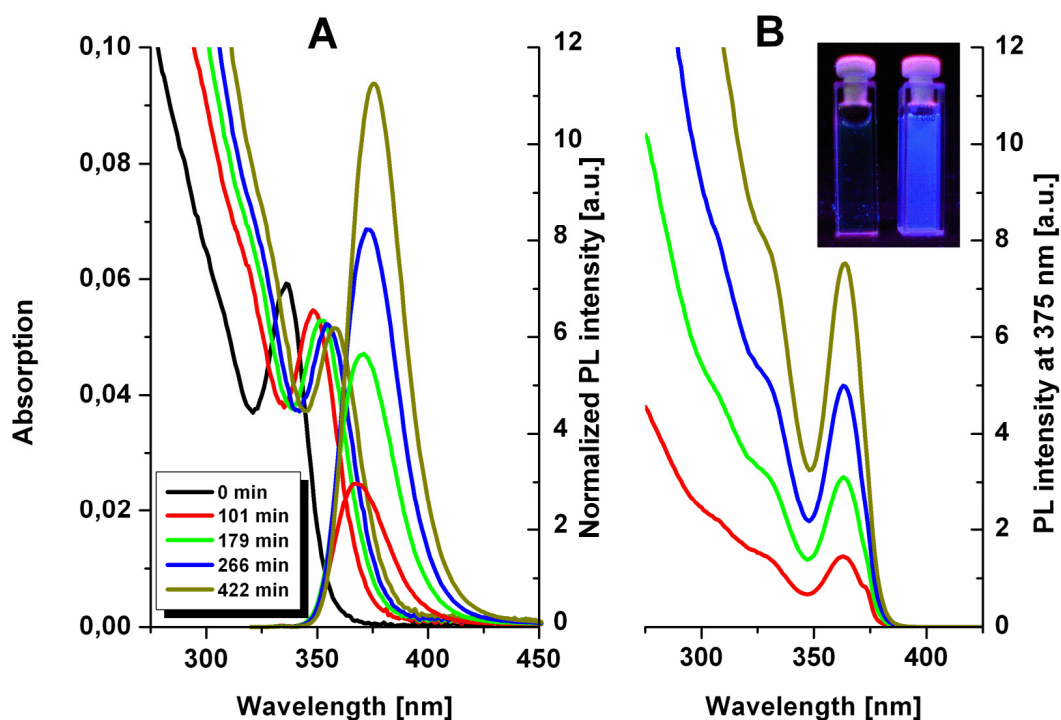


Figure 3.2.1. Evolution of the absorption and PL spectra (A) and excitation spectra (B) (emission wavelength 375 nm) of ZnSe NCs during illumination with white light (Xenon lamp, 100 W with a water filter to cut off the NIR part of the spectrum). Inset shows a color photograph of two solutions of the ZnSe NCs before (left) and after (right) illumination. Solutions are excited by 366 nm line of the Hg UV-lamp. Total irradiation time: 422 minutes.

To understand the nature of the photoinduced processes the influence of the chemical composition of the solution on the resulting PL QE was studied. The ZnSe QDs were precipitated from the crude solution by addition of a non-solvent (2-propanol) and subsequent centrifugation. The precipitate was separated from the supernatant and was redissolved in pure water giving a stable colloidal solution with its optical properties being generally similar to the initial one. Purified by this way the QDs were used for preparation of 3 different solutions (S1-S3, see the **Table**). In addition, the crude solution of NCs was divided into fractions with narrower size distribution (by size-selective precipitation technique [5]) and one of the fractions was used for the preparation of solution S4. The experiments with these solutions as well as with the crude solution (S0) were done under the same conditions and were repeated 3 times to avoid possible mistakes and confirm reproducibility.

3. Post preparative phototreatment of semiconductor nanocrystals

As is seen from the **Table** the phototreatment of the ZnSe QDs proceeds efficiently only in the presence of an excess amount of both TGA and Zn^{2+} ions in solution. Note that free unreacted stabilizer molecules and Zn^{2+} ions are present also in the crude solution because they are used for the synthesis in excess over the Se source (see above the reaction recipe).

Table. Chemical composition of the QDs solutions used for irradiation (pH 6.5 by adding NaOH).

Sample Number	ZnSe QDs, mmol/L (ref. to Se)	TGA, mmol/L	Zn^{2+} , mol/L (in form of $Zn(ClO_4)_2$)	Result of Phototreatment
S0 (crude)	10.2	not added	not added	Stable; PL QE of up to 10%
S1	10.2	-	-	Coagulation after 10 min; no improvement of PL QE
S2	10.2	42.2	-	Stable; increase of PL QE is negligible
S3	10.2	42.2	17.4	Stable; PL QE of up to 10%
S4 (selected fraction)	10.2 ^a	42.2	17.4	Stable; PL QE of up to 25-30%

^aThe absorption is equal to the crude solution in the region of the first excitonic maximum.

As is seen from **Figure 3.2.1**, the PL efficiency of the TGA-capped QDs increases mainly due to the appearance of a pronounced narrow band gap emission band, while the trap-associated emission is negligible. The position of the PL maximum and the absorption edge shifted to the lower energy region, which is in contrast to the high-energy shift observed recently for the photoetching of thiol-stabilized CdTe nanocrystals [6]. Since the QDs studied are in the regime of size-confinement, i.e. a low energy band edge corresponds to larger particles, it can be assumed, that the colloidal ZnSe particles grow under irradiation.

These findings together with the data of the **Table** allow us to consider that the growth proceeds not through the Ostwald ripening mechanism but instead consumes mainly Zn^{2+} ions and TGA from the solution. In the case of Ostwald ripening the smaller particles in an ensemble dissolve giving the “monomer” species for the growth of the

larger ones. It is noted, that the observed evolution of the PL properties of the ZnSe(S) NCs is generally followed by a decrease of the Stokes shift.

The appearance of the strong band-gap emission and the small level of the trap-associated one allow us to suggest that such a photoinduced growth is accompanied with a transition of the nanoparticles in the direction of sulfur enriched alloyed particles. Moreover, the small level of surface trap emission can be a result of the formation of an efficient passivating shell. More detailed information can be obtained from the XRD and TEM data (Figures 3.2.2 and 3.2.3).

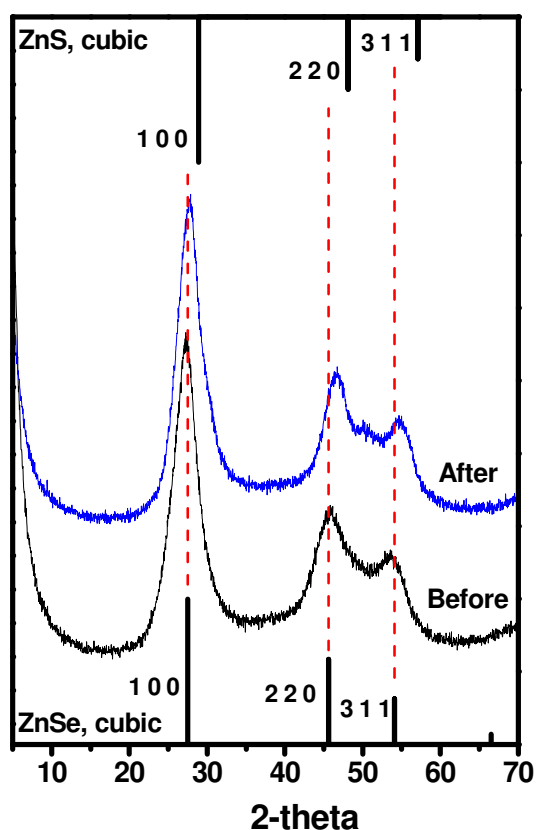


Figure 3.2.2 XRD patterns of ZnSe NCs before (down) and after (up) irradiation by white light. The line spectra show the cubic ZnSe and ZnS reflection with their relative intensities.

The position of the XRD peaks exhibits a small shift from their normal position for the ZnSe cubic structure. EDX data show that the content of sulfur continually rises during

the irradiation from 19 at% before to 29 at% after the process (the sulfur in the EDX data of the initial samples appears mainly due to the stabilizer (TGA)). Indeed, the particles' growth under these conditions can proceed only by involving the sulfur as a chalcogenide source, which appears as a product of the photodecomposition or hydrolysis of the thioglycolic acid in solution. As a result, the XRD lines shift to values which are characteristic for ZnSe-ZnS alloys, i.e. located between the positions of the corresponding lines for pure ZnSe and ZnS (**Figure 3.2.2**). Such kind of XRD-spectrum evolution accompanied also with the growth of thiol-stabilized CdTe(S) QDs is reported in detail recently [4, 22]. The sulfur enriched phase is formed during the phototreatment as a kind of an alloyed shell on the surface of the preformed ZnSe particle cores, followed by a reorganization of the particles' structure and by this the content of sulfur increases towards the surface of the nanoparticles. The formation of such an alloyed shell constructed from larger band gap material can explain the improvement of the optical properties (higher PL QE and stability) [6, 11].

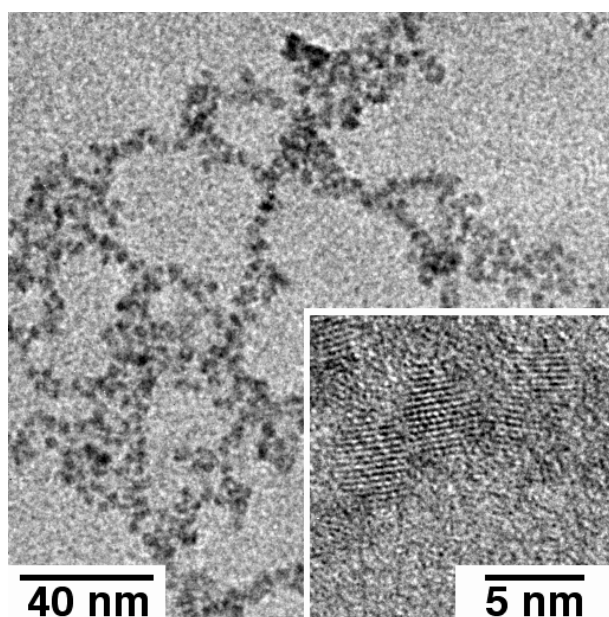


Figure 3.2.3. High-resolution transmission electron microscopy (HRTEM) image of luminescent ZnSe(S) NCs.

It has to be emphasized, that distinctions between true core-shell and the above mentioned alloyed crystals, with a gradient of the sulfur content, are probably not possible from the point of view of their physical properties. In fact, such small crystals (2-3 nm in

size) have only a few lattice planes per crystal (the lattice constant a is near 0.56 nm for the ZnSe cubic structure, see also **Figure 3.2.3**). From this, a removal and/or intermixing of a second chalcogenide (S) into the surface layer leads almost automatically to an alloyed crystal structure.

3.3. Post preparative improvement of luminescence efficiency of the CdTe NCs

Commonly used approach for the aqueous synthesis of the CdTe allows to produce NCs with quantum efficiency about 5-10% for “as prepared” particles and up to 40% after applying the size selective precipitation procedure [6]. At the same time the organometallic approach to the synthesis of CdTe NCs leads to QE of nanocrystals up to 65% [26, 27]. Improvement of the QE of water soluble nanocrystals is the important task especially for small green emitting NCs which are normally less stable and emit with less efficiencies. This chapter is devoted to the investigation of the possibility of the improving the QE of CdTe NCs by utilizing both photoetching and photoassisted inorganic shell formation.

The CdTe aqueous nanocrystals were synthesized according to the procedure described in **Chapter 2**, by using 2.45 TGA/Cd ratio and pH 11.2-11.8. See **Appendix 2** and Ref [6] for more details of synthetic procedure. The solution of the NCs was irradiated by the light of 450 W Xenon lamp equipped with the water filter to cut off NIR irradiation. Photoassisted shell formation was performed in solution containing the metal ions and thioglycolic acid. Oppositely, the photoetching can be performed in pure solution of the CdTe NCs in MilliQ water.

The phototreatment was done according to the following procedure. The solutions for treatment were prepared by dissolving $\text{Me}(\text{ClO}_4)_2$ ($\text{Me} = \text{Zn, Cd}$) and TGA in MilliQ water with 4-fold excess of all components in comparison with concentration commonly used for the NCs synthesis. The pH of these solutions was adjusted to 11.4-11.6 by dropwise addition of 1 M solution of NaOH. These solutions are named below as “Zn-TGA” and “Cd-TGA” solutions.

The certain amount of CdTe NCs solution was added to the 0.5 mL of “Zn-TGA” or “Cd-TGA” solutions and volume was adjusted to 2 mL. Final concentrations of metal ions and thioglycolic acid were 0.019M ($\text{Me}(\text{ClO}_4)_2$) and 0.046M (TGA) correspondingly. Irradiation was performed in quartz vessel under permanent flow of nitrogen.

Worth to mention, that addition of the TGA leads at the beginning to the decreasing of PL intensity (near 25% of initial QY for 630 nm emitting particles in 10^{-4} M TGA solution). Decreasing of QY after addition TGA to the solution of the CdTe NCs size selected fraction can be explain by the partial dissolution of nanoparticles surface due to formation of the stable complexes of cadmium with TGA. Actually, the instability constant for CdL , CdL_2 and CdL_3 are $10^{11.45}$, $10^{15.63}$ and $10^{19.11}$ correspondingly [28] and solubility product constant for CdTe is near 10^{-42} [29, 30] (see **Appendix 1** for more details about complexes formations). Irradiation of such system leads to the establishment of the new equilibrium in the system followed by the recovering of initial PL intensity and finally to the improving of the PL properties of the CdTe NCs.

Figure 3.3.1 shows the typical changes in the absorption and photoluminescence properties of CdTe NCs irradiated by UV-white light in the Cd-TGA and Zn-TGA solutions. Such solutions of nanocrystals may absorb light only with wavelength in region between 200 nm (limit for quartz, material of flask for irradiation) and 500 nm (band gap absorption of CdTe NCs). The illumination of small (green emitting) nanocrystals both in Zn-TGA and Cd-TGA solution leads to the drastic improvement of the luminescence of NCs. Both solutions demonstrate the red shift in absorption and luminescence spectra which can be attributed to the growing of nanoparticles during photo-assisted ZnS- and CdS-shell formation. Formation of the CdS and ZnS NCs as by product in the solution should not be excluded.

The aqueous synthesis of thiol capped CdTe NCs at basic pH (11.2-11.8) resulted in the incorporation of the sulfur in to the nanoparticles [6, 31]. Sulfur atoms are incorporated in the nanoparticles during thermal decomposition of the stabilizer molecules, but photo-assisted decomposition should not be excluded (as a result of using unprotected flask). The big particles can contain relatively large amount of sulfur atoms (8 day of reflux) in comparison with the small (green emitting) which synthesis takes only 1-2 hours. Continuous shift of CdTe-cubic phase XRD reflexes during the synthesis of CdTe NCs toward the position of reflexes corresponding to the CdS-cubic phase has been demonstrated in Ref [6]. The direct heat-assisted synthesis of CdS NPs from water soluble thiols and cadmium salt [32] as well as the irradiative-assisted CdS formation [33] are well known.

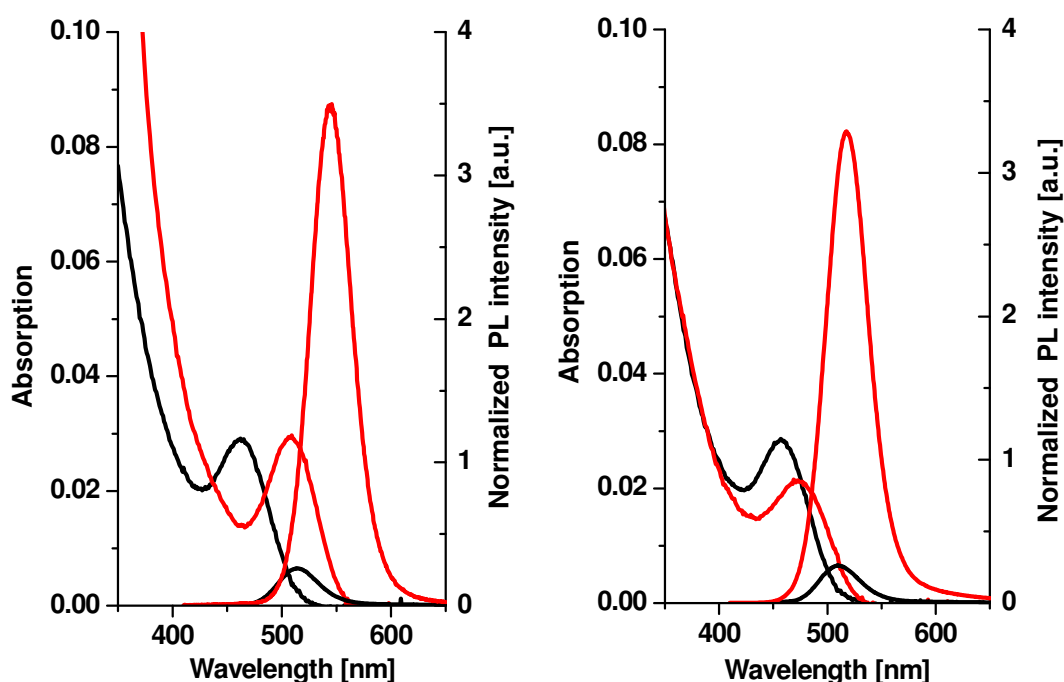


Figure 3.3.1 Absorption and normalized PL spectra of CdTe NCs before (black) and after (red) irradiation in the presence of Cd-TGA (left) and Zn-TGA (right) solutions. The irradiation time is 800 minutes.

Therefore, for small CdTe nanocrystals, which have only a few lattice planes and relatively small sulfur content, shell growing leads to formation of CdTe(CdS) and CdTe(ZnS) alloyed shells. In this case it is impossible to distinguish between pure core/shell system and S or ZnS enriched external alloyed shell. **Figure 3.3.1** also shows that irradiation of the CdTe NCs in the Zn-TGA solution leads to the smaller red shift than irradiation in Cd-TGA solution. Smaller red shift appears, in the case of ZnS shell, due to large band gap of the ZnS and as a result due to the smaller possibility for distribution of the electron-wave function in the nanoparticles.

Thus the large CdTe particles have the surface enriched with sulfur and further incorporation of sulfur can not lead to the improvement of PL and pronounced red shift. Oppositely a small, wide band gap particle can consume sulfur from solution more efficiently. As a result, the competition of processes of photoetching and shell formation leads mainly to the etching in case of large (red and IR emitting) nanoparticles and to the shell formation for small (green emitting) nanoparticles. Therefore effectiveness of shell growing is size dependent. (See **Figure 3.3.2**).

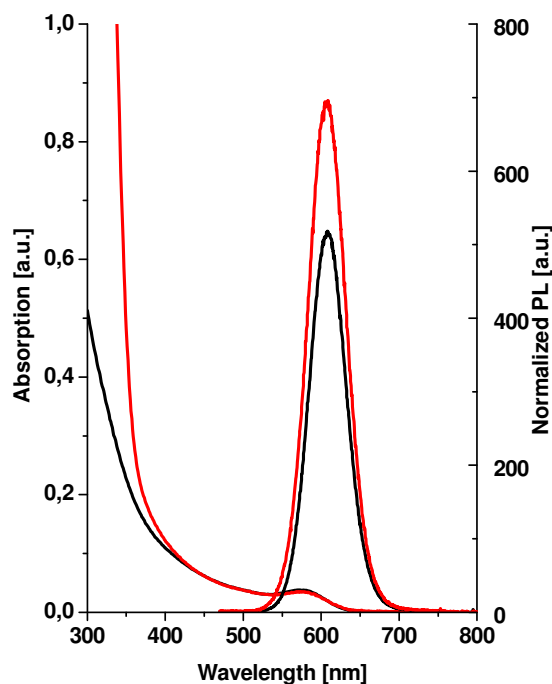


Figure 3.3.2 Absorption and normalized PL spectra of CdTe NCs before (black) and after (red) irradiation in the Cd-TGA solution. Irradiation time is 805 min.

In order to investigate the possibility of the formation of CdS NCs as a “by product” the solution of red-emitting CdTe nanocrystals was irradiated during 24 hours. **Figure 3.3.3** shows the absorption and PL spectra of irradiated CdTe together with PLE spectrum.

A PL spectra of irradiated sample have two clear distinguishable peaks: broad and weak peak at 400-500 nm and strong narrow at 585 nm correspondingly (**Figure 3.3.3A**, black line). A PLE spectrum (emission 470 nm, **Figure 3.3.3C**) shows that this emission can be assigned to the trap-related luminescence of CdS NPs. Oppositely, the emission at 585 nm can be assigned to a band gap luminescence of the CdTe/CdS core/shell structure (**Figure 3.3.3B**). Panel A shows the increase of band gap emission during irradiation (blue line shows emission before phototreatment). Increasing of QE of nanoparticles together with the appearance of “blue” shoulder in absorption spectra allow assume that shell formation is followed by the CdS NCs by-product formation.

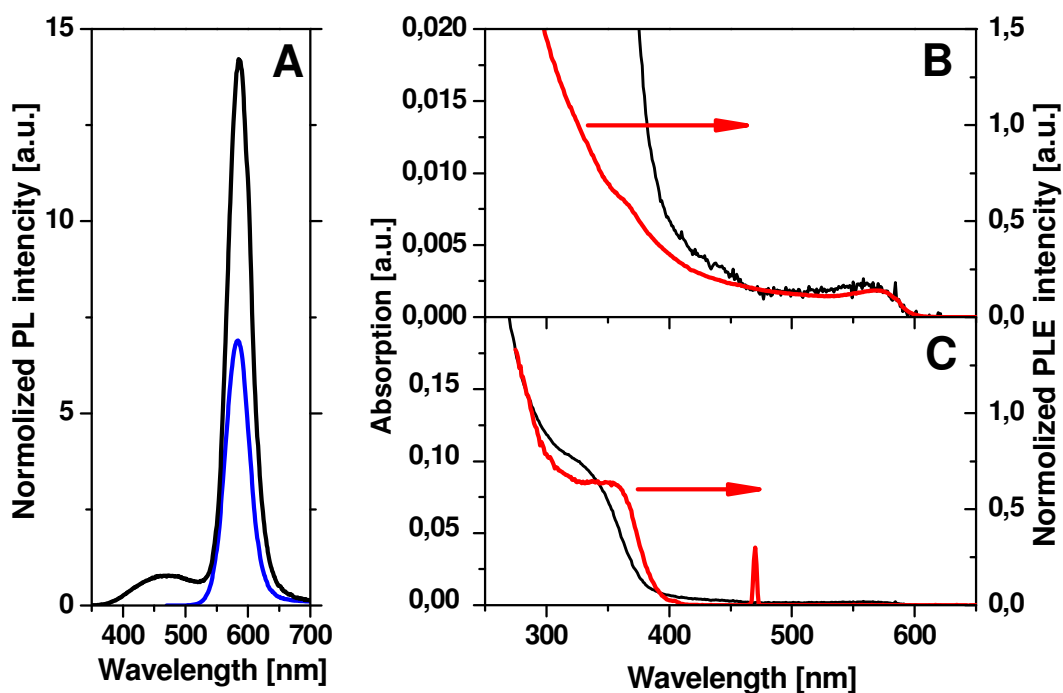


Figure 3.3.3 Absorption, luminescence and excitation spectra of the CdTe/CdS core/shell NCs obtained by the phototreatment during 24 hours. Panel A presents PL (excitation at 300 nm) spectra before (blue) and after (black) phototreatment. Panels B and C (black lines) present the same absorption spectrum, but the scale of the Y axes in B is chosen to be 10 times smaller compares to that C in order to pronounce absorption maximum of ca 560 nm. The PLE spectra (red lines) measured at 600 nm (B) and at 470 nm (C) are also shown.

In general, the irradiation of the aqueous solution of semiconductor NCs can initiate at least two processes i) photodissolution (photoetching) of the NCs and ii) photoassisted modification of NC surface [3].

Photoetching is a process of photo-assisted degradation of nanoparticles with releasing of cadmium ions and by product in the solution followed by decrease of the particle size. Photoetching leads to the blue shift both in absorption and luminescence spectra. At the initial stage photoetching improves PL properties of nanocrystals as a result of removing of surface defects. Further irradiation can lead to the complete degradation of the nanocrystals, which are losing their stability and precipitate as a result of decomposition of molecules of the stabilizers.

Oppositely to the photoetching, the photoassisted modification can lead to the increasing of particles size, i.e. shell formation. Shell formation is followed by the red shift in optical spectra as a result of a weaker confinement of electron–hole pairs. The appearance of electron transitions corresponding to the shell materials in absorption spectra is also possible. Shell formation in aqueous media is going through consumption of cadmium ions and molecules of stabilizer. Shell formation leads to the drastic improvement of quantum efficiency as a result of passivation of the surface states by material of inorganic shell.

Irradiation of the pure solution of nanocrystals may lead only to the photoetching of nanoparticles. The addition of some amount of molecules of stabilizer improves drastically the stability of the nanocrystals suspension under irradiation.

Results of competition of photoetching and photo-assisted shell formation depend on the nature of semiconductor material and stabilizer. Materials with different band gaps possess different energy of electrons and holes which can be involved in photochemical processes. From the other side, different stabilizer molecules have different ability to take part in the photo-assisted processes. In particular, the post-preparative photochemical treatment of thiol-stabilized ZnSe and CdTe nanocrystals leads to the improvement of their luminescence properties with different contribution of photoetching and shell formation mechanisms.

3.4. Conclusions.

The post-preparative photochemical treatment of thiol-stabilized ZnSe and CdTe nanocrystals has been investigated.

Phototreatment of ZnSe NCs is going mainly through inorganic shell formation. The illumination of “dark” ZnSe NCs leads to the strong (up to 25-30% PL QE) band gap luminescence. Phototreatment is followed by increase of NC’s size, due to incorporation of the sulfur in to the particles, which results in the formation of ZnSe(S) alloyed protective shell on the surface of nanoparticles.

Oppositely, photo-treatment of CdTe NCs goes through the competition of i) photoetching of nanocrystals and ii) photo-assisted shell formation. Both processes are size

dependent. Small (green emitting) CdTe NCs undergo mainly the shell formation and show pronounced red shift both in absorption and luminescence spectra. Increase of particles' size is followed by the improvement of the photoetching efficiency due to the increasing of sulfur content.

The post preparative irradiation of aqueous CdTe nanocrystals allows achieving the PL quantum efficiency as high as 50-60% which is comparable with quantum efficiencies of CdTe NCs synthesized by hot injection procedure in organic media.

3.5. References.

1. Dabbousi, B.O., J. RodriguezViejo, F.V. Mikulec, J.R. Heine, H. Mattoussi, R. Ober, K.F. Jensen and M.G. Bawendi, *(CdSe)ZnS core-shell quantum dots: Synthesis and characterization of a size series of highly luminescent nanocrystallites*. J. Phys. Chem. B, 1997. **101**(46): p. 9463-9475.
2. Peng, X.G., M.C. Schlamp, A.V. Kadavanich and A.P. Alivisatos, *Epitaxial growth of highly luminescent CdSe/CdS core/shell nanocrystals with photostability and electronic accessibility*. J. Am. Chem. Soc., 1997. **119**(30): p. 7019-7029.
3. Bao, H., Y. Gong, Z. Li and M. Gao, *Enhancement Effect of Illumination on the Photoluminescence of Water-Soluble CdTe Nanocrystals: Toward Highly Fluorescent CdTe/CdS Core-Shell Structure*. Chemistry of Materials, 2004. **16**(20): p. 3853-3859.
4. Harrison, M.T., S.V. Kershaw, A.L. Rogach, A. Kornowski, A. Eychmüller and H. Weller, *Wet chemical synthesis of highly luminescent HgTe/CdS core/shell nanocrystals*. Adv. Mater., 2000. **12**(2): p. 123-125.
5. Talapin, D.V., A.L. Rogach, E.V. Shevchenko, A. Kornowski, M. Haase and H. Weller, *Dynamic distribution of growth rates within the ensembles of colloidal II-VI and III-V semiconductor nanocrystals as a factor governing their photoluminescence efficiency*. J. Am. Chem. Soc., 2002. **124**(20): p. 5782-5790.
6. Gaponik, N., D.V. Talapin, A.L. Rogach, K. Hoppe, E.V. Shevchenko, A. Kornowski, A. Eychmüller and H. Weller, *Thiol-capping of CdTe nanocrystals: An alternative to organometallic synthetic routes*. J. Phys. Chem. B, 2002. **106**(29): p. 7177-7185.
7. Wang, Y., Z. Tang, M.A. Correa-Duarte, L.M. Liz-Marzan and N.A. Kotov, *Multicolor Luminescence Patterning by Photoactivation of Semiconductor Nanoparticle Films*. J. Am. Chem. Soc., 2003. **125**(10): p. 2830-2831.
8. Wang, Y., Z. Tang, M.A. Correa-Duarte, I. Pastoriza-Santos, M. Giersig, N.A. Kotov and L.M. Liz-Marzan, *Mechanism of Strong Luminescence Photoactivation of Citrate-Stabilized Water-Soluble Nanoparticles with CdSe Cores*. J. Phys. Chem. B, 2004. **108**(40): p. 15461-15469.

9. Talapin, D.V., N. Gaponik, H. Borchert, A.L. Rogach, M. Haase and H. Weller, *Etching of Colloidal InP Nanocrystals with Fluorides: Photochemical Nature of the Process Resulting in High Photoluminescence Efficiency*. J. Phys. Chem. B, 2002. **106**(49): p. 12659-12663.
10. Jang, E., S. Jun, Y. Chung and L. Pu, *Surface Treatment to Enhance the Quantum Efficiency of Semiconductor Nanocrystals*. J. Phys. Chem. B, 2004. **108**(15): p. 4597-4600.
11. Myung, N., Y. Bae and A.J. Bard, *Enhancement of the Photoluminescence of CdSe Nanocrystals Dispersed in CHCl₃ by Oxygen Passivation of Surface States*. Nano Lett., 2003. **3**(6): p. 747-749.
12. Gao, M.Y., S. Kirstein, H. Mohwald, A.L. Rogach, A. Kornowski, A. Eychmüller and H. Weller, *Strongly photoluminescent CdTe nanocrystals by proper surface modification*. J. Phys. Chem. B, 1998. **102**(43): p. 8360-8363.
13. Kalyuzhny, G. and R.W. Murray, *Ligand Effects on Optical Properties of CdSe Nanocrystals*. J. Phys. Chem. B, 2005. **109**(15): p. 7012-7021.
14. Wuister, S.F., C. De Donega and A. Meijerink, *Influence of thiol capping on the exciton luminescence and decay kinetics of CdTe and CdSe quantum dots*. J. Phys. Chem. B, 2004. **108**(45): p. 17393-17397.
15. Wuister, S.F., C. De Donega and A. Meijerink, *Luminescence Temperature Antiquenching of Water-Soluble CdTe Quantum Dots: Role of the Solvent*. J. Am. Chem. Soc., 2004. **126**(33): p. 10397-10402.
16. Manna, L., E.C. Scher, L.-S. Li and A.P. Alivisatos, *Epitaxial Growth and Photochemical Annealing of Graded CdS/ZnS Shells on Colloidal CdSe Nanorods*. J. Am. Chem. Soc., 2002. **124**(24): p. 7136-7145.
17. Tsay, J.M., S. Doose, F. Pinaud and S. Weiss, *Enhancing the Photoluminescence of Peptide-Coated Nanocrystals with Shell Composition and UV Irradiation*. J. Phys. Chem. B, 2005. **109**(5): p. 1669-1674.
18. Cordero, S.R., P.J. Carson, R.A. Estabrook, G.F. Strouse and S.K. Buratto, *Photoactivated luminescence of CdSe quantum dot monolayers*. J. Phys. Chem. B, 2000. **104**(51): p. 12137-12142.
19. Nazzal, A.Y., X. Wang, L. Qu, W. Yu, Y. Wang, X. Peng and M. Xiao, *Environmental Effects on Photoluminescence of Highly Luminescent CdSe and CdSe/ZnS Core/Shell Nanocrystals in Polymer Thin Films*. J. Phys. Chem. B, 2004. **108**(18): p. 5507-5515.
20. Kimura, J., T. Uematsu, S. Maenosono and Y. Yamaguchi, *Photoinduced Fluorescence Enhancement in CdSe/ZnS Quantum Dot Submonolayers Sandwiched between Insulating Layers: Influence of Dot Proximity*. J. Phys. Chem. B, 2004. **108**(35): p. 13258-13264.
21. Nazzal, A.Y., L. Qu, X. Peng and M. Xiao, *Photoactivated CdSe Nanocrystals as Nanosensors for Gases*. Nano Lett., 2003. **3**(6): p. 819-822.

22. Jones, M., J. Nedeljkovic, R.J. Ellingson, A.J. Nozik and G. Rumbles, *Photoenhancement of Luminescence in Colloidal CdSe Quantum Dot Solutions*. J. Phys. Chem. B, 2003. **107**(41): p. 11346-11352.
23. Murase, N., M.Y. Gao, N. Gaponik, T. Yazawa and J. Feldmann, *Synthesis of water dispersible ZnSe nanocrystals showing whitish blue photoluminescence*. Springer Proceedings in Physics, 2001. **87**(Proceedings of the 25th International Conference on the Physics of Semiconductors, 2000, Part II): p. 1191-1192.
24. Shavel, A., N. Gaponik and A. Eychmüller, *Efficient UV-Blue Photoluminescing Thiol-Stabilized Water-Soluble Alloyed ZnSe(S) Nanocrystals*. Journal of Physical Chemistry B, 2004. **108**(19): p. 5905-5908.
25. Crosby, G.A. and J.N. Demas, *Measurement of photoluminescence quantum yields. Review*. J. Phys. Chem., 1971. **75**(8): p. 991-1024.
26. Talapin, D.V., S. Haubold, A.L. Rogach, A. Kornowski, M. Haase and H. Weller, *A novel organometallic synthesis of highly luminescent CdTe nanocrystals*. J. Phys. Chem. B, 2001. **105**(12): p. 2260-2263.
27. Wuister, S.F., I. Swart, F. van Driel, S.G. Hickey and C.d.M. Donega, *Highly Luminescent Water-Soluble CdTe Quantum Dots*. Nano Lett., 2003. **3**(4): p. 503-507.
28. Turyan, I. and D. Mandler, *Electrochemical study of the Cd(II)/Cd(Hg) system in 2-mercaptopoacetic acid solutions*. Electrochimica Acta, 1995. **40**(9): p. 1093-1100.
29. Buketov, E.A., M.Z. Ugorets and A.S. Pashinskin, *Solubility product and entropy of sulfides, selenides, and tellurides*. Zhurnal Neorganicheskoi Khimii, 1964. **9**(3): p. 526-529.
30. Erdenbaeva, M.I., *Solubility product of selenium and tellurium compounds*. Vestnik Akademii Nauk Kazakhskoi SSR, 1975(2): p. 51-57.
31. Rogach, A.L., *Nanocrystalline CdTe and CdTe(S) particles: wet chemical preparation, size-dependent optical properties and perspectives of optoelectronic applications*. Materials Science & Engineering, B: Solid-State Materials for Advanced Technology, 2000. **B69-70**: p. 435-440.
32. Doellefeld, H., K. Hoppe, J. Kolny, K. Schilling, H. Weller and A. Eychmüller, *Investigations on the stability of thiol stabilized semiconductor nanoparticles*. Phys. Chem. Chem. Phys., 2002. **4**(19): p. 4747-4753.
33. Swayambunathan, V., D. Hayes, K.H. Schmidt, Y.X. Liao and D. Meisel, *Thiol surface complexation on growing cadmium sulfide clusters*. J. Am. Chem. Soc., 1990. **112**(10): p. 3831-3837.

Chapter 4

Electrochemical properties of aqueous nanocrystals.

Electrochemical studies of aqueous thiol-capped CdTe and ZnSe nanocrystals have demonstrated several distinct oxidation and reduction peaks in the voltammograms. The peak positions are dependent on the nanocrystals' size and on the post preparative treatment. Experimental observations allow to assign these peaks to the oxidation of Se- or Te-related surface traps for ZnSe and CdTe NCs, respectively. The intra-band-gap energy levels of aqueous NCs assigned to these Te- and Se- related trap states shift towards the top of the valence band as the nanocrystal size increases. The position of these intra band gap states are linearly depend on the position of the first excitonic transition of the NCs and move towards higher potentials with size. The photo-assisted formation of ZnSe(S) NCs leads to even more pronounced and nonlinear shift of the intra band gap levels. Finally, the trap level merges into the valence band. Moving of the trap level is followed by a drastic increase of the luminescence of the ZnSe(S) nanocrystals (from negligible to up to 25-30%).

4.1. Introduction

As opposed to other important physicochemical properties of colloidal semiconducting nanocrystals less attention has been paid to their electrochemical behavior [1-5]. Several reports have been devoted to the study of a correlation between the optical band gap of the NCs and the band gap estimated from the oxidation and reduction peak positions in cyclic voltammograms [1, 2]. These studies have been performed in non-aqueous media and the results obtained are somewhat contradictory. Whereas Kucur et al. [2] found good agreement between electrochemical and optical E_g values for CdSe NCs with different sizes, Bard and coworkers [1] revealed that the electrochemical band gaps were smaller than the optical gaps for CdS NCs. In their recent work, Bard et al. found that the electrochemical band gap (~ 2.1 eV) between the first anodic and cathodic peaks was close to the optical E_g value (2 eV) for TOPO-capped CdTe nanoparticles [6]. The authors of the electrochemical studies noted that upon changing the particle size the reduction and oxidation peaks in the voltammograms were shifted in the direction predicted by theory [1-3, 6].

Thus, since the size dependent electrochemical behavior of nanoparticles is not studied properly yet here we report on the study of the correlations between the electrochemical properties of MPA and TGA capped CdTe NCs of different sizes and their optical properties. Another point of our interest is the size dependent behavior of ZnSe NCs, a material not being studied so far, and especially an *in situ* observation of a light induced formation on alloyed ZnSe(S) NCs.

4.2. Size dependent electrochemical properties of CdTe nanocrystals.

The CdTe NCs stabilized by thioglycolic (TGA) or 3-mercaptopropionic (MPA) acids were synthesized according to the procedure described previously (see details of the procedure in **Appendix 2** and Ref [7]). Portions of CdTe NCs of different sizes were taken from the crude solution at different refluxing times and size selective precipitation was applied to the crude solutions of the nanocrystals. Each portion of the crude solution was divided into a series of fractions with narrower size distributions by this means [7, 8]. This procedure allowed also washing out reaction by-products and excessive stabilizing agents, which is important taking into account the high-sensitivity of the electrochemical methods.

A series of the electrochemical experiments was carried out using pre-adsorbed NCs. The cleaned electrodes were dipped into the deaerated colloidal solutions of the NCs for 5 min. This procedure results in the adsorption of NCs on the electrode surface (see **Figure 4.2.1**) giving a surface concentration corresponding to approximately 50% surface coverage. The nanocrystal-coated electrodes were then washed with buffer solution and transferred to the electrochemical cell under Ar atmosphere. The cell electrolyte was deaerated by purging purified Argon for 30 min (see **Appendix 2** and Ref [9] for experimental details).

The cyclic voltammogram (CV) of the bare Au electrode in buffer solution is shown in **Figure 4.2.2** (black line). The current is negligible in the wide potential region from 1.0 to 0.5 V. Oxidation of the gold electrode surface starts from 0.5 V with an anodic current peak at 0.67 V that gives a cathodic current peak at 0.36 V during the reverse potential scan.

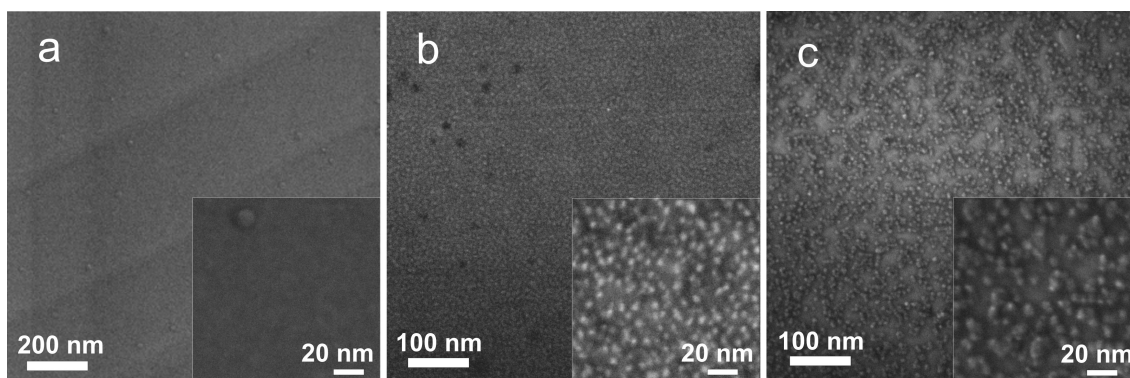


Figure 4.2.1. High-resolution SEM images of the surface of the Au electrode before (a) and after adsorption of CdTe nanocrystals stabilized with TGA (b) and MPA (c).

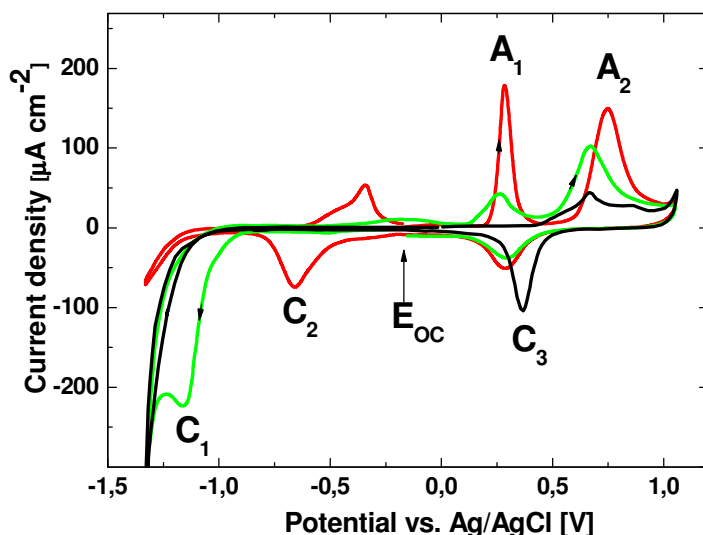


Figure 4.2.2. Voltammograms of the Au electrode with pre-adsorbed CdTe nanocrystals in blank buffer solution. The black line presents the CV of the bare Au electrode. Scan from E_{OC} in anodic direction (red) Scan from E_{OC} in cathodic direction (green). The potential sweep rate was 20 mV s^{-1} . E_{OC} : open circuit potential.

The CV curves of the gold electrode with preadsorbed CdTe NCs shows several additional electrochemical peaks. When the potential of the electrode is swept from the open circuit potential (E_{OC}) in the positive direction (red line), two distinct anodic peaks can be recorded in the potential regions from 0.3 to 0.4 V and from 0.75 to 0.8 V. The peak positions depend on the CdTe NC size (see **Figure 4.2.3**). The subsequent potential cycling between -0.5 and 1.2 V results in the disappearance of the anodic peaks, and the CV curves become similar to those recorded in the supporting electrolyte, suggesting that the oxidation products block the electrode surface. **Figure 4.2.2** (green line) also shows the

first CV curve for the Au electrode with preadsorbed CdTe NCs by scanning the potential in the negative direction from the open circuit potential. A cathodic current peak is observed at about -1.2 V, which is most likely associated with the reduction of the NCs. This peak is absent if the potential is initially scanned in the positive direction through the anodic peaks.

Figure 4.2.3 shows the first CV curves of CdTe NCs of four different sizes at the Au electrode in the blank buffer solution both for TGA stabilized CdTe NCs (left) and for MPA stabilized CdTe NCs right (right). In both cases the first anodic peak moves in the negative direction with decreasing the NCs size.

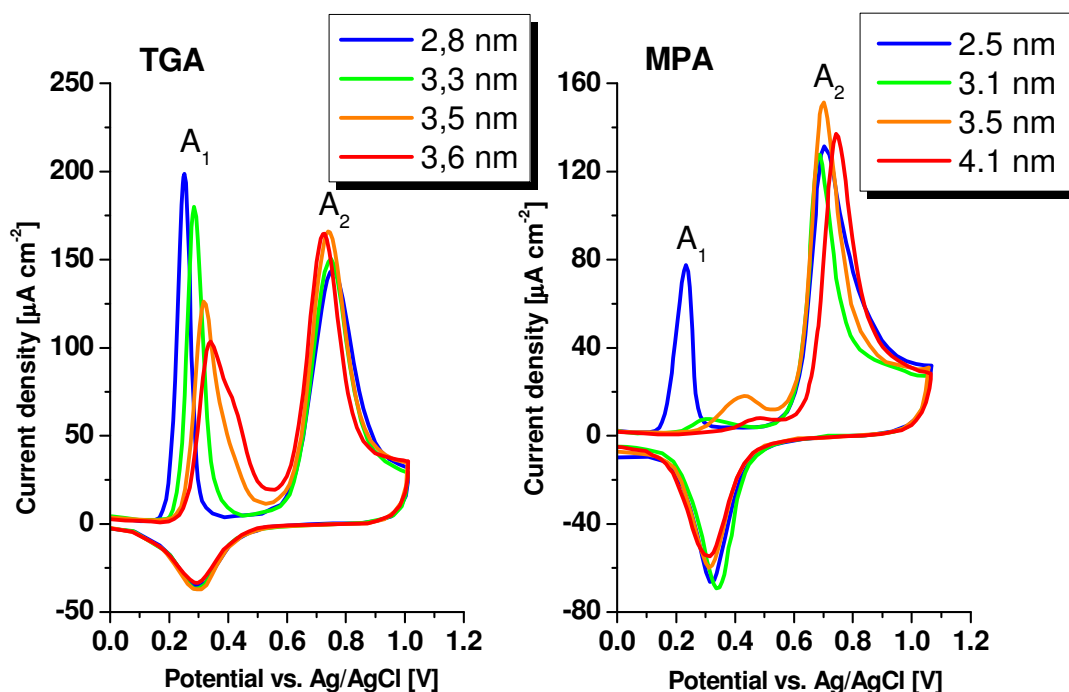


Figure 4.2.3 Voltammograms of the Au electrode in blank buffer solution after preadsorption of the TGA- (left) and MPA-capped (right) CdTe nanocrystals of four different sizes. The potential sweep rate was 20 mV s^{-1} .

The dependence of the potential corresponding to the first anodic peak for the NCs of different sizes on the PL peak energy is shown in **Figure 4.2.4**. To assure reproducibility, three different size-series of TGA-capped CdTe NCs were investigated. As can be seen, this dependence is practically linear both for TGA-capped and for MPA-capped CdTe NCs and the potential of the first oxidation peak increases with increasing the particle size or with decreasing the NCs band gap. Characteristically, the slope of the E_{A1}

vs. E_{\max}^{PL} curve is markedly greater for MPA-capped NCs in comparison with TGA-capped ones.

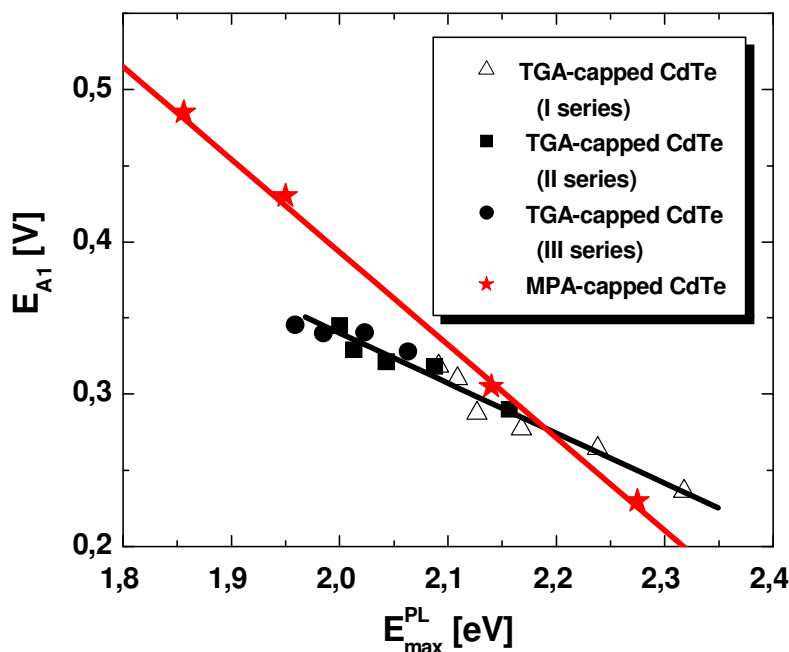


Figure 4.2.4. Dependence of the peak A_1 potential on the photon energy corresponding to the PL peak for three series of TGA-capped CdTe NC size-selected fractions and for a series of MPA-capped CdTe NC size-selected fractions.

Figure 4.2.5 depicts the first cyclic voltammograms of the cathodic reduction of TGA-capped CdTe NCs of two different sizes. The reduction peak also moves in the negative direction with decreasing NC size.

Since the positions of both the anodic and the cathodic current peaks depend on the NC size, it was of interest to elucidate the relationship between the electrochemical redox potentials and the semiconductor band gap energies. The separation between the peaks A_1 and C_1 is 1.4 – 1.6 V which is markedly smaller than the optical band gap of the CdTe NCs (2.0 – 2.3 eV) estimated from their spectra. At the same time, the $A_2 - C_1$ peak separation correlates better with the optical gap, remaining slightly smaller than the latter value (cf. **Table 4.1**).

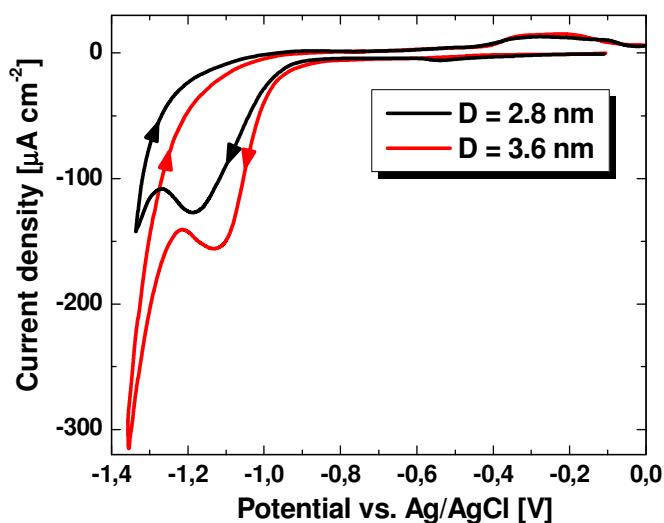


Figure 4.2.5. Cathodic voltammograms of the Au electrode in buffer solution after the pre-adsorption of TGA-capped CdTe nanocrystals of different sizes on the electrode surface. The potential sweep rate was 20 mV s^{-1} .

Table 4.1. Comparison of the band gap energies estimated for TGA-capped CdTe NCs of three different sizes from the PL maximum (E_g^{lum}) position with the electrochemical estimates ΔE (the difference between oxidation and reduction peaks).

Size of CdTe NCs ^a , nm	$\Delta E_1 (A_1-C_1)^b$, V	$\Delta E_2 (A_2-C_1)^b$, V	E_g^{lum} , eV
2.8	1.43	1.95	2.26
3.3	1.445	1.91	2.13
3.6	1.47	1.85	1.96

^a the NC size was estimated using the energy of the first absorption peak [10]

^b peak separation at the scan rate of 20 mV s^{-1} .

According to our expectation, the smaller CdTe NCs should be oxidized at more positive potentials and reduced at more negative ones than the larger NCs since the top of the valence band is shifted towards lower energies and the bottom of the conduction band is moved to higher energies with decreasing the particle size. It is important to note that the direction of the size dependent shift of the second anodic peaks and cathodic peaks is in accord with this expectation. In contrast, the first oxidation peak behaves abnormally, i.e. it shifts to the negative direction with decreasing the NC size.

These observations allow us to assume that the first anodic peak can be related to the oxidation of surface defects forming intra-band-gap surface states. The existence of trap states has been proven by fluorescence studies on CdS, CdSe and CdTe NCs prepared in

aqueous media [11, 12]. Generally, the traps can be associated with both Cd and Te dangling bonds on the nanocrystal surface where the oxidation of CdTe NCs will start. A previous high resolution photoelectron spectroscopy study of TGA-capped CdTe NCs has revealed that a larger amount of Te atoms occurs on the surface of low luminescent NCs in comparison with highly luminescing ones [13]. The traps at the NC surface may give rise to non-radiative recombination pathways. Since the low luminescent samples possess much more Te atoms at the surface than the high luminescent ones, it becomes apparent why the peak A_1 , tentatively related to the oxidation of these traps, is markedly higher for the lowly luminescing fractions.

The shift of this peak to more positive potentials with increasing the NC size indicates that the energy levels of Te-related traps move to lower energies when the NC size increases. Here it is important to note that this effect is markedly dependent on the chain length of the thiol ligands. **Figure 4.2.4** clearly demonstrates that the first anodic peak is shifted more drastically to the positive direction with decreasing the CdTe band gap for MPA-coated NCs as compared to TGA-coated ones. The shift becomes so large for the largest available NCs synthesized with MPA (PL maximum at about 800 nm), that the peak simply merges into the second anodic peak. This allows us to assume that for these NCs the energy levels of Te-related traps appear inside the valence band. For such kind of particles the highest possible photostability and PL life-times are expected, which corresponds very well with our preliminary observations [14].

Whereas the detailed mechanism of the electrochemical oxidation of the CdTe NCs remains largely unknown at the moment, the second anodic peak is most likely to be due to the oxidation of the rest of the CdTe core. The adsorption of reaction products on the electrode surface (both at the Au and ITO electrodes) suppresses the nanocrystal electrooxidation at the second and further scans. The electrochemical activity of thus passivated electrodes can be again restored by cleaning the electrode surface (see Experimental section). Since the second anodic peak shifts only slightly in the positive direction with decreasing the NCs size, the electrochemical band gap calculated as a separation between the second anodic peak and the cathodic peak ($A_2 - C_1$) is less than the optical band gap especially for the smallest NCs. A similar difference has been previously observed for thioglycerol-capped CdS NCs and was attributed to a multielectron transfer process where the electrons (or holes) are consumed by fast coupled chemical reactions due to decomposition of the particles [1]. A total multielectron reaction usually involves

several consecutive steps and the redox potential of the rate-limiting step may be different from that of the total reaction.

4.3. *In situ* electrochemical observation of photo induced formation of alloyed ZnSe(S) nanocrystals.

The photochemical treatment is a successful method for improving the photoluminescence quantum yields [7, 15-18] of semiconductor nanocrystals as well as for narrowing of their size distribution [7, 19]. (See **Chapter 3** for details of the photochemical treatment of ZnSe and CdTe NCs.)

Taking into account the high sensitivity of the electrochemical methods to the NC surface states as well as the similarity of ZnSe and CdTe NCs (TGA-capping, aqueous synthesis, etc) the evolution of the ZnSe NC surface properties under light irradiation was chosen to be an object for a cyclic voltammetric study.

The nanocrystals as-prepared possess a weak broad whitish-blue emission that is mainly associated with trap states. The irradiation of thus obtained ZnSe NCs with “white light” led to a dramatic improving of the PL properties, i.e. narrow UV-blue band-edge emission appeared and reached in the best cases quantum efficiencies of up to 25-30%. The improvement was explained in terms of the formation of a sulfur enriched shell on the surface of the nanocrystals. Photodestruction of the excess thiol molecules is assumed to be the source of the sulfur which together with the also present zinc ions are consumed for the shell formation [17]. (See for example **Figure 3.2.1** for a typical evolution of the absorption and PL spectra of thioglycolic acid (TGA) stabilized ZnSe NCs under irradiation with a 100 W Xe lamp.)

The photochemical treatment was performed as follows. A size selected fraction of nanocrystals (83 μ L) was added to 10 mL of a fresh solution of Zn(ClO₄)₂·6H₂O (16mM) and TGA (40mM) at pH 6.6. In order to assign the anodic peaks and understand better the details of the shell formation the behavior of the ZnSe NCs in a solution of TGA only (40mM, pH 6.6.) and in pure water has also been studied. The solution was illuminated by the light of a high-pressure Hg lamp equipped with an aqueous IR filter and a filter to cut the UV irradiation with $\lambda < 300$ nm. The total intensity of the photochemically active light in the wavelength range from 300 to 400 nm was about 75 mW cm⁻². All experiments were

performed in a quartz cell under open air conditions and intensive stirring. Aliquots of the solution were taken for spectroscopic and electrochemical measurements after different periods of time.

For electrochemical measurements the aliquots were precipitated by 2-propanol and centrifuged. The precipitates were separated from the supernatant and redissolved in acetate buffer giving stable colloidal solutions. After that, the gold foil was dipped for 5 minutes into the buffer solution of ZnSe NCs. Our previous study on CdTe NCs showed that efficient adsorption (at least 50% of surface coverage) of thiol-capped NCs on the gold surface took place under these conditions (cf. **Chapter 4.2** and ref. [9]). The electrode with adsorbed ZnSe NCs was thoroughly washed in fresh buffer solution and re-placed into the electrochemical cell as working electrode for the investigations. Electrochemical measurements were performed in a standard three-electrode two-compartment cell with a platinum counter electrode and an Ag | AgCl | KCl(sat.) electrode as the reference electrode. See **Appendix A2.6** for experimental details.

Typical cyclic voltammograms of four different fractions of the “as prepared” ZnSe NCs preadsorbed on the Au electrode are shown in **Figure 4.3.1A**. The anodic scans of the electrodes have three different peaks in the potential region 0.35 – 0.50 V (A_1), 0.66-0.67V (A_2) and 0.93-0.94 V (A_3), correspondingly. **Figure 4.3.1B** presents the size dependent behavior of the potentials A_1 and A_3 of this series of differently sized ZnSe NCs.

The evolution of the cyclic voltammograms of the ZnSe NCs during the photochemical treatment in the solution of TGA and zinc ions is shown in **Figure 4.3.2A**. The position of the first anodic peak (A_1) drastically shifts, while the positions of the second (A_2) and the third (A_3) peaks appear to be stable during the illumination. However, it has to be noted that the position of the second peak (A_2) becomes unrecognizable due to the masking by the moving first anodic peak. The evolution of the peak positions A_1 and A_3 and the PL intensity as a function of the illumination time are shown in **Figure 4.3.2B** and **4.3.2D**, respectively. The figure shows a clear correlation between first peak (A_1) position and the PL properties of the NCs. The increasing of QY of ZnSe NCs is followed by the shifting of the A_1 peak toward valence band. Finally peak merges the valence band and the PL intensity decreases due to the photodegradation of the solution of the ZnSe NCs as a result of long-time irradiation with the powerful light source.

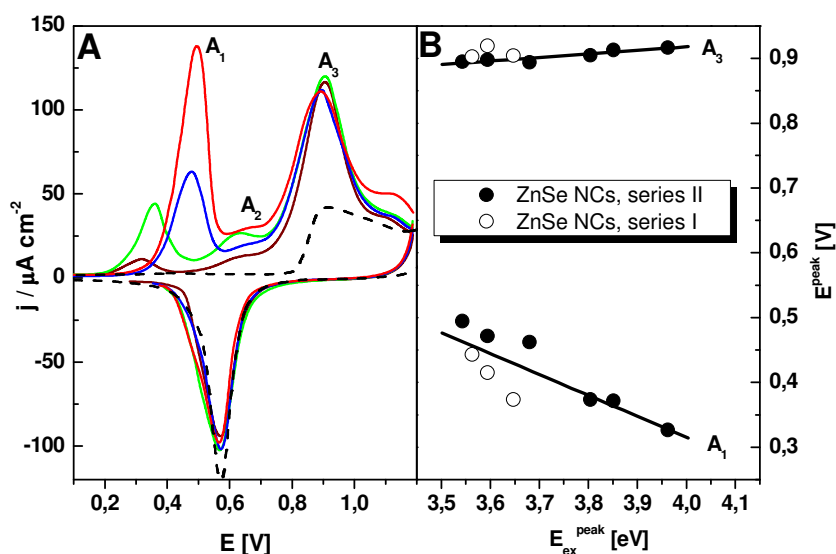


Figure 4.3.1 Four examples of typical anodic voltammograms of the ZnSe NCs (A) and dependence of the peak positions A_1 and A_3 on the photon energy corresponding to the first excitonic maxima for the full series of the TGA-capped ZnSe NC size-selected fractions (B). ZnSe NCs preadsorbed on Au electrodes in acetic buffer solution (pH 6). The black dashed line presents the voltammogram of the bare Au electrode. The potential sweep direction was $-0.15 > 1.19 > +0.375$ V. The potential sweep rate was 20 mV s^{-1} .

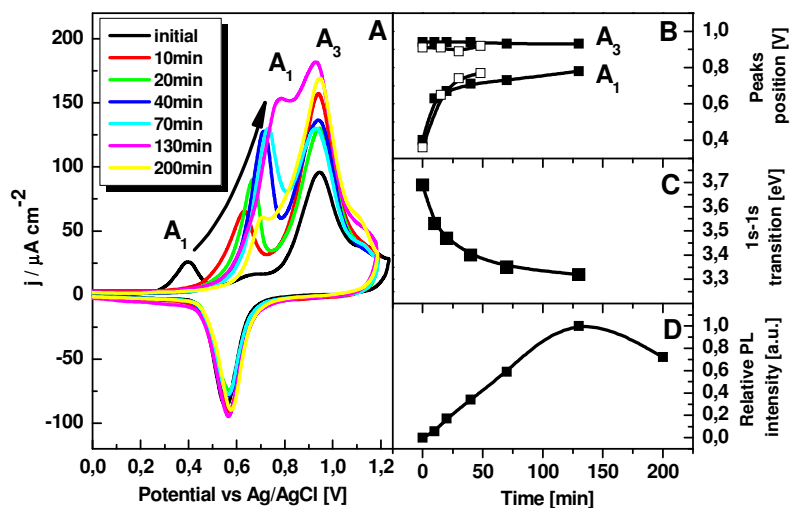


Figure 4.3.2 Evolution of the cyclic voltammograms of ZnSe NCs preadsorbed on the Au electrodes upon the time of the photochemical treatment (A), evolution of the relative positions of first (A_1) and third (A_3) anodic electrochemical peaks (B), Position of the 1s-1s electronic transition (C), and the PL intensity (D) during the photochemical treatment of the ZnSe NCs. Open and full squares present the evolution of the ZnSe NCs in the solution containing TGA and Zn^{2+} ions and TGA only, respectively. The potential sweep direction was $-0.18 > 1.05 > 1.33 > -0.18$ V. The potential sweep rate was 20 mV s^{-1} .

According to our previous findings for analogously prepared CdTe NCs (cf. ref. [9] and **Chapter 4.2**), the first anodic peak (A_1) can be associated with the oxidation of the intra-band-gap surface states. Moreover, the position of this peak in the case of the CdTe NCs was shown to be size dependent, i.e. it was moving to lower energies (higher electrochemical potentials) with the increase of the NCs' size [9]. The maximum size dependent shift of the A_1 peak was about 120 mV for the first excitonic transition range of the NCs from 550 nm to ca. 635nm. In the case of the ZnSe NCs studied, the size-span is more limited compared to the CdTe series. However, ZnSe NCs exhibiting a first excitonic transition between 312 and 350 nm are available and the maximum size dependent shift of the potential A_1 is about 170 mV. The shift depends linearly on the optical band gap of the nanoparticles (**Figure 4.3.1B**) which is consistent with the findings for the CdTe NCs.

Under irradiation by white light the shift of the first excitonic maximum from 336 nm to 365 nm (about 340 meV) is accompanied by a shift of the A_1 peak of as much as 400 mV. The observed behavior can be explained as a simultaneous influence of both increasing of NCs' size and changing of the surface composition during the assumed shell formation. Thus, the photochemical growing of the protecting shell improves the PL quantum yields of the ZnSe NCs and is followed by the moving of the surface states towards the valence band.

The irradiation of the solution of the ZnSe NCs in a mixture with TGA only demonstrates neither PL increasing nor a shift in the absorption spectra while the CV curves show the typical shift of the first peak (A_1) towards the positive direction (see **Figure 4.3.2**, squares). In fact, the absence of the zinc ions in the solution makes impossible the photo-assisted formation of the ZnS shell which is necessary for the PL improvement [17]. At the same time photoexcitation of the ZnSe NCs may lead to the dissolution of the relatively unstable surface selenium atoms or to their replacement by the sulfur being present as a result of the TGA degradation. The presence of an excess of TGA in this case provides an additional stabilization to the NCs. Both dissolution and replacement of the Se atoms should result in an anodic shift of the oxidation peak corresponding to the surface Se atoms (peak A_1) which corresponds to the experimental finding (**Figure 4.3.2A**, open squares). Neither a PL improvement nor changes in the electrochemical behavior were observed when the phototreatment was done in the absence of both, Zn ions and TGA in solution. A degradation of the colloidal solution took place during only a few minutes under these conditions making impossible further investigations.

This supports our assumption that TGA plays a role of both a sulfur source and stabilizing agent for the NCs under phototreatment.

The small second peak (A_2) may be associated with oxidation of TGA molecules. The position of this peak matches the oxidation potential of the TGA solution [9] as found recently. A small amount of TGA may appear in the solution due to the incomplete washing as well as due to the existence of an equilibrium between the TGA on the surface of the NCs and in the solution [20].

The third anodic peak (A_3) can be assigned to the direct oxidation of the core of the ZnSe NCs. The slight shift of this peak (about 10 mV) towards lower potentials can be the result of a band gap decrease of the ZnSe NCs during the shell formation. The photochemical treatment gives rise a competition of two processes: i) the increase of the band gap due to the incorporation of sulfur into the NCs, and ii) the decrease of the band gap as a result of the nanocrystal growth (size-confinement effect). The overall result of this competition is a decrease of the band gap [17]. It is noted that the decrease of the optical band gap during illumination reached about 0.35 eV which is considerably higher than the electrochemically observed shift of the position of the A_3 peak. This founding can be explained by the more effective shift of the conductive band in comparison with valence one.

4.4. Conclusions

Electrochemical studies of thiol-capped CdTe NCs in an aqueous buffer solution (pH 9.2) have demonstrated several distinct oxidation and reduction peaks in the voltammograms, with the peak positions being size dependent. While the size-dependence of the reduction (C_1) and oxidation (A_2) potentials can be attributed to moving the energetic band positions owing to the quantum size effect, an extraordinary behavior was found for the oxidation peak A_1 observed at less positive potentials. This peak moves to more negative potentials as the NCs size decreases. This peak is assigned to the oxidation of Te-related surface traps. The results obtained indicate that the energy levels of these traps are shifted to lower energies as the NCs size increases, allowing thus to explain the higher photostability of the larger NCs.

The thiol-capped aqueous ZnSe NCs demonstrate the same type of behavior. The A_1 anodic peak is responsible for the general quality of the nanocrystals and correlate very

well with the QY of the ZnSe NCs. The evolution of the position of anodic peak A₁ in the voltammetric curves of the ZnSe NCs is a function of the improving NCs quality (i.e. the formation of a sulfur-enriched surface shell) during the photochemical treatment. Thus, the cyclic voltammetry confirms the previously proposed mechanism of the ZnSe NC phototreatment.

Thus the current research has demonstrated that the CV method is very sensitive to the nanocrystal surface state, providing complimentary information for better understanding of special size-dependent optical properties of semiconductor NCs.

4.5. References

1. Haram, S.K., B.M. Quinn and A.J. Bard, *Electrochemistry of CdS nanoparticles: A correlation between optical and electrochemical band gaps*. J. Am. Chem. Soc., 2001. **123**(36): p. 8860-8861.
2. Kucur, E., J. Riegler, G.A. Urban and T. Nann, *Determination of quantum confinement in CdSe nanocrystals by cyclic voltammetry*. J. Chem. Phys., 2003. **119**(4): p. 2333-2337.
3. Ogawa, S., K. Hu, F.-R.F. Fan and A.J. Bard, *Photoelectrochemistry of films of quantum size lead sulfide particles incorporated in self-assembled monolayers on gold*. J. Phys. Chem. B, 1997. **101**(29): p. 5707-5711.
4. Chen, S.W., L.A. Truax and J.M. Sommers, *Alkanethiolate-protected PbS nanoclusters: Synthesis, spectroscopic and electrochemical studies*. Chem. Mat., 2000. **12**(12): p. 3864-3870.
5. Ding, Z., B.M. Quinn, S.K. Haram, L.E. Pell, B.A. Korgel and A.J. Bard, *Electrochemistry and electrogenerated chemiluminescence from silicon nanocrystal quantum dots*. Science, 2002. **296**(5571): p. 1293-1297.
6. Bae, Y., N. Myung and A.J. Bard, *Electrochemistry and Electrogenerated Chemiluminescence of CdTe Nanoparticles*. Nano Letters, 2004. **4**(6): p. 1153-1161.
7. Gaponik, N., D.V. Talapin, A.L. Rogach, K. Hoppe, E.V. Shevchenko, A. Kornowski, A. Eychmüller and H. Weller, *Thiol-capping of CdTe nanocrystals: An alternative to organometallic synthetic routes*. J. Phys. Chem. B, 2002. **106**(29): p. 7177-7185.
8. Talapin, D.V., A.L. Rogach, E.V. Shevchenko, A. Kornowski, M. Haase and H. Weller, *Dynamic distribution of growth rates within the ensembles of colloidal II-VI and III-V semiconductor nanocrystals as a factor governing their photoluminescence efficiency*. J. Am. Chem. Soc., 2002. **124**(20): p. 5782-5790.
9. Poznyak, S.K., N.P. Osipovich, A. Shavel, D.V. Talapin, M. Gao, A. Eychmüller and N. Gaponik, *Size-Dependent Electrochemical Behavior of Thiol-Capped CdTe*

- Nanocrystals in Aqueous Solution*. Journal of Physical Chemistry B, 2005. **109**(3): p. 1094-1100.
10. Yu, W.W., L. Qu, W. Guo and X. Peng, *Experimental Determination of the Extinction Coefficient of CdTe, CdSe, and CdS Nanocrystals*. Chem. Mat., 2003. **15**(14): p. 2854-2860.
 11. Eychmüller, A., *Structure and Photophysics of Semiconductor Nanocrystals*. J. Phys. Chem. B, 2000. **104**(28): p. 6514-6528.
 12. Weller, H. and A. Eychmüller, *Photochemistry and photoelectrochemistry of quantized matter: properties of semiconductor nanoparticles in solution and thin-film electrodes*. Advances in Photochemistry, 1995. **20**: p. 165-216.
 13. Borchert, H., D.V. Talapin, N. Gaponik, C. McGinley, S. Adam, A. Lobo, T. Moeller and H. Weller, *Relations between the Photoluminescence Efficiency of CdTe Nanocrystals and Their Surface Properties Revealed by Synchrotron XPS*. J. Phys. Chem. B, 2003. **107**(36): p. 9662-9668.
 14. Franzl, T., A. Shavel, N. Gaponik, A.L. Rogach, A. Eychmüller and J. Feldmann, *Manuscript in preparation*.
 15. Jones, M., J. Nedeljkovic, R.J. Ellingson, A.J. Nozik and G. Rumbles, *Photoenhancement of Luminescence in Colloidal CdSe Quantum Dot Solutions*. J. Phys. Chem. B, 2003. **107**(41): p. 11346-11352.
 16. Bao, H., Y. Gong, Z. Li and M. Gao, *Enhancement Effect of Illumination on the Photoluminescence of Water-Soluble CdTe Nanocrystals: Toward Highly Fluorescent CdTe/CdS Core-Shell Structure*. Chemistry of Materials, 2004. **16**(20): p. 3853-3859.
 17. Shavel, A., N. Gaponik and A. Eychmüller, *Efficient UV-Blue Photoluminescing Thiol-Stabilized Water-Soluble Alloyed ZnSe(S) Nanocrystals*. Journal of Physical Chemistry B, 2004. **108**(19): p. 5905-5908.
 18. Talapin, D.V., N. Gaponik, H. Borchert, A.L. Rogach, M. Haase and H. Weller, *Etching of Colloidal InP Nanocrystals with Fluorides: Photochemical Nature of the Process Resulting in High Photoluminescence Efficiency*. J. Phys. Chem. B, 2002. **106**(49): p. 12659-12663.
 19. van Dijken, A., A.H. Janssen, M.H.P. Smitsmans, D. Vanmaekelbergh and A. Meijerink, *Size-selective photoetching of nanocrystalline semiconductor particles*. Chem. Mat., 1998. **10**(11): p. 3513-3522.
 20. Döllefeld, H., K. Hoppe, J. Kolny, K. Schilling, H. Weller and A. Eychmüller, *Investigations on the stability of thiol stabilized semiconductor nanoparticles*. Phys. Chem. Chem. Phys., 2002. **4**(19): p. 4747-4753.

Chapter 5

The Assembling of Semiconductor Nanocrystals

The arranging of the semiconductor nanoparticles in superstructures is shown in this chapter. Coupling mechanisms utilized for this purpose include electrostatic and covalent interactions. The layer-by-layer assembly and covalent attachment of nanoparticles to the functionalized surface (aminated) are employed. The fast Förster energy transfer in nanocrystal superstructures is observed.

5.1. Introduction

Ordered assemblies of nanocrystalline materials receive increasing interest in recent years. Nanoparticles (often referred to as artificial atoms) are used to build up artificial molecules and solids [1]. These arrays and superlattices offer new perspectives for the application of nanoparticles for example in optoelectronic devices. Various approaches toward assembling nanocrystals are known. Three dimensional superlattices of semiconductor nanoparticles have been built up via self organization [2] and crystallization [3-5]. Another main route towards ordered structures of nanocrystals is covalent binding with and without special linker molecules. These efforts have a direct correlation to the investigations in the fields of covalent coupling of nanoparticles to biomolecules and surface functionalization of nanocrystals [6].

Worth to mention that, still only little is known about the properties of solids evolving from these assembled structures. Some work has been published by Heath et al. on collective properties of interacting metal nanoparticles [7, 8]. Depending on the interparticle distance, those solids reflect dipole-dipole interaction followed by pure electronic coupling when the particles come into closest contact. Later, Remacle and Levine studied theoretically electron transfer processes in arrays of quantum dots [9]. A shift of the first electronic absorption of small cadmium sulfide clusters to lower energies compared to their solutions was first published by Vossmeier et al. [10] for closely packed layers of cadmium sulfide nanocrystals. The layers were built up from solutions of the

clusters by a spin-coating technique and were examined by absorption spectroscopy. Besides some further studies on Förster energy transfer in semiconductor quantum solids consisting of particles of different sizes [11, 12] little is known about the interaction between semiconductor nanoparticles.

This chapter is devoted to the layer-by-layer assembling of semiconductor nanocrystals with and without interfacial polyelectrolytes as well as direct covalent linking of nanocrystals with aminated surface.

5.2. Layer-by-layer assembly of semiconductor nanocrystals

Uniform and multicomponent thin films consisting of functional molecules and/or nanocrystals may be formed by applying the so-called layer-by-layer (LbL) assembly technique. **Figure 5.2.1** shows schematically the LbL procedure which was originally introduced for the assembly of polymer electrolytes [13] and which was recently adapted to the deposition of charged nanocrystals both on flat [14, 15] and on curved surfaces [16, 17]. As seen from the figure the formation of monolayers of deposited material is based on the electrostatic interaction between the nanocrystals and the surface. Alternation of the sign of the charges of the species to be deposited allows to grow quite thick multilayers while the introduction of new components in one of the layers yields the opportunity of virtually non-limited but controllable variations of LbL-multistructure compositions [18, 19]. The application of the method described for the modification of artificial opals allowed to obtain intrinsically light emitting photonic crystals which were successfully used for investigations on photonic confinement phenomena [20, 21].

The following standard cyclic procedure is normally used for the preparation of layered structures of negatively charged nanocrystals: (i) dipping of the substrate into a solution of polyelectrolyte (PE) (e.g. 5 mg/ml in 0.5 M NaCl) for 10 min (poly(ethyleneimine) - PEI was used for the first layer and poly(diallyldimethylammonium chloride) - PDDA for the 2nd and further layers); (ii) rinsing with water for 1 min; (iii) dipping into aqueous dispersions of the nanocrystals for 20 min; (iv) rinsing with water again for 1 min (cf. **Figure 5.2.1**). On each surface exposed this procedure results in a 'bilayer' consisting of a polymer/NC composite. **Figure 5.2.2** shows spectra of an example of a polymer/CdTe "bilayer".

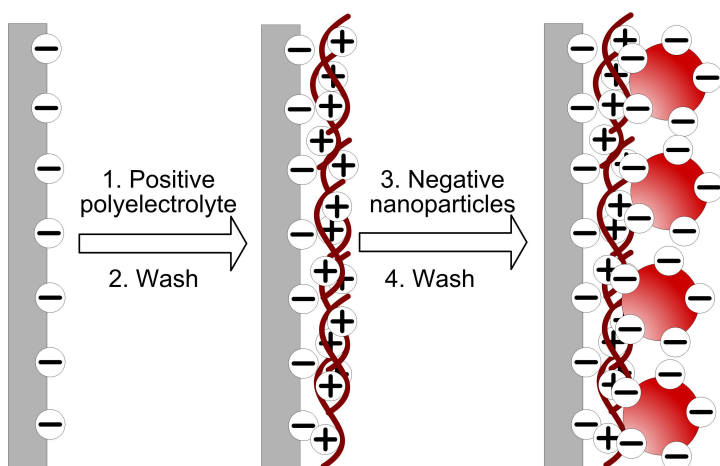


Figure 5.2.1. Schematic representation of the LbL assembly involving polyelectrolyte molecules and oppositely charged nanoparticles. The procedures 1-4 can be repeated to assemble more PE/nanoparticles bilayers.

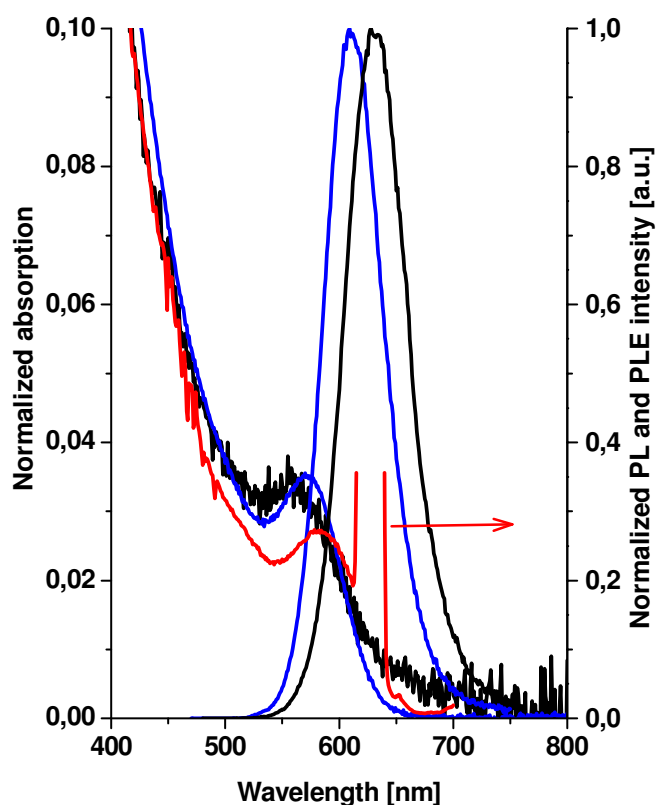


Figure 5.2.2 PL and absorption spectra of a polymer/CdTe “bilayer” (black lines) in comparison with a solution of CdTe NCs (blue lines) together with a PLE spectrum of a layered structure (red line).

The cycle can be repeated as many times as necessary to obtain a multilayer film of desired thickness. The thickness of the LbL film depends linearly on the number of “bilayers”. Moreover, a linear dependence of the absorption in the region of the first absorption maximum on the number of bilayers was observed [22, 23]. **Figure 5.2.3** presents an example of a PDDA-ZnSe layered structure.

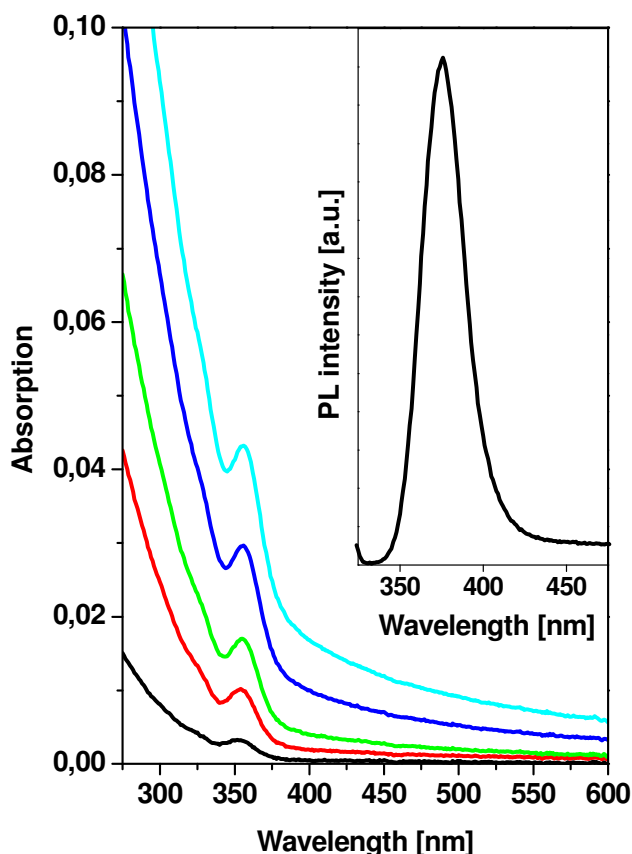


Figure 5.2.3 Example of the evolution of film absorption during the LbL assembly of PDDA/ZnSe film. The inset shows the PL of a structure constructed from 5 “bilayers”.

Worth to mention that in some cases the LbL-assembly appeared to be non-efficient. When using freshly prepared colloidal solutions of nanocrystals occasionally incomplete layer formation was observed. Low-molecular weight by-products of the synthesis as well as nanocrystal precursors can be responsible for this because they may be attracted by the polyelectrolyte sub-layers with higher efficiency than the nanocrystals themselves. Aging of nanocrystal colloidal solutions might lead to the reduction of the activity of those poisoning species due to their association with particle shells, aggregation

and precipitation, etc. To avoid this problem, i.e. to make nanocrystal colloidal solutions useful for LbL without aging them, an electrophoretic activation of the colloidal solutions of thiol-capped nanocrystals has been developed. The nanocrystal solution to be activated is placed in a 2-electrode electrochemical cell and 1.5-2 V potential is applied to the cell. The commonly used electrodes are flat stainless steel or ITO-glass plates of 1 cm² working surface and 5 mm gap in-between. The current density drops from ca. 100-120 μAcm^{-2} in the very beginning down to 5-10 μAcm^{-2} after one hour of this treatment. The above mentioned by-products and possibly other charged species are electrophoretically assembled or reacted at the electrodes and thus the cleaned activated solutions can be used for the LbL-deposition as usual after removal from the cell.

5.3. Electrostatic assembly of semiconductor nanocrystals

However, in these LbL systems the distance between donors and acceptors can not be shorter than the thickness of the polyelectrolyte monolayer. In order to avoid this limitation which may be unfavorable for efficient interparticle interactions (see below) a new kind of LbL structure has been generated [24]. The building blocks of the system were water soluble CdTe NCs with opposite surface charges (the charge of the CdTe NCs depends on the kind of stabilizer [25]) which were LbL assembled without polyelectrolytes between the particle layers. However, we encountered intrinsic limitations like an easy removal of the already deposited layers and the unbeneficial balance of charges during the film growth [26]. These limitations might have less influence in the case of the assembly of only one NC bilayer, while at the same time the inter-layer distance in this case would be further reduced leading to more efficient interactions. Bilayers of oppositely charged NCs can indeed be formed by a direct assembly of water-soluble CdTe NCs capped with amino- and carboxyl-group terminated short chain thiols (see inset **figure 5.3.1**).

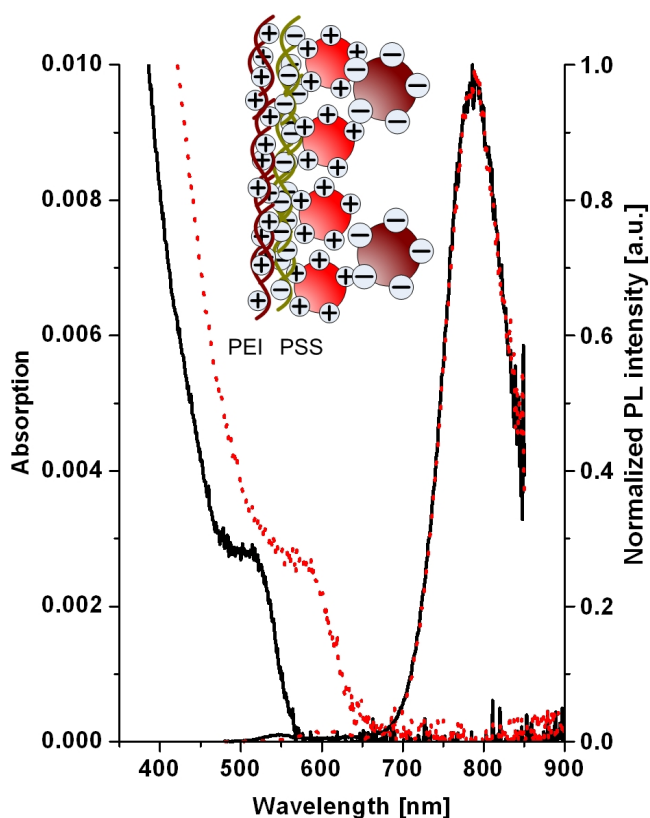


Figure 5.3.1 Examples of two close-packed structures utilizing MA-capped CdTe NCs (positively charged) of approximately 2 nm (black solid lines) and 4 nm (red dotted lines) as the bottom layer. MPA-capped nanocrystals (negatively charged) of 6-8 nm in diameter were used as the top layer in both structures shown. Whereas the absorption spectra of the structures show only the features corresponding to the bottom layer, the photoluminescence of the top layer (centered at ca. 780 nm) dominates in both structures.

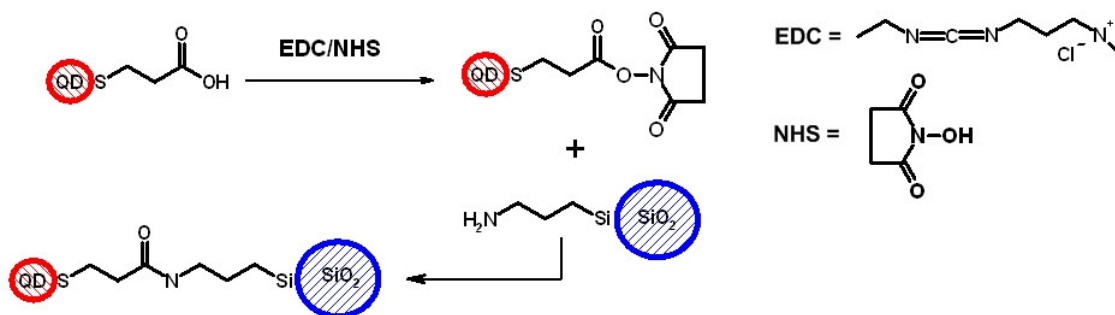
The preparation of this layered structure was performed in two steps. In the first step a polyelectrolyte sub-layer was formed by this standard procedure: (i) dipping of the substrate into PEI solution for 20 min; (ii) rinsing with water for 1 min; and (iii) dipping into PSS solution (iv) and final rinsing in water. The first PEI-layer was used to improve the quality of the layered structure in terms of uniform surface coverage [15]. In a second step, close-packed nanoparticle structures were assembled on the surface of the polyelectrolyte bilayer as follows. The substrate with the PE bilayer was (i) dipped into aqueous dispersions of the 2-mercaptoethylamine (MA) -capped nanocrystals for 20 min, (ii) rinsed with water for 1 min and finally (iii) dipped into an aqueous dispersion of the mercaptopropionic acid (MPA) or thioglycolic acid (TGA) capped nanocrystals again for 20 min. Such a procedure results in a layered structure consisting of a support/polymer/NCs-NCs composite. Typical absorption and photoluminescence spectra

of the system are shown in **figure 5.3.1**. The composite of the nanoparticles exhibits absorption only from the bottom layer of NCs (the absorption from the top NC layer is below the limit of the sensibility of our spectrophotometer). At the same time emission associated mainly with the top layer is observed which is taken as a first hint to efficient energy transfer (see below).

5.4. Covalent coupling of SC NCs

5.4.1. Covalent linking of CdTe NCs to flat surfaces

Besides electrostatic coupling of NCs the generation of covalent bonds between selected nanocrystalline entities constitutes a very attractive and vast field. As an example of bridging two different sorts of NCs the linkage of CdTe nanocrystals stabilized by TGA and MA can be shown [27]. The coupling has been carried out directly at the ligands without using an additional bridging molecule only with the aid of carbodiimide acting as a mediator for the reaction. The reaction between nanocrystal and silica bead is described in **Scheme 5.1**.



Scheme 5.1 of carbodiimide assisted amide bond formation.

While the covalent coupling of SC NCs is still in an infant status the acting chemistry may well be applied to the coupling of NCs to pre-treated surfaces. Accordingly, the appropriate fractions of CdTe NCs for the conjugation with various substrates like glass, silica or silicon with different surfaces shapes have been used [28]. A general illustration of the binding of the acid-stabilized NCs to aminated surfaces with the aid of carbodiimide as a mediator in the formation of the amide bond is shown in **Figure 5.4.1 (inset)**.

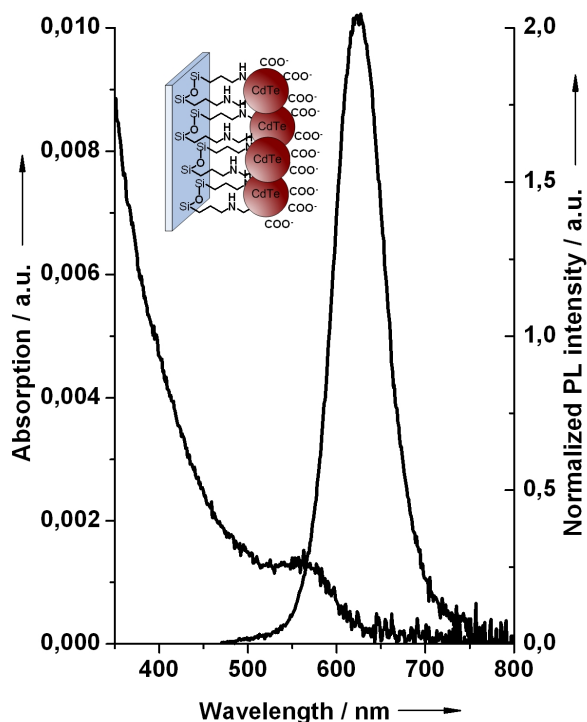


Figure 5.4.1. Absorption and luminescence spectra of CdTe NCs conjugated with a flat glass substrate. Excitation wavelength is 450 nm. The inset shows a schematic representation of the structure.

The silicon wafers, the quartz and the glass slides were pre-treated before conjugation in the following manner: the glass (Menzel-Glaser, Germany) and the quartz slides (Hellma Optic GmbH, Germany) as well as the silicon wafers (with a 400nm SiO₂ layer) were cleaned by sonication first in 0.1 M NaOH solution, then in methanol, and finally in pure water for 15 min each. To form an amino-terminated layer on their surface, the substrates were immersed in a 3 vol% solution of 3-(aminopropyl)-triethoxysilane (Fluka) in 95 % methanol (named below “3APTES solution”) under sonication for 15 min followed by thorough rinsing with methanol. Drying was performed by a thermal treatment at 120°C for half an hour in an oven.

The details of the linking of the CdTe NCs to flat substrates are as follows. An appropriate amount (0.1-0.5 mL) of aqueous solutions of CdTe NCs was mixed with 0.5 mL of MES buffer (2-(N-morpholino)ethanesulfonic acid 0,1 mM, Sigma) and 8 mL of Milli-Q water. The preliminarily cleaned aminated substrate was dipped into this solution. Subsequently, 0.5 mL of a solution of 1-Ethyl-3-[3-(dimethylamino)propyl]carbodiimide hydrochloride (Sigma) 0.025 M and N-hydroxysuccinimide (Aldrich) 0.025M (named

below “EDC/NHS solution”) was added under vigorous stirring which was continued for another 10 min. After conjugation, the slides were washed three times in Milli-Q water and rinsed thoroughly in acetone and toluene and dried under vacuum conditions. **Figure 5.4.1** shows optical spectra of the modified slides. The PL properties of the films prepared were found to be more stable in time as compared to analogously LbL-assembled monolayer films. Although the surface coverage estimated from the optical densities of the modified glass slides is roughly 100% (i.e. one monolayer), the formation of island-like multilayers could not be excluded [14].

5.4.2 Covalent linking of CdTe NCs to silica and glass beads.

The method described is not limited to flat substrates but is of more generality as shown by successful attempts to coat glass spheres of micron size by CdTe NCs [28]: A dispersion (5 wt % in 10% solution of ethanol in water) of borosilicate glass microspheres ($2 \pm 0.5 \mu\text{m}$, Duke Sci. Co., USA) was treated with 0.1 M NaOH for 15 minutes under sonication and washed three times in methanol by centrifugation. The treated microspheres were immersed in the 3APTES solution under sonication for 15 min and washed thoroughly with methanol by centrifugation. The final methanol dispersion was heated up to the boiling point for 1 hour. After that, the microspheres were separated from the methanol, redispersed in 0.5 ml of MES buffer and subsequently 0.1 ml of an aqueous solution of CdTe NCs and 0.5 ml of the EDC/NHS solution was added to the dispersion under vigorous shaking which was continued for another 10 min. The conjugation was terminated by the addition of an excess amount of 0.1 M glycine solution. The spheres were washed three times with Milli-Q water and stored in an appropriate solvent like water or DMF. In **Figure 5.4.2** displayed a fluorescence microscopy image of the glass spheres conjugated with the CdTe NCs. The persistency of the luminescence of the NCs is nicely seen. This luminescence is not altered for at least 3 months. The inset shows a SEM image of one particle of the same sample providing an impression of the coverage of the spheres with nanoparticles.

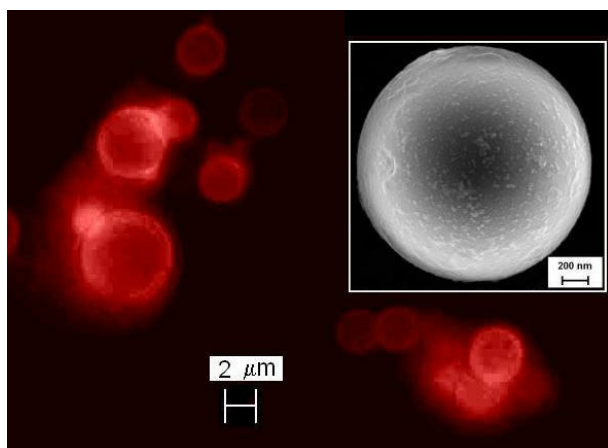


Figure 5.4.2. Fluorescence microscopy image of glass spheres conjugated with CdTe NCs. The inset shows a SEM image of one of those particles.

Figure 5.4.3 shows some optical properties of conjugates of CdTe NCs with silica beads. For the generation of these conjugates the CdTe NCs of two different sizes, namely 3 – 4 nm in diameter and 6 – 8 nm in diameter, respectively have been used. The absorption spectra of the conjugates possess well pronounced first electronic transitions and strong emissions. The positions of the absorption and luminescence maxima relate well to the sizes of the NCs in accord with the size quantization effect being operative in semiconductor nanoparticles of such sizes. It is seen that the emission of the larger particles reaches into the near-IR spectral region and that absorption spectra of monolayers of NCs have been gained in this study.

For the preparation of the silica beads we used a well known literature method [29]. Tetraethyl orthosilicate (1,5ml) was added to a solution of ammonium hydroxide (2 ml) in ethanol (50 ml) in order to prepare particles at around 100 nm in diameter. The reaction mixture was stirred for 24 h to yield silica nanoparticles. The amino-functionalization of the particles' surfaces was accomplished by the addition of 25 μl of 3APTES to the reaction mixture and continuing stirring for additional 24 hours. After this, the mixture was heated up to the boiling point for 1 hour. The cooled mixture was washed three times with ethanol by centrifugation to give a stable dispersion of amino-functionalized silica spheres. Before conjugation, the silica particles were transferred into DMF by consecutive centrifugation and adding of fresh portions of DMF.

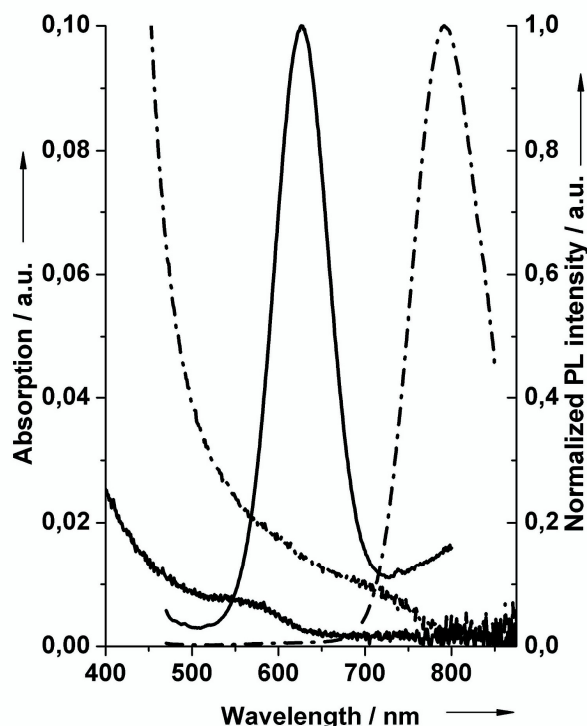


Figure 5.4.3. Absorption and luminescence spectra of silica particles conjugated with CdTe NCs of two different sizes.

Conjugates of CdTe NCs with aminated silica beads have been prepared as follows. 0.05 ml of aqueous solutions of the CdTe NCs and 0.25 ml of the dispersion of the aminated silica particles in DMF were added to 0.70 ml of DMF. Then, 0.5 mL of the EDC/NHS solution (in DMF) was added under vigorous shaking. The shaking was continued for another 5-20 min. The conjugation was stopped by centrifugation of the silica particles. The conjugated silica particles were washed 3 times with pure DMF and stored as dispersions in the dark.

5.4.3 Covalent linking of CdTe NCs to the functionalized Latex beads.

The method of carbodiimide-assisted linking may also be used for formation of ester bonds in non aqueous media. In order to demonstrate conjugation through ester bond formation the CdTe NCs with surface OH groups were coupled with latex beads whose surface were modified by $-\text{COOH}$ and $-\text{SO}_2\text{OH}$ groups.

The linking solution contained N,N'-diisopropylcarbodiimide (DIC, 0.1M) and 4-dimethylaminopyridine (DMAP, 0.01M) in methanol. In order to prepare the non-aqueous suspension of latex beads consecutive centrifugation and redispersion in fresh methanol have been used. Finally, a methanol suspension of latex beads with 4.8×10^{-6} mol of the –COOH group per mL was obtained. The methanol soluble CdTe NCs (1.6×10^{-6} M, 3.6 nm in diameter; see **Appendix 2.3** for details) were used for the coupling reaction (see **Appendix 2.2** for details of the CdTe NCs synthesis).

Conjugates of CdTe NCs with functionalized latex beads have been prepared as follows. 100 μ L of the latex beads dispersion were added to 1 mL of methanol solution of CdTe NCs and afterwards 10 μ L of linker solution were added under extensive stirring. The mixture was stirred overnight and washed through consecutive centrifugation and adding of fresh methanol. Finally a stable suspension of CdTe–modified latex beads in methanol was obtained. **Figure 5.4.5** shows the SEM images and optical spectra of the conjugated latex beads.

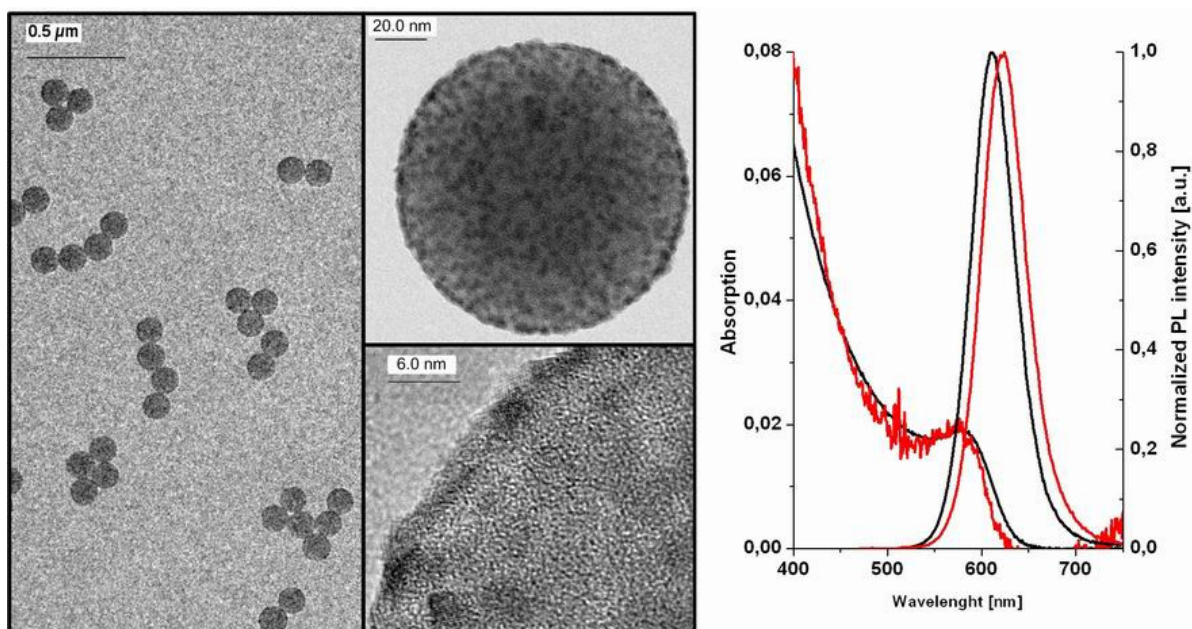


Figure 5.4.5. SEM images of latex beads conjugated with CdTe NCs (left) and optical spectra of the conjugates (red lines) in comparison with methanol solution of CdTe NCs (black lines).

The formation of ester bonds between methanol and the latex beads can not be excluded. Actually, there is a competition between the conjugation of latex beads with OH-groups of thioglycerol-capped CdTe NCs and with OH-groups of the solvent (methanol). The conjugation of methanol molecules does the beads' surface still accessible for the CdTe NCs since each latex bead has one carboxy-group per 0.92 nm^2 which is much smaller than cross section of the CdTe nanoparticles (for 3.6 nm particles). Thus, only few carboxy-groups have the possibility to be conjugated with CdTe nanoparticles. Other carboxy-groups are still free for conjugation with molecules of methanol (solvent). Both i) steric effects and ii) kinetic competition of molecules of stabilizer and solvent lead to the high amount of linked methanol molecules. Nevertheless, conjugation of latex beads with CdTe NCs is sufficiently effective to produce nicely covered surfaces.

5.5. Rapid Förster energy transfer

To investigate the Förster energy transfer from smaller (green emitting, PL maximum at approx. 555 nm) to bigger NCs (red emitting, 650 nm) in LbL layered assemblies two different structures both consisting of 10 polyelectrolyte/NCs bilayers have been prepared. The first structure consists of 5 bilayers of the same NCs size followed by 5 bilayers of the other NCs size on top while the second structure consists of alternating bilayers of NCs of both sizes, as is schematically shown in **Figure 5.5.1**. The disappearance of the green PL band and the simultaneous relative amplification of the red emission is inherent for both structures and is a consequence of the Förster energy transfer (FRET), i.e. energy transfer takes place between donor and acceptor NCs, when the interparticle distance is smaller than the so-called Förster radius. At the same time the efficiency of the FRET appears to be relatively higher in the case of alternating layers. Indeed, the mean distance between the NCs of different sizes is smaller in the case of the alternating structure. In the other case only the closest red and green NC layers participate in the energy transfer efficiently, while others are too far apart. Furthermore, the applicability of the LbL method for the creation of even more complex structures has been demonstrated. This structure consisted of alternating bilayers of NCs of three different sizes with a gradual decrease of the electronic band gap and it shows PL originating from the biggest NCs only, while the features corresponding to all NCs' sizes appear in the absorption spectrum (**Figure 5.5.2**)

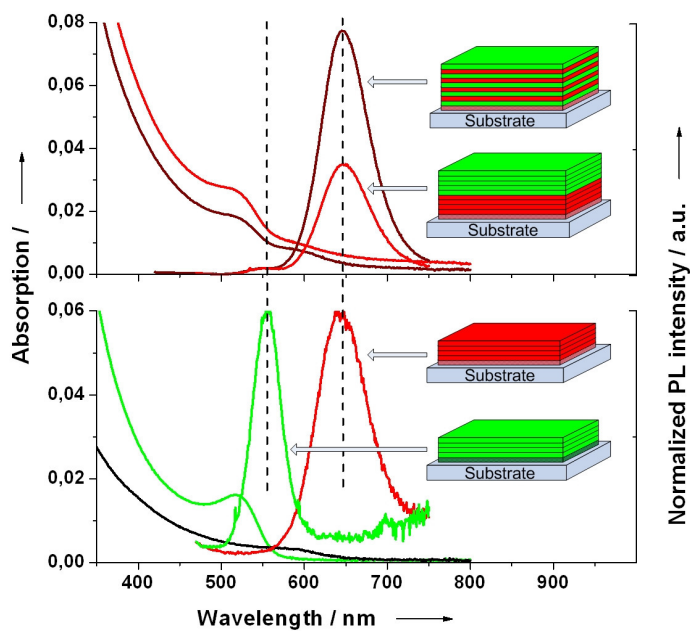


Figure 5.5.1. Absorption and PL spectra of the LbL formed assemblies sketched on the right hand side. Green and red layers correspond to the emission colour of the particles constituting the assembled PE/NCs bilayers.

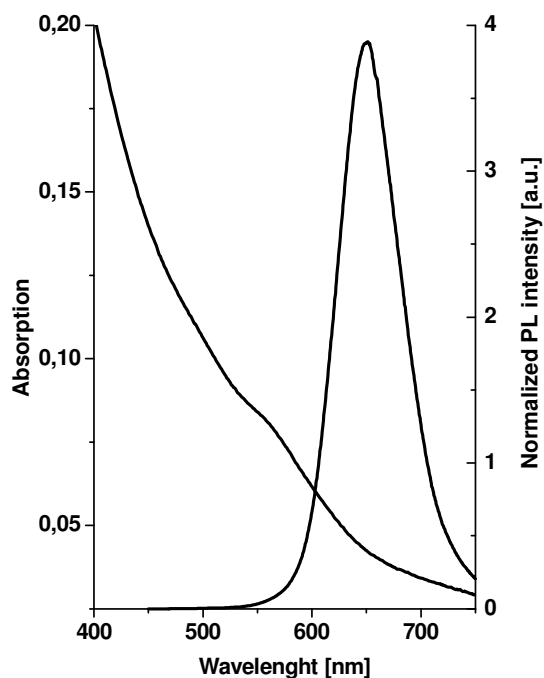


Figure 5.5.2. Absorption and PL spectra of the LbL structure consisted of alternating bilayers of NCs of three different sizes.

The FRET efficiency of thin alternating films of NCs of 2.4 and 3.5 nm in size with PDDA as opposite polyelectrolyte was estimated to be as high as 50% with an average interlayer energy transfer rate of $(254 \text{ ps})^{-1}$ reaching the value of $(134 \text{ ps})^{-1}$ for certain subspecies in the inhomogeneous distribution of the donor NCs having larger spectral overlap with the acceptor NCs [30].

5.5.1 Förster energy transfer in the close-packed structures.

As described above LbL-composite can be prepared with NCs as building blocks only, i.e. without polyelectrolytes in between the NC layers. These structures have been made in order to study Förster energy transfer in nanocrystal solids, assuming that the FRET will be facilitated by a smaller mean interlayer distance. The bilayer structure is supposed to be composed of MA-capped CdTe NCs (donors) in the bottom layer and TGA-capped CdTe NCs (acceptors) in the top layer (**Figure 5.3.1**). For comparison, two monolayer samples comprising only donors (MA-capped CdTe NCs) or only acceptors (TGA-capped CdTe NCs) are also deposited on the polymer underlayer. For both NC sizes the electronic transitions can be distinguished in the absorption spectrum of the bilayer sample, although the contribution of the acceptor NCs is reduced in comparison to the monolayer sample. This is not surprising because the bottom layer of the donor NCs is deposited on a polymer underlayer in both cases, favoring the attachment of the NCs, while the top layer of acceptor NCs in the bilayer sample is deposited onto a pre-formed donor NC layer, which is apparently limited in its ability to attract and accommodate oppositely charged NCs in comparison to a polymer underlayer. This is indicated schematically by an incomplete layer of acceptor NCs in the inset of **Figure 5.3.1**. The use of electric-field directed layer-by-layer assembly (EFDLA)[31] which relies on the additional attraction of NCs by applying an electric field to the substrate may allow to overcome this problem. The absorption spectrum of the bilayer sample can be reproduced by a linear superposition of $1.0\times$ the donor and $0.33\times$ the acceptor absorption spectra. PL spectra show that almost all of the emission from the bilayer sample originates from the acceptor NCs, while the contribution from the donor NCs is strongly diminished. From the quenching of the donor and the enhancement of the acceptor NC PL in the bilayer sample, the efficiency of energy transfer in the bilayer structure is estimated to be $\sim 80\%$.

In order to figure out the energy transfer rate, the streak camera data binned by wavelengths rather than time was analyzed. **Figure 5.5.3** compares the PL decay of the

donor NCs in the bilayer sample with the PL decay of the donor NCs in the monolayer sample at the same wavelength.

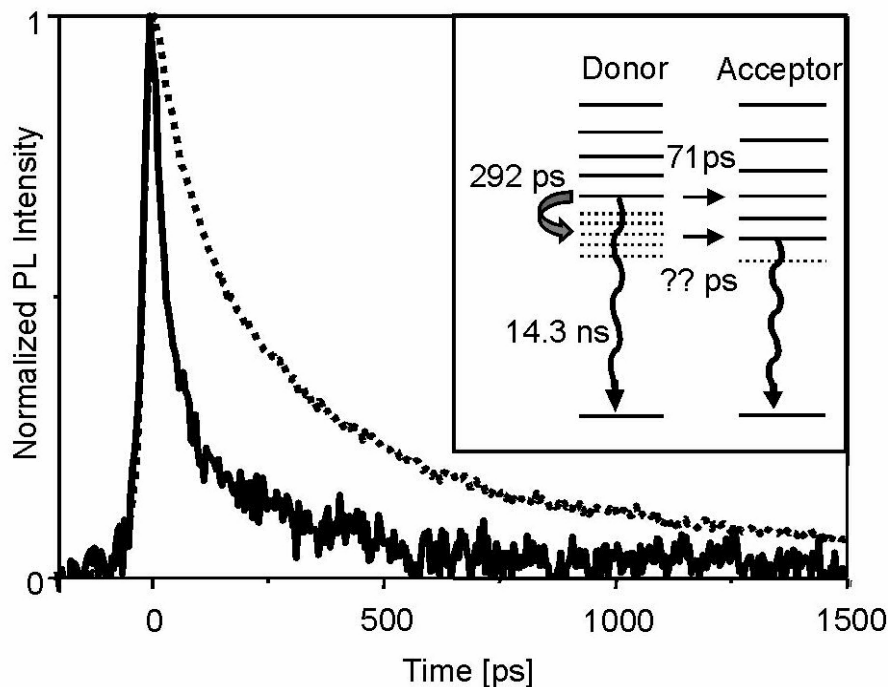


Figure 5.5.3. Fluorescence decays of the donor NCs in the monolayer donor sample (dotted line) and the donor NCs in the bilayer sample (solid line). In both samples the PL is integrated from 500 to 525 nm. The $1/e$ times are 286 ps and 57 ps, respectively. The inset sketches the different decay channels of an exciton in a NC of the donor layer including the corresponding timescales. Thick solid lines represent the first excitonic transition, thin lines represent vibronic progressions and dashed lines indicate trap states from where the excitons decay nonradiatively. Apart from a resonant energy transfer of excitons in donor NC groundstates, a recycling of trapped excitons by resonant transfer to a radiating state in an acceptor NC is also possible on an unknown timescale.

To ensure that the donor decay in the bilayer sample is not affected by PL cross-talk from the acceptor NCs a wavelength-binning region of interest from 500 nm to 525 nm has been chosen. For both samples the PL transients appear as non-exponential decays as it is typical for thiol-capped CdTe NCs [30, 32]. Nevertheless, one can deduce a $1/e$ decay time which decreases from 286 ps for the monolayer sample down to 57 ps for the bilayer sample. A transfer rate of $(71 \text{ ps})^{-1}$ is calculated from these numbers which is 3.5 times higher than the average transfer rate reported before for a CdTe NC bilayer structure with a polymer linker between the layers [30]. If one chooses the wavelength binning region of interest being more shifted to the high energy side of the donor spectrum (from 475 to 500

nm), an energy transfer time as low as 50 ps is derived, which is very close to the energy transfer rates of $(38 \text{ ps})^{-1}$ predicted by Klimov et al. [33]. We attribute this increase of the energy transfer rate to the reduced average distance between the NC layers by eliminating a polymer linker in between. From the decay times provided above we derive an energy transfer efficiency of 80%, consistent with the efficiency we have calculated from time integrated PL spectra.

5.6. Conclusions

The arranging of semiconductor nanoparticles in superstructures has been shown. The layer-by-layer assembly and direct electrostatic assembling of CdTe NCs were used for the preparation of layered structures. A system with alternating layers of nanocrystals with different sizes (i.e. band gaps) has been constructed. Effective FRET is possible in these structures. The layer-by-layer assembly may also be applied for the preparation of a “mono-layered” structure through formation of “sandwich” PE-CdTe layers. Fast Förster energy transfer in such nanocrystal superstructures is observed.

The covalent attachment of nanoparticles to functionalized surfaces (aminated inorganic substrates and carboxy-functionalized latex beads) is used for the formation of monolayered structures. The carbodiimide assisted amide- or ester- bond formation was used in order to link nanocrystals with substrates at mild conditions in various media (water and methanol). The higher stability of such structures in comparison with conventional LbL techniques has been shown. Covalent coupling was applied to various flat (glass, silicon and quartz slides) and spherical (silica, glass and latex beads) substrates. Therefore, using carbodiimide chemistry opens the possibility to form stable layers of semiconducting nanocrystals on surfaces of various functionalized substrates.

5.7. References

1. Collier, C.P., T. Vossmeier and J.R. Heath, *Nanocrystal superlattices*. Annu. Rev. Phys. Chem., 1998. **49**: p. 371-404.
2. Murray, C.B., C.R. Kagan and M.G. Bawendi, *Synthesis and characterization of monodisperse nanocrystals and close-packed nanocrystal assemblies*. Annu. Rev. Mater. Sci., 2000. **30**: p. 545-610.
3. Vossmeier, T., G. Reck, L. Katsikas, E.T.K. Haupt, B. Schulz and H. Weller, A *"double-diamond superlattice"* built up of $Cd_{17}S_4(SCH_2CH_2OH)_{26}$ clusters. Science, 1995. **267**(5203): p. 1476-1479.
4. Talapin, D.V., E.V. Shevchenko, A. Kornowski, N. Gaponik, M. Haase, A.L. Rogach and H. Weller, *A new approach to crystallization of CdSe nanoparticles into ordered three-dimensional superlattices*. Adv. Mater., 2001. **13**(24): p. 1868-1871.
5. Rogach, A.L., D.V. Talapin, E.V. Shevchenko, A. Kornowski, M. Haase and H. Weller, *Organization of matter on different size scales: monodisperse nanocrystals and their superstructures*. Adv. Funct. Mater., 2002. **12**(10): p. 653-664.
6. Michalet, X., F.F. Pinaud, L.A. Bentolila, J.M. Tsay, S. Doose, J.J. Li, G. Sundaresan, A.M. Wu, S.S. Gambhir and S. Weiss, *Quantum dots for live cells, in vivo imaging, and diagnostics*. Science, 2005. **307**(5709): p. 538-544.
7. Collier, C.P., R.J. Saykally, J.J. Shiang, S.E. Henrichs and J.R. Heath, *Reversible tuning of silver quantum dot monolayers through the metal-insulator transition*. Science, 1997. **277**(5334): p. 1978-1981.
8. Markovich, G., C.P. Collier, S.E. Henrichs, F. Remacle, R.D. Levine and J.R. Heath, *Architectonic Quantum Dot Solids*. Accounts Chem. Res., 1999. **32**(5): p. 415-423.
9. Remacle, F. and R.D. Levine, *Superexchange, Localized, and Domain-Localized Charge States for Intramolecular Electron Transfer in Large Molecules and in Arrays of Quantum Dots*. J. Phys. Chem. B, 2001. **105**(11): p. 2153-2162.
10. Vossmeier, T., L. Katsikas, M. Giersig, I.G. Popovic, K. Diesner, A. Chemseddine, A. Eychmüller and H. Weller, *CdS Nanoclusters: Synthesis, Characterization, Size Dependent Oscillator Strength, Temperature Shift of the Excitonic Transition Energy, and Reversible Absorbance Shift*. J. Phys. Chem., 1994. **98**(31): p. 7665-7673.
11. Kagan, C.R., C.B. Murray, M. Nirmal and M.G. Bawendi, *Electronic energy transfer in CdSe quantum dot solids*. Phys. Rev. Lett., 1996. **76**(9): p. 1517-1520.
12. Kagan, C.R., C.B. Murray and M.G. Bawendi, *Long-range resonance transfer of electronic excitations in close-packed CdSe quantum-dot solids*. Phys. Rev. B, 1996. **54**(12): p. 8633-8643.

13. Decher, G., *Fuzzy nanoassemblies: toward layered polymeric multicomposites*. Science, 1997. **277**(5330): p. 1232-1237.
14. Rogach, A.L., D.S. Koktysh, M. Harrison and N.A. Kotov, *Layer-by-layer assembled films of HgTe nanocrystals with strong infrared emission*. Chem. Mat., 2000. **12**(6): p. 1526-1528.
15. Gao, M.Y., C. Lesser, S. Kirstein, H. Mohwald, A.L. Rogach and H. Weller, *Electroluminescence of different colors from polycation/CdTe nanocrystal self-assembled films*. J. Appl. Phys., 2000. **87**(5): p. 2297-2302.
16. Susha, A.S., F. Caruso, A.L. Rogach, G.B. Sukhorukov, A. Kornowski, H. Mohwald, M. Giersig, A. Eychmüller and H. Weller, *Formation of luminescent spherical core-shell particles by the consecutive adsorption of polyelectrolyte and CdTe(S) nanocrystals on latex colloids*. Colloid Surf. A-Physicochem. Eng. Asp., 2000. **163**(1): p. 39-44.
17. Crisp, M.T. and N.A. Kotov, *Preparation of Nanoparticle Coatings on Surfaces of Complex Geometry*. Nano Lett., 2003. **3**(2): p. 173-177.
18. Klar, T.A., T. Franzl, A.L. Rogach and J. Feldmann, *Super-efficient exciton funneling in layer-by-layer semiconductor nanocrystal structures*. Adv. Mater., 2005. **17**(6): p. 769-773.
19. Mamedov, A.A., A. Belov, M. Giersig, N.N. Mamedova and N.A. Kotov, *Nanorainbows: graded semiconductor films from quantum dots*. J. Am. Chem. Soc. **123**(31): p. 7738-7739.
20. Gaponik, N., A. Eychmüller, A.L. Rogach, V.G. Solovyev, C.M. Sotomayor Torres and S.G. Romanov, *Structure-related optical properties of luminescent hetero-opals*. J. Appl. Phys., 2004. **95**(3): p. 1029-1035.
21. Romanov, S.G., D.N. Chigrin, C.M. Sotomayor Torres, N. Gaponik, A. Eychmüller and A.L. Rogach, *Emission stimulation in a directional band gap of a CdTe-loaded opal photonic crystal*. Phys. Rev. E, 2004. **69**(4 Pt 2): p. 046606/046601 - 046606/046604.
22. Shavel, A., N. Gaponik and A. Eychmüller, *Efficient UV-Blue Photoluminescing Thiol-Stabilized Water-Soluble Alloyed ZnSe(S) Nanocrystals*. Journal of Physical Chemistry B, 2004. **108**(19): p. 5905-5908.
23. Ostrander, J.W., A.A. Mamedov and N.A. Kotov, *Two Modes of Linear Layer-by-Layer Growth of Nanoparticle-Polyelectrolyte Multilayers and Different Interactions in the Layer-by-layer Deposition*. J. Am. Chem. Soc., 2001. **123**(6): p. 1101-1110.
24. Franzl, T., A. Shavel, A.L. Rogach, N. Gaponik, T.A. Klar, A. Eychmüller and J. Feldmann, *High-rate unidirectional energy transfer in directly assembled CdTe nanocrystal bilayers*. Small, 2005. **1**(4): p. 392-395.
25. Gaponik, N., D.V. Talapin, A.L. Rogach, K. Hoppe, E.V. Shevchenko, A. Kornowski, A. Eychmüller and H. Weller, *Thiol-capping of CdTe nanocrystals: An*

- alternative to organometallic synthetic routes*. J. Phys. Chem. B, 2002. **106**(29): p. 7177-7185.
26. Kotov, N.A., in *Multilayer Thin Films*, J.B. Schlenoff, Editor. 2003, Wiley-VCH: Weinheim. p. 207-270.
 27. Hoppe, K., E. Geidel, H. Weller and A. Eychmüller, *Covalently bound CdTe nanocrystals*. Phys. Chem. Chem. Phys., 2002. **4**(10): p. 1704-1706.
 28. Shavel, A., N. Gaponik and A. Eychmüller, *Covalent linking of CdTe nanocrystals to amino-functionalized surfaces*. Chemphyschem : a European journal of chemical physics and physical chemistry, 2005. **6**(3): p. 449-451. .:
 29. Shipway, A.N., M. Lahav, R. Gabai and I. Willner, *Investigations into the Electrostatically Induced Aggregation of Au Nanoparticles*. Langmuir, 2000. **16**(23): p. 8789-8795.
 30. Franzl, T., D.S. Koktysh, T.A. Klar, A.L. Rogach, J. Feldmann and N. Gaponik, *Fast energy transfer in layer-by-layer assembled CdTe nanocrystal bilayers*. Appl. Phys. Lett., 2004. **84**(15): p. 2904-2906.
 31. Gao, M., J. Sun, E. Dulkeith, N. Gaponik, U. Lemmer and J. Feldmann, *Lateral Patterning of CdTe Nanocrystal Films by the Electric Field Directed Layer-by-Layer Assembly Method*. Langmuir, 2002. **18**(10): p. 4098-4102.
 32. Kapitonov, A.M., A.P. Stupak, S.V. Gaponenko, E.P. Petrov, A.L. Rogach and A. Eychmüller, *Luminescence properties of thiol-stabilized CdTe nanocrystals*. J. Phys. Chem. B, 1999. **103**(46): p. 10109-10113.
 33. Crooker, S.A., J.A. Hollingsworth, S. Tretiak and V.I. Klimov, *Spectrally Resolved Dynamics of Energy Transfer in Quantum-Dot Assemblies: Towards Engineered Energy Flows in Artificial Materials*. Physical Review Letters, 2002. **89**(18): p. 186802/1-186802/4.

Chapter 6

Summary

The present thesis focusses on the synthesis of aqueous thiol-stabilized II-VI semiconductor nanocrystals, their post-preparative photo-treatment, their electrochemical characterization and the preparation of ordered superstructures using nanocrystals (NCs) as building blocks.

In particular, the first successful synthesis of aqueous ZnSe NCs has been developed and its optimal conditions have been found. The “as prepared” aqueous ZnSe NCs possess a narrow size distribution but have negligible and broad (deep trap) emission. The photoluminescence (PL) quantum yield (QY) of the ZnSe NCs is improved by a post-preparative photochemical treatment. The illumination of ZnSe NCs by “white light” of a xenon lamp leads to strong (up to 25-30 % QY) band gap PL. This phototreatment leads to the formation of a ZnSe(S) alloyed shell. Due to the incorporation of sulfur into the particles their size increases. The proposed mechanism has been confirmed by an electrochemical study.

An improvement of the PL properties of the CdTe NCs synthesized in aqueous media is shown. The influence of the initial conditions of the synthesis (structure and concentration of the Cd-thiol complexes in the syntheses solution before injection of the H_2Te) on the quality of the CdTe nanocrystals is revealed. The distribution of the complexes of cadmium with the stabilizer thioglycolic acid (TGA) is calculated in a wide range of pH values and concentrations of the cadmium ions. It is found that only CdL_3^{4-} , CdL_2^{2-} and CdL (where L is $(SCH_2COO)^{2-}$) complexes play an important role under the synthetic conditions used (pH 9.0-12.5). The results of the numerical simulation show that the CdL concentration in the initial solution correlates clearly with the PL QY of the CdTe NCs. An improvement of the QY of the CdTe NCs is achieved by decreasing the TGA/Cd ratio which leads to an increasing concentration of the CdL complex. Reducing the TGA/Cd ratio allows the preparation of strongly luminescing (PL QY up to 50% for the crude solution) CdTe NCs.

Another possibility to improve the PL of CdTe NCs is again the photochemical treatment. The illumination of a solution of the CdTe NCs leads to i) photoetching of the nanocrystals and ii) to a photo-assisted formation of a protective shell. Both processes are size dependent. Small CdTe NCs undergo mainly the process of shell formation and show a pronounced red shift both in absorption and in the luminescence. Thus, the post preparative irradiation of aqueous CdTe nanocrystals as well as the changing of the initial conditions in the synthesis results in PL QYs as high as 50-60% which is comparable with the QY of CdTe NCs synthesized by the hot injection procedure in organic media. The CdTe NCs exhibiting this sufficiently high PL QY and this simple water based synthetic procedure offers a good compatibility with biological surroundings and superior stability against oxidation.

Electrochemical properties of thiol-capped CdTe and ZnSe NCs which were pre-adsorbed on an electrode are studied. The voltammograms demonstrate several distinct oxidation and reduction peaks with the peak positions being size dependent. The size-dependence of the reduction and the second oxidation peaks can be attributed to moving the energetic band positions owing to the quantum size effect. An extraordinary behavior (moving to more negative potentials as the NC size decreases) was found for the first oxidation peak (observed at less positive potentials). This peak can be assigned to the oxidation of Se- and Te-related surface traps, respectively. The results obtained indicate that the energy levels of these traps are shifted to lower energies as the NCs size increases leading finally to an enhanced emission QY. The process of the photo-assisted shell formation (ZnSe NCs) is reflected by the position of the first oxidation peak. This peak moves towards the direction of the conduction band of the ZnSe NCs correlating with an improvement of the PL QY of the NCs. Finally, the peak merges with the valence band of the ZnSe NCs. Thus, the current research has demonstrated that electrochemical methods provide important information about surface states and the size-dependent behavior of semiconductor NCs.

The arranging of semiconductor nanoparticles in superstructures has been studied. The layer-by-layer assembly and the direct electrostatic assembly of CdTe NCs is used for the preparation of layered structures. A system with alternating layers of nanocrystals with different sizes (i.e. band gaps) has been constructed. Effective Förster resonant energy transfer (FRET) is possible in this kind of structures. The layer-by-layer assembly may also be applied to the preparation of “mono-layered” structures through

the formation of “sandwich” polyelectrolyte-CdTe layers. Extremely fast FRET in such nanocrystal superstructures is observed.

The covalent attachment of nanoparticles to functionalized surfaces (aminated inorganic substrates and carboxy-functionalized latex beads) is utilized for the formation of monolayer structures. The carbodiimide assisted bond formation is used in order to link nanocrystals with substrates under mild conditions. The covalent attachment of semiconductor NCs through an amide- and an ester-bond formation in various media (water and methanol) is shown. A higher stability of such structures in comparison with the conventional LbL techniques is observed. Covalent coupling is applied to various flat (glass, silicon and quartz slides) and spherical (silica, glass and latex beads) substrates. Therefore, the use of the carbodiimide chemistry opens the possibility to form stable layers of semiconducting nanocrystals on the surface of various functionalized substrates.

Appendix 1

Calculation of the distribution of the complexes of cadmium with thioglycolic acid.

Here the calculation of the distribution of the concentration of cadmium complexes as a function of the pH and TGA/Cd ratio is presented. This calculation is carried out to compare its result with experimental data (quantum yield, stokes shift etc) and assumes the importance of different complexes for the successful synthesis of aqueous NCs. The stability constants of cadmium complexes with thioglycolic acid were taken from ref [1]. These data together with information about the stability constants of the hydroxy-complexes of cadmium [2] which may play an important role at very high pH, provides us with a full set of information about complexes in solution (see table).

Table. Stability constants of Cadmium(II) complexes in solution containing thioglycolic acid.

Complex.	Initial ions	Logarithm of stability constants	Ref.
$\text{Cd}(\text{SCH}_2\text{CO}_2)_3^{4-}$	$\text{Cd}^{2+}, 3 \text{SCH}_2\text{CO}_2^{2-}$	$\text{Log}\beta_{103} = 19.11 \pm 0.04$	[1]
$\text{Cd}(\text{SCH}_2\text{CO}_2)_2^{2-}$	$\text{Cd}^{2+}, 2 \text{SCH}_2\text{CO}_2^{2-}$	$\text{Log}\beta_{102} = 15.63 \pm 0.1$	[1]
$\text{Cd}(\text{SCH}_2\text{CO}_2)$	$\text{Cd}^{2+}, \text{SCH}_2\text{CO}_2^{2-}$	$\text{Log}\beta_{101} = 11.45 \pm 0.2$	[1]
$\text{CdH}(\text{SCH}_2\text{CO}_2)^+$	$\text{Cd}^{2+}, \text{H}^+, \text{SCH}_2\text{CO}_2^{2-}$	$\text{Log}\beta_{111} = 18.68 \pm 0.1$	[1]
$\text{CdH}(\text{SCH}_2\text{CO}_2)_2^-$	$\text{Cd}^{2+}, \text{H}^+, 2 \text{SCH}_2\text{CO}_2^{2-}$	$\text{Log}\beta_{112} = 24.30 \pm 0.2$	[1]
$\text{CdH}(\text{SCH}_2\text{CO}_2)_3^{3-}$	$\text{Cd}^{2+}, \text{H}^+, 3 \text{SCH}_2\text{CO}_2^{2-}$	$\text{Log}\beta_{113} = 28.35 \pm 0.1$	[1]
$\text{CdH}_2(\text{SCH}_2\text{CO}_2)_2$	$\text{Cd}^{2+}, 2 \text{H}^+, 2 \text{SCH}_2\text{CO}_2^{2-}$	$\text{Log}\beta_{122} = 30.88 \pm 0.1$	[1]
$\text{CdH}_2(\text{SCH}_2\text{CO}_2)_3^{2-}$	$\text{Cd}^{2+}, 2 \text{H}^+, 3 \text{SCH}_2\text{CO}_2^{2-}$	$\text{Log}\beta_{123} = 36.34 \pm 0.2$	[1]
$\text{Cd}(\text{OH})^+$	$\text{Cd}^{2+}, \text{OH}$	$\text{Log}\beta_{10} = 3.92$	[2]
$\text{Cd}(\text{OH})_2$	$\text{Cd}^{2+}, 2\text{OH}$	$\text{Log}\beta_{20} = 7,65$	[2]
$\text{Cd}(\text{OH})_3^-$	$\text{Cd}^{2+}, 3\text{OH}$	$\text{Log}\beta_{30} = 8,7$	[2]
$\text{Cd}(\text{OH})_3^{2-}$	$\text{Cd}^{2+}, 4\text{OH}$	$\text{Log}\beta_{40} = 8,65$	[2]

A1. Calculation of distribution of the cadmium complexes with thioglycolic acid.

The expression for the total concentration of cadmium and thioglycolic acid through the equilibrium concentration of cadmium ions and concentration of fully dissociated thioglycolic acid allows to find the equilibrium concentration of each ion. The equilibrium concentration of all ions and complexes depends only on the total concentration of TGA, cadmium salt and pH (at a given temperature). Knowledge about the equilibrium concentration of cadmium ions and the concentration of completely dissociated thioglycolic acid allows the calculation of the concentration of each complex in solution.

Details of the calculation of the concentration and composition of cadmium complexes are shown below:

Eq 1 expresses the total concentration of TGA in solution:

$$C_{TGA} = [L^{2-}] + [HL^-] + [H_2L] + 3[CdL_3^{4-}] + 2[CdL_2^{2-}] + [CdL] + [CdH_1L_1^{1+}] + 2[CdH_1L_2^{1-}] + 3[CdH_1L_3^{3-}] + 2[CdH_2L_2] + 3[CdH_2L_3^{2-}] \quad (1)$$

In order to express the concentrations of the cadmium complexes through the equilibrium concentration of cadmium ions $[Cd^{2+}]$, the concentration of fully dissociated thioglycolic acid $[L^{2-}]$ and pH the equations for the stability constant:

$$\beta_{1ij} = \frac{[Cd(H)_i(L)_j]^{(2+i-2j)}}{[Cd^{2+}][H^+]^i[L^{2-}]^j} \quad (2)$$

and for the protonation constant of thioglycolic acid

$$\beta_i = \frac{[(H_iL)^{i-2}]}{[L^{2-}][H^+]^i} \quad (3)$$

can be used.

Substitution of **eqs 2** and **3** in to **eq 1** and by using the values of the stability constants (**see table**) and protonation constants of thioglycolic acid ($\beta_1 = 5.62 \times 10^9$ and $\beta_2 = 1.41 \times 10^{13}$ correspondingly [1]; in 1M NaClO₄) allows the expression of the total concentration of TGA through the equilibrium concentration of cadmium ions $[Cd^{2+}]$ and fully dissociated thioglycolic acid $[L^{2-}]$:

A1. Calculation of distribution of the cadmium complexes with thioglycolic acid.

$$\begin{aligned}
 C_{TGA} = & [L^{2-}] + \beta_1[L^{2-}][H^+] + \beta_2[L^{2-}][H^+]^2 + \\
 & + 3\beta_{103}[Cd^{2+}][L^{2-}]^3 + 3\beta_{113}[H^+][Cd^{2+}][L^{2-}]^3 + 3\beta_{123}[H^+]^2[Cd^{2+}][L^{2-}]^3 + \\
 & + 2\beta_{102}[Cd^{2+}][L^{2-}]^2 + 2\beta_{112}[H^+][Cd^{2+}][L^{2-}]^2 + 2\beta_{122}[H^+]^2[Cd^{2+}][L^{2-}]^2 + \\
 & + \beta_{101}[Cd^{2+}][L^{2-}] + \beta_{111}[H^+][Cd^{2+}][L^{2-}]
 \end{aligned} \tag{4}$$

Grouping the like terms together in to **eq 4**:

$$\begin{aligned}
 C_{TGA} = & [L^{2-}] \left(1 + \beta_1[H^+] + \beta_2[H^+]^2 \right) + \\
 & + [Cd^{2+}] \left(3[L^{2-}]^3 (\beta_{103} + \beta_{113}[H^+] + \beta_{123}[H^+]^2) + \right. \\
 & \left. + 2[L^{2-}]^2 (\beta_{102} + \beta_{112}[H^+] + \beta_{122}[H^+]^2) + [L^{2-}] (\beta_{101} + \beta_{111}[H^+]) \right)
 \end{aligned} \tag{5}$$

where all expressions in brackets depend only on the pH of the solution.

$$B_0 = \beta_2[H^+]^2 + \beta_1[H^+] + 1 \tag{6}$$

$$B_1 = \beta_{111}[H^+] + \beta_{101} \tag{7}$$

$$B_2 = \beta_{122}[H^+]^2 + \beta_{112}[H^+] + \beta_{102} \tag{8}$$

$$B_3 = \beta_{123}[H^+]^2 + \beta_{113}[H^+] + \beta_{103} \tag{9}$$

Using the pH dependent parameters B_0 , B_1 , B_2 , B_3 finally allows the expression of the total TGA concentration through equilibrium concentration of cadmium $[Cd^{2+}]$ and thioglycolic acid $[L^{2-}]$:

$$C_{TGA} = B_0[L^{2-}] + [Cd^{2+}](3B_3 [L^{2-}]^3 + 2B_2 [L^{2-}]^2 + B_1 [L^{2-}]). \tag{10}$$

It is possible to express the total concentration of cadmium in solution in the same way. The overall cadmium in solution is in the form of cadmium (II) ions, complexes with TGA and hydroxo-complexes:

$$\begin{aligned}
 C_{Cd} = & [Cd^{2+}] + \\
 & + [CdL_3^{4-}] + [CdL_2^{2-}] + [CdL] + [CdH_1L_1^{1+}] + [CdH_1L_2^{1-}] + \\
 & + [CdH_1L_3^{3-}] + [CdH_2L_2] + [CdH_2L_3^{2-}] + \\
 & + [Cd(OH)_1^{1+}] + [Cd(OH)_2] + [Cd(OH)_3^{1-}] + [Cd(OH)_4^{2-}]
 \end{aligned} \tag{11}$$

The equation for the stability constant **eq 2** allows to express the complex's concentration through the equilibrium concentration of cadmium (II) and the concentration of fully deprotonated TGA ions:

A1. Calculation of distribution of the cadmium complexes with thioglycolic acid.

$$\begin{aligned}
 C_{Cd} = & [Cd^{2+}] + \beta_{103}[Cd^{2+}][L^{2-}]^3 + \beta_{113}[H^+][Cd^{2+}][L^{2-}]^3 + \beta_{123}[H^+]^2[Cd^{2+}][L^{2-}]^3 + \\
 & + \beta_{102}[Cd^{2+}][L^{2-}]^2 + \beta_{112}[H^+][Cd^{2+}][L^{2-}]^2 + \beta_{122}[H^+]^2[Cd^{2+}][L^{2-}]^2 + \\
 & + \beta_{101}[Cd^{2+}][L^{2-}] + \beta_{111}[H^+][Cd^{2+}][L^{2-}] + \\
 & + \beta_{10}[Cd^{2+}][OH^-] + \beta_{20}[Cd^{2+}][OH^-]^2 + \beta_{30}[Cd^{2+}][OH^-]^3 + \beta_{40}[Cd^{2+}][OH^-]^4 \quad (12)
 \end{aligned}$$

Grouping the like terms together:

$$\begin{aligned}
 C_{Cd} = & [Cd^{2+}] \left(1 + \beta_{103}[L^{2-}]^3 + \beta_{113}[H^+][L^{2-}]^3 + \beta_{123}[H^+]^2[L^{2-}]^3 + \right. \\
 & + \beta_{102}[L^{2-}]^2 + \beta_{112}[H^+][L^{2-}]^2 + \beta_{122}[H^+]^2[L^{2-}]^2 + \beta_{101}[L^{2-}] + \beta_{111}[H^+][L^{2-}] + \\
 & \left. + \beta_{10}[OH^-] + \beta_{20}[OH^-]^2 + \beta_{30}[OH^-]^3 + \beta_{40}[OH^-]^4 \right) + \quad (13a)
 \end{aligned}$$

or:

$$\begin{aligned}
 C_{Cd} = & [Cd^{2+}] \left(1 + [L^{2-}]^3 (\beta_{103} + \beta_{113}[H^+] + \beta_{123}[H^+]^2) + \right. \\
 & + [L^{2-}]^2 (\beta_{102} + \beta_{112}[H^+] + \beta_{122}[H^+]^2) + [L^{2-}] (\beta_{101} + \beta_{111}[H^+]) + \\
 & \left. + \beta_{10}[OH^-] + \beta_{20}[OH^-]^2 + \beta_{30}[OH^-]^3 + \beta_{40}[OH^-]^4 \right) + \quad (13b)
 \end{aligned}$$

Substituting eqs 6-9 in to eq 13b, one can get the expression for the concentration of all cadmium in solution as a function of the equilibrium concentration of ions of cadmium ($[Cd^{2+}]$) and thioglycolic acid in solution ($[L^{2-}]$):

$$C_{Cd} = [Cd^{2+}] (1 + B_3[L^{2-}]^3 + B_2[L^{2-}]^2 + B_1[L^{2-}] + K) \quad (14)$$

Where $K = \beta_{10} [OH^-] + \beta_{20} [OH^-]^2 + \beta_{30} [OH^-]^3 + \beta_{40} [OH^-]^4$ which depends only on the pH as for eqs 6-9.

Finally, we have equations for overall concentrations of TGA (eq 10) and cadmium (eq 14) which are expressed only through the equilibrium concentration of cadmium, thioglycolic acid and the pH of the solutions.

The equilibrium concentration of cadmium (II) ions from eqs 14 may be expressed as:

$$[Cd^{2+}] = \frac{C_{Cd}}{1 + B_3[L^{2-}]^3 + B_2[L^{2-}]^2 + B_1[L^{2-}] + K} \quad (15)$$

Substitution of the equilibrium concentration of cadmium in eq 10 allows expression of the equilibrium concentration of fully dissociated thioglycolic acid only

A1. Calculation of distribution of the cadmium complexes with thioglycolic acid.

through the external parameters – overall concentration of cadmium, TGA and pH of solution:

$$C_{TGA} = B_0[L^{2-}] + \frac{C_{Cd}(3B_3[L^{2-}]^3 + 2B_2[L^{2-}]^2 + B_1[L^{2-}])}{1 + B_3[L^{2-}]^3 + B_2[L^{2-}]^2 + B_1[L^{2-}] + K} \quad (16)$$

Rearranging of equation **16** allows writing of the following expressions:

$$\left(C_{TGA} - B_0[L^{2-}] \right) \left((1 + K) + B_3[L^{2-}]^3 + B_2[L^{2-}]^2 + B_1[L^{2-}] \right) = C_{Cd} \left(3B_3[L^{2-}]^3 + 2B_2[L^{2-}]^2 + B_1[L^{2-}] \right) \quad (17)$$

$$\begin{aligned} C_{TGA}(1 + K) + C_{TGA} \left(B_3[L^{2-}]^3 + B_2[L^{2-}]^2 + B_1[L^{2-}] \right) - B_0[L^{2-}](1 + K) \\ - B_0[L^{2-}] \left(B_3[L^{2-}]^3 + B_2[L^{2-}]^2 + B_1[L^{2-}] \right) = \\ = C_{Cd} \left(3B_3[L^{2-}]^3 + 2B_2[L^{2-}]^2 + B_1[L^{2-}] \right) \end{aligned} \quad (18)$$

$$\begin{aligned} C_{TGA}(1 + K) + C_{TGA}B_3[L^{2-}]^3 + C_{TGA}B_2[L^{2-}]^2 + C_{TGA}B_1[L^{2-}] - B_0[L^{2-}](1 + K) - \\ - B_0B_3[L^{2-}]^4 - B_0B_2[L^{2-}]^3 - B_0B_1[L^{2-}]^2 = \\ = 3C_{Cd}B_3[L^{2-}]^3 + 2C_{Cd}B_2[L^{2-}]^2 + C_{Cd}B_1[L^{2-}] \end{aligned} \quad (19)$$

Now by grouping the like terms together in the parenthesis we have an expression for the equilibrium concentration of TGA ions in the solution which depends only on the pH of the solution.

$$\begin{aligned} -[L^{2-}]^4 B_0 B_3 + [L^{2-}]^3 \left(C_{TGA} B_3 - 3C_{Cd} B_3 - B_0 B_2 \right) + \\ + [L^{2-}]^2 \left(C_{TGA} B_2 - 2C_{Cd} B_2 - B_0 B_1 \right) + \\ + [L^{2-}] \left(C_{TGA} B_1 - C_{Cd} B_1 - B_0(1 + K) \right) + C_{TGA}(1 + K) = 0 \end{aligned} \quad (20)$$

Numerical simulation of eqs **20** allows to find the equilibrium concentration of TGA ($[L^{2-}]$) ions. Substitution of the $[L^{2-}]$ value in equation **15** allows the calculation of the concentration of cadmium ions ($[Cd^{2+}]$) in solution. Finally, knowledge about the equilibrium concentration of Cd(II) and TGA ions in solution allows to find the concentrations of each of the complexes in solution at the given pH and total concentration

A1.Calculation of distribution of the cadmium complexes with thioglycolic acid.

of cadmium and thioglycolic acid. Results of the numerical simulation are shown below (Figure A1-A4).

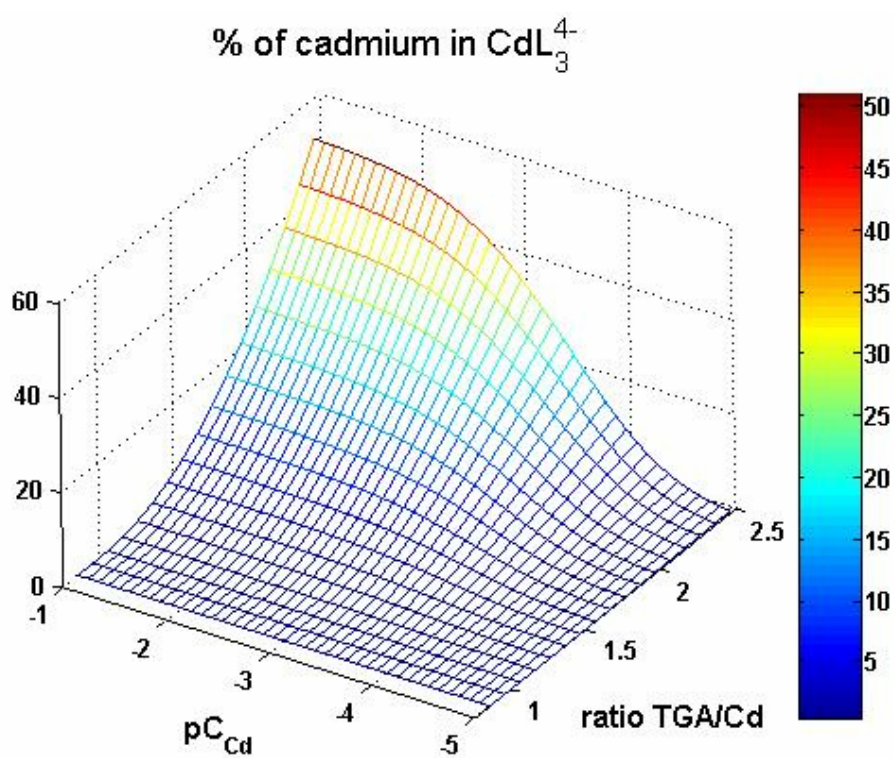


Figure A1. Concentration of Cd(L)_3^{4-} versus the total concentration of cadmium and the TGA/Cd ratio.

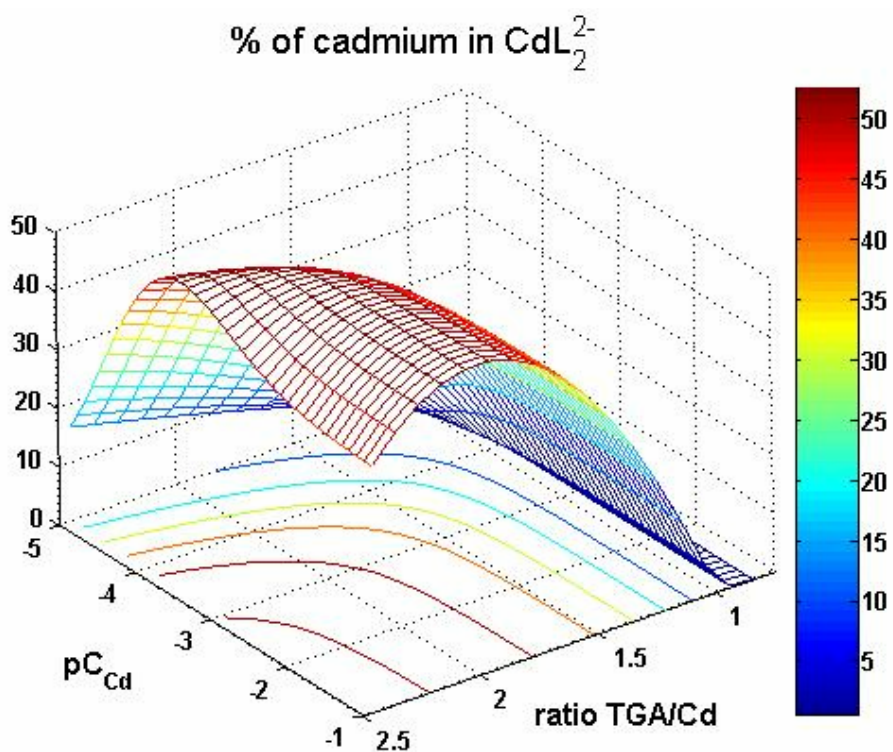


Figure A2. Concentration of $Cd(L)_2^{2-}$ versus the total concentration of cadmium and the TGA/Cd ratio.

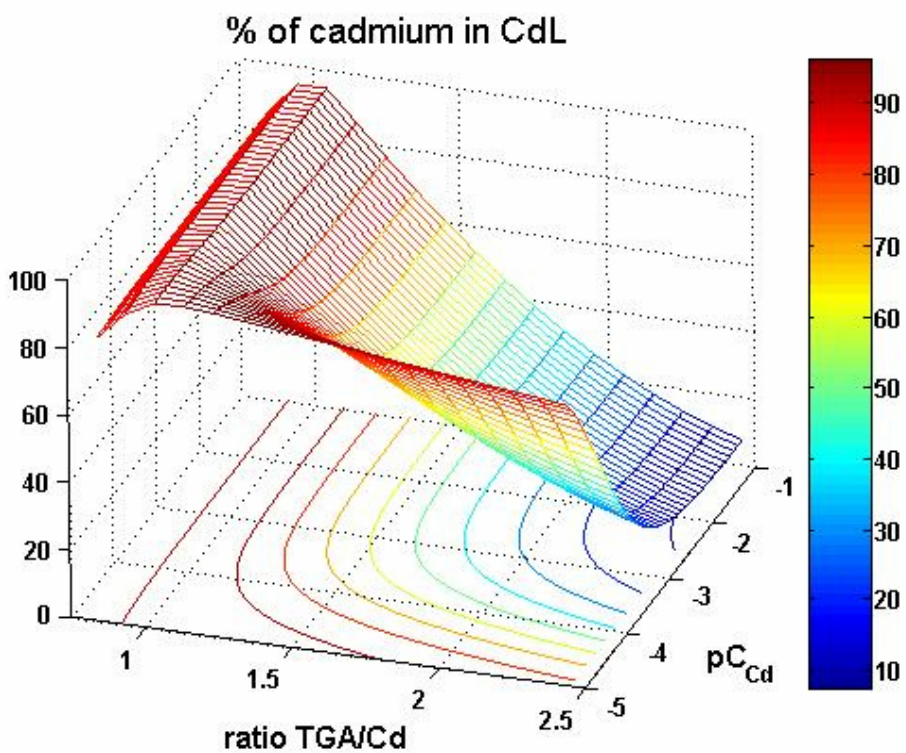


Figure A3. Concentration of $Cd(L)$ versus the total concentration of cadmium and the TGA/Cd ratio.

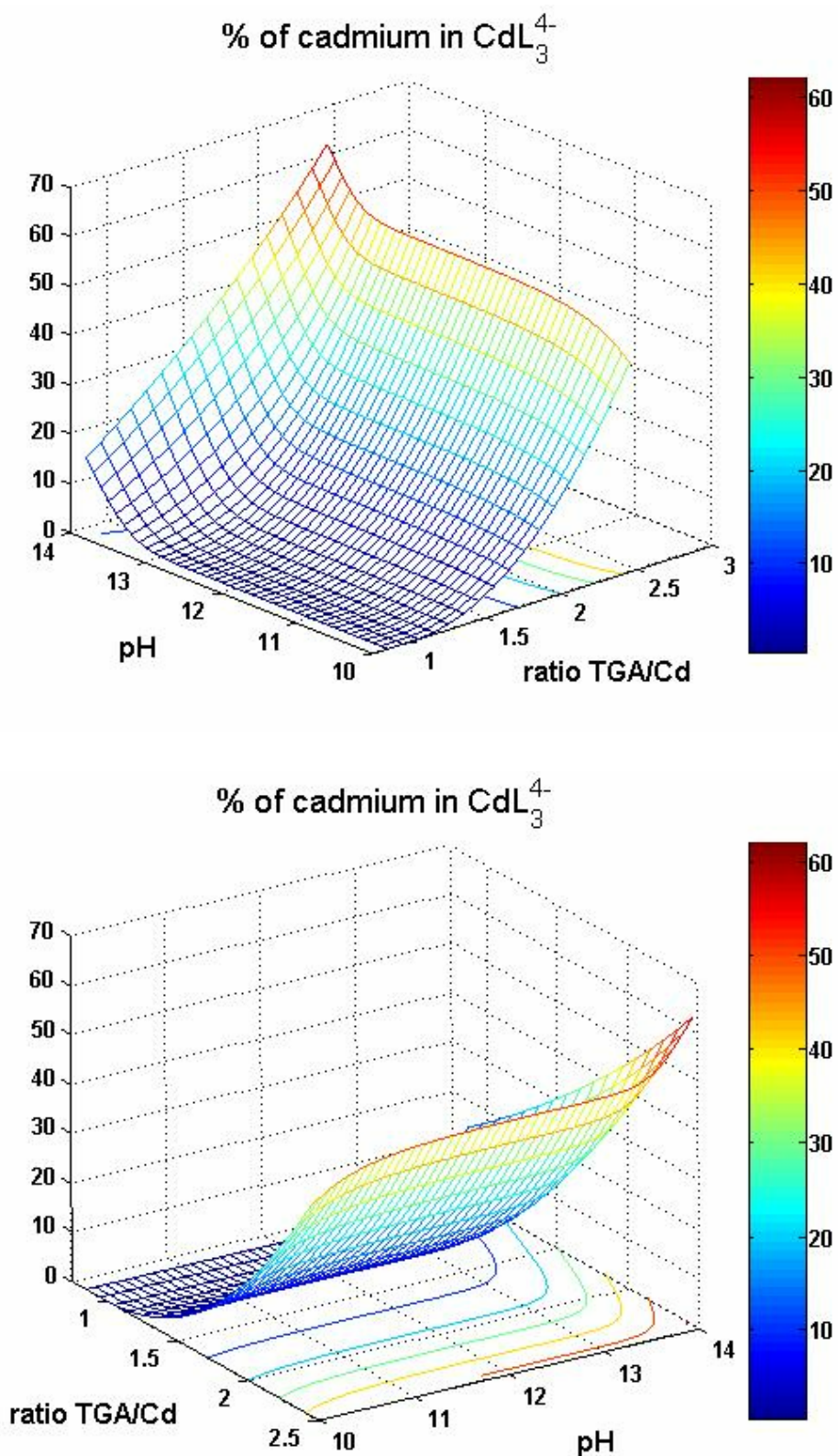


Figure A4. Concentration of $\text{Cd}(\text{L})_3^{4-}$ versus the total concentration of cadmium and the pH of the solution.

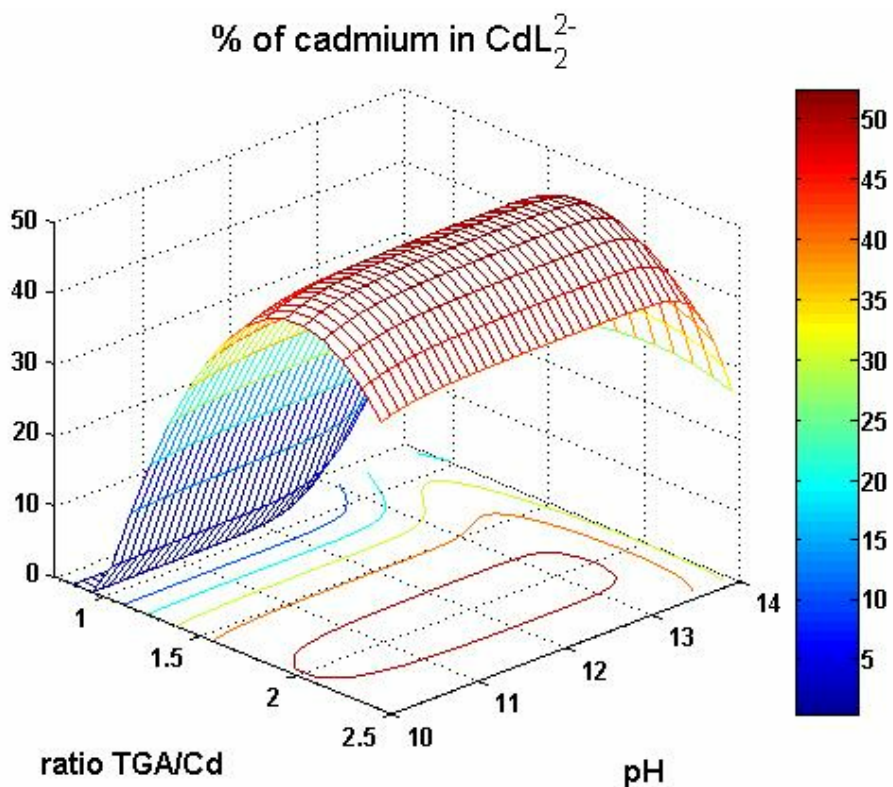
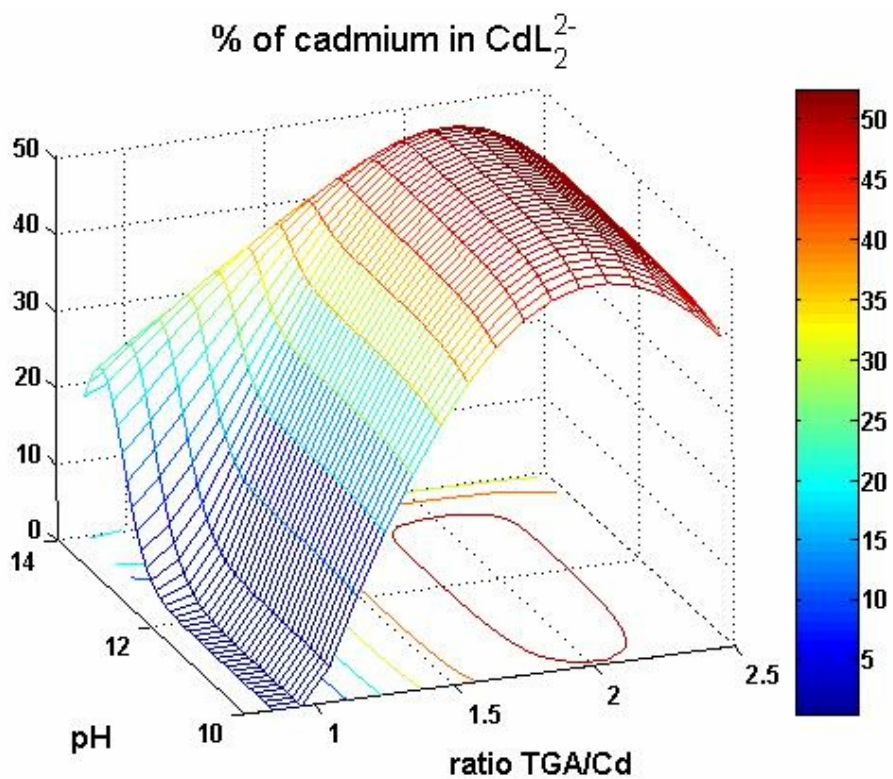


Figure A5. Concentration of Cd(L)_2^{2-} versus the total concentration of cadmium and the pH of the solution.

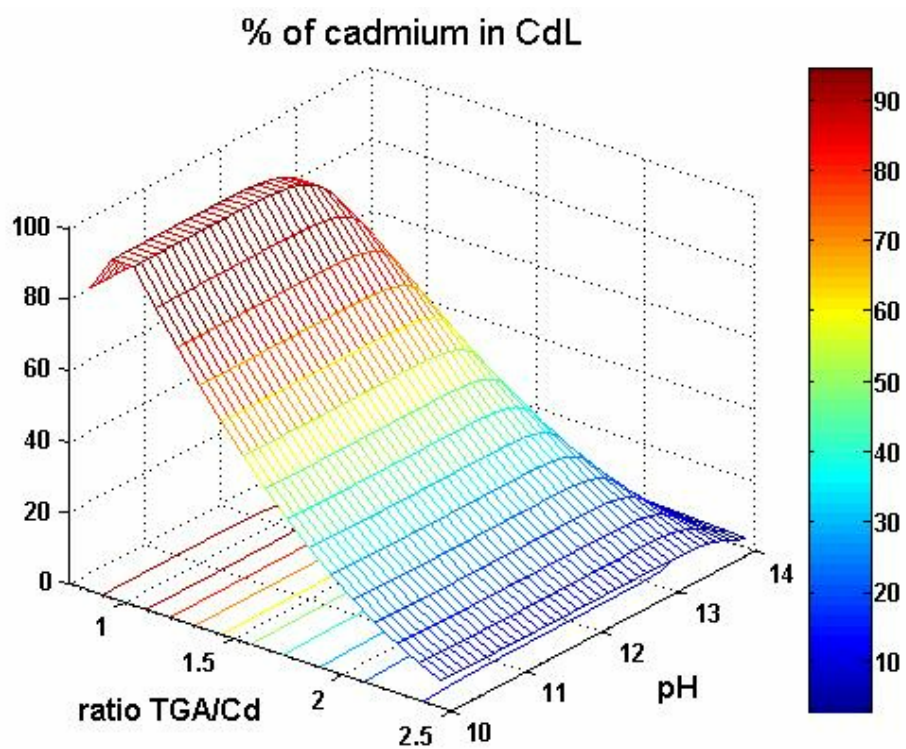
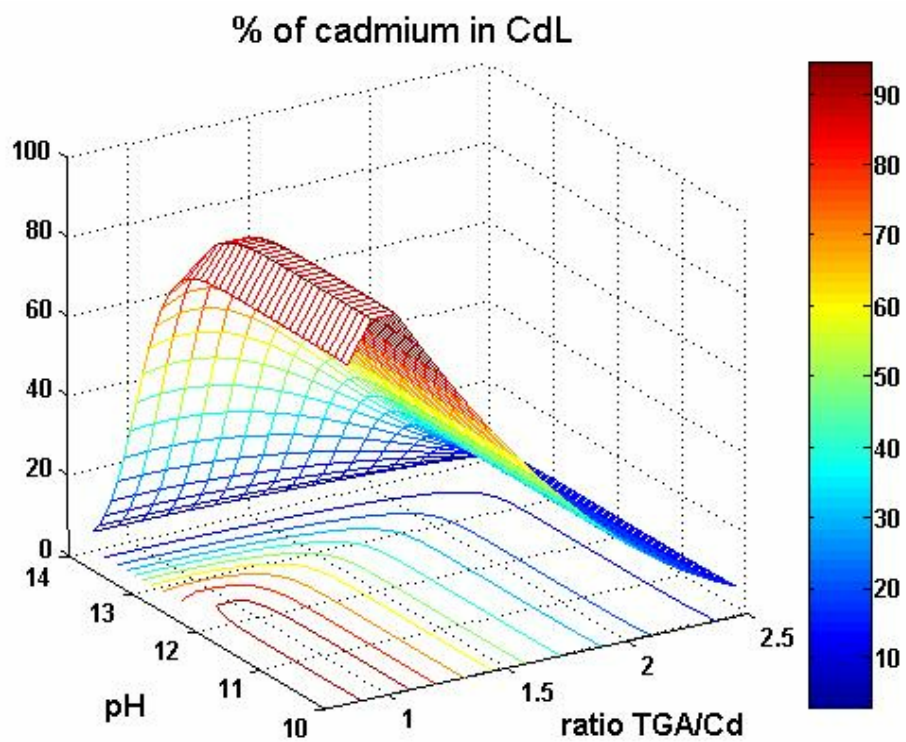


Figure A6. Concentration of Cd(L) versus the total concentration of cadmium and the pH of the solution.

A1.1. Estimation of the calculation validity.

In this calculation the several presumptions which can reduce the validity of the calculation have been made. The most important source of deviation is using the concentration of the ions instead the activity for calculation. In order to estimate the relative deviation of the calculation the ionic strength of the solution has been calculated using the following equation:

$$I = \frac{1}{2} \sum C_i z_i^2 \quad (1)$$

Using Davis' equation allows the calculation of the activity coefficient of the ions in the solution:

$$-\frac{\log f_i}{z_i^2} = \frac{0.511\sqrt{I}}{1 + 1.5\sqrt{I}} - 0.2I \quad (2)$$

In fact, the activity of hydrogen ions instead the concentrations in this calculation has been used. Practically, the substitution of activities instead the correspondent concentrations is not influence on the result of calculation. Comparing of calculated complexes concentration with a real system where pH is measured by pH-meter (see below) lead to the using activity for hydrogen ions.

Taking into account that the activity coefficient for neutral species is nearly equal to the concentration, we may estimate the deviation for the dissociation constant of thioglycolic acid:

$$K_1 = \frac{a_{(H^+)}[HL^-]}{[H_2L]} = \frac{a_{(H^+)}a_{(HL^-)}f_{(HL^-)}}{a_{(H_2L)}}$$

Taking the logarithm gives:

$$\log(K_1) = \log\left(\frac{a_{(H^+)}a_{(HL^-)}}{a_{(H_2L)}}\right) + \log(f_{(HL^-)}) = \log(K_1^T) + \log(f_{(HL^-)})$$

K_1^T is the thermodynamic constant which does not depend on the concentrations of the species and the value of the $\log(f_{(HL^-)})$ can be calculated from **eq 2**.

Numerical calculation shows that the parameter on the left side of the Davis equation is 0.081 at ionic strength 0.064 M (pH 12; TGA/Cd ratio 1.3) which gives a deviation of about 3% ($pK_{A1} = 3.31$ [1]). The same result shows the calculation for the second ionization step. In fact the ionic strength is even smaller (about 6%) because the pH

value in the synthesis is fixed by adding a portion of the solution of 0.1M NaOH (7.3 mL for pH 12.0 at TGA/Cd ratio 1.3).

A second source of deviation is the low solubility of the uncharged complexes of cadmium (for example CdL). The precipitation of the uncharged species leads to the shifting of the equilibrium and further production of those substances. Thus, precipitation leads to the underestimation of the overall amount of the purely soluble complexes. Here we assume that the mistake induced by the all our presumptions is within 10 %.

References

1. Turyan, I. and D. Mandler, *Electrochemical study of the Cd(II)/Cd(Hg) system in 2-mercaptoacetic acid solutions*. *Electrochimica Acta*, 1995. **40**(9): p. 1093-1100.
2. Lur'e, Y.Y., *Handbook on Analytical Chemistry*. 6th Ed. 1989. 446 pp.

Appendix 2

Experimental part.

All chemicals used were of analytical grade or of the highest purity available and were used without additional purification. All aqueous solutions were prepared using MilliQ water (Millipore) as the solvent. Cadmium lactate (ABCR) and $\text{Cd}(\text{ClO}_4)_2 \times 6\text{H}_2\text{O}$ (Alfa Aesar) were used as precursors for the syntheses of CdTe NCs. Thioglycerol (TG, Fluka), thioglycolic acid (TGA, Fluka), mercaptosuccinic acid (Fluka) or 3-mercaptopropionic acid (MPA, Fluka) were used as the stabilizing agents.

A2.1 Synthesis of water soluble CdTe NCs.

The nanocrystals synthesized according to this method are used for the electrochemical studies as well as for all kinds of linking procedures. Improving of the synthesis of aqueous CdTe nanocrystals are described in **Chapter 2.3**.

The “standard” synthesis of CdTe nanocrystals was done according to a well known experimental procedure [1]. In a typical synthesis 3.98 g (9.5 mmol) of $\text{Cd}(\text{ClO}_4)_2 \times 6\text{H}_2\text{O}$ is dissolved in 500 mL of water, and 23.3 mmol of the thiol stabilizer (MPA or TGA) are added under stirring, followed by adjusting the pH to 11.2-11.8 by dropwise addition of an appropriate amount of 1M NaOH solution. The mentioned pH values were experimentally found to be optimal for the synthesis of stable colloids [1]. The solution is placed into a three-necked flask fitted with a septum and valves and is deaerated by N_2 bubbling for 1.5 hours. Under stirring, H_2Te gas (generated by the reaction of 0.8 g (1.83 mmol) of Al_2Te_3 lumps with an excess amount of 1N H_2SO_4 under N_2 atmosphere) is passed through the solution together with a slow nitrogen flow for nearly 20 min. CdTe precursors are formed at this stage. The further nucleation and growth of the nanocrystals proceeds when refluxing at 100°C under open-air conditions with a condenser attached.

A2.2 Synthesis of CdTe NCs in DMF.

The synthesis of DMF soluble CdTe NCs is done according to a slightly modified procedure from ref [2]. In a typical synthesis 664 mg (2.28 mmol) of cadmium lactate is mixed with 50 mL of DMF and this mixture is stirred overnight giving a slightly turbid suspension. The suspension of the cadmium precursor is placed in a three-necked flask fitted with a septum and valves and 2.73 mmol of the thiol stabilizer (thioglycerol) are added. The reaction mixture is deaerated by N₂ bubbling for one hour. Under stirring, H₂Te gas (generated by the reaction of 0.08 g (0.183 mmol) of Al₂Te₃ lumps with an excess amount of 1 N H₂SO₄ under N₂ atmosphere) is passed through the solution together with a slow nitrogen flow for nearly 20 min. CdTe precursors are formed at this stage. The further nucleation and growth of the nanocrystals proceeds when refluxing at the boiling temperature of DMF under open-air conditions with a condenser attached. It takes approximately 1.5 hours to prepare nanoparticles emitting near 600 nm. The clear solution of red-emitting CdTe NCs is cooled down and precipitated by adding an equivalent amount of diethyl ether. The precipitate is redispersed in pure MeOH giving a clear transparent solution. Solutions of CdTe NCs in methanol are stable for at least 6-8 months.

A2.3 Determination of the size and concentration of CdTe NCs.

The size and the extinction coefficient are determined according to procedure by X. Peng [3]. Peng's data together with the data about aqueous NCs from Reference [4] allow finding the sizes and the extinction coefficient of various CdTe NCs.

A2.4 Optical spectra.

UV-Vis absorption spectra are recorded either with a Cary 50 or Cary 500 spectrophotometers (Varian). Photoluminescence measurements were carried out at room temperature using FluoroMax-2 and FluoroLog-3 spectrometers (Instruments SA). The scattering samples were measured on the Cary 500 spectrophotometer (Varian) equipped with a LabSphere (Varian).

A2.5 HRTEM and HRSEM.

High-resolution scanning electron microscopy was done using a LEO 1550 microscope operating at 20 kV. High-resolution transmission electron microscopy (HRTEM) and energy-dispersive X-ray analysis (EDX) were performed on a Philips CM-300 microscope operating at 300 kV.

Samples for electron microscopy were prepared by transferring aqueous nanocrystals in organic solvent (chloroform or toluene) according ref [5] (for CdTe NCs) or by dilution of aqueous NCs' solution by DMF ($H_2O : DMF = 1 : 10$) (for ZnSe NCs). Diluted solutions were dropped onto 400-mesh carbon-coated copper grids and the excessive solvent is evaporated immediately. A mixture with DMF was chosen for ZnSe NCs to facilitate uniform drying of the drop on the hydrophobic grid surface.

A2.6 XRD.

Powder X-ray diffraction (XRD) measurements were carried out with a Philips X'Pert diffractometer (Cu $K\alpha$ -radiation, variable entrance slit, Bragg-Brentano geometry, secondary monochromator). Samples for this study were prepared by placing finely dispersed powders of nanocrystals on standard Si supports.

A2.7 Electrochemical measurements.

Electrochemical measurements were performed in a standard three-electrode two-compartment cell with a platinum counter-electrode and an $Ag|AgCl|KCl(sat.)$ electrode as the reference electrode (+0.201 V vs. SHE). All potentials were determined with respect to this reference electrode and were controlled by a conventional potentiostat with a controller. The working electrode compartment of the electrochemical cell was separated from the counter-electrode compartment by a fine porous glass membrane.

Gold plates or ITO films on a glass substrate were used as working electrodes. The surface of the gold plates was polished by diamond paste followed by boiling in concentrated HNO_3 and H_2SO_4 . Then, the gold electrodes were thoroughly washed with

doubly distilled water and annealed at 700°C for 15 min in air. ITO electrodes were cleaned with a mixture of aqueous solutions of NH₃ and H₂O₂ and rinsed thoroughly with doubly distilled water. Before the measurements, the electrodes were cycled in the supporting electrolyte in the potential region from -0.5 to 1.1 V.

For electrochemical measurements, CdTe NC colloidal solutions (particle concentration in the range of $2 \cdot 10^{-6}$ - $4 \cdot 10^{-6}$ M) in a buffer containing 0.1 M Na₂SO₄ and 0.02 M Na₂B₄O₇ (pH 9.2) were prepared. The CdTe NC colloids were sufficiently stable in the presence of this supporting electrolyte in the dark. After addition of the buffer solution, no noticeable changes of the colloids were found at least for periods of weeks judging from their absorption and fluorescence spectra.

The electrochemical measurements of ZnSe NCs' solutions were performed in acetate buffer solution (0.1M CH₃COONa + 0.0046M CH₃COOH (pH6)).

A2.8 Referenses

1. Gaponik, N., D.V. Talapin, A.L. Rogach, K. Hoppe, E.V. Shevchenko, A. Kornowski, A. Eychmüller and H. Weller, *Thiol-capping of CdTe nanocrystals: An alternative to organometallic synthetic routes*. J. Phys. Chem. B, 2002. **106**(29): p. 7177-7185.
2. Rogach, A.L., *Nanocrystalline CdTe and CdTe(S) particles: wet chemical preparation, size-dependent optical properties and perspectives of optoelectronic applications*. Materials Science & Engineering, B: Solid-State Materials for Advanced Technology, 2000. **B69-70**: p. 435-440.
3. Yu, W.W., L. Qu, W. Guo and X. Peng, *Experimental Determination of the Extinction Coefficient of CdTe, CdSe, and CdS Nanocrystals*. Chem. Mat., 2003. **15**(14): p. 2854-2860.
4. S.V. Gaponenko and U. Woggon, *Landolt-Börnstein New Series III/34C2 Optical Properties of Semiconductor Nanostructures*, C. Klingshirn, Editor. 2004. p. 284-347.
5. Gaponik, N., D.V. Talapin, Andrey L. Rogach, A. Eychmüller and H. Weller, *Efficient Phase Transfer of Luminescent Thiol-Capped Nanocrystals: From Water to Nonpolar Organic Solvents*. Nano Lett., 2002. **2**(8): p. 803-806.

Appendix 3

Safety precaution information on the used chemicals.

Substance	R-phrases	S-phrases	Hazard signs
3-(aminopropyl)-triethoxysilane	22-34	26-36/37/39-45	[C]
Acetone	11-36-66-67	9-16-26	[F][Xi]
Al ₂ Te ₃	Not fully examined compound	-	-
Al ₂ Se ₃	Not fully examined compound	-	-
Cd(ClO ₄) ₂ ·6H ₂ O	20/21/22-50/53	60-61	[Xn][N]
Ethanol	11-20/21/22-68/20/21/22	16-36/37	[F] [Xn]
i-propanol	11-36-67	7-16-24/25-26	[F][Xi]
N,N'-diisopropylcarbodiimide	10-26-36/37/38-41-42/43	26-36/37/39-45	[T ⁺]
N,N-Dimethylformamide	61-20/21-36	53-45	[T]
4-dimethylaminopyridine	25-27-36/37/38	26-28-36/37/39-45	[T ⁺]
1-Ethyl-3-[3-(dimethylamino)propyl]carbodiimide hydrochloride	20/21/22-34-42/43	23-36/37/39-45	[C]
N-Hydroxysuccinimide	-	22-24/25	-
H ₂ SO ₄ 1M	35	26-30-45	[C]
2-mercaptoethylamine	22-36/37/38	26-36	[Xn]
Mercaptopropionic acid	25-34	7-26-36/37/39-45	[T]
Methanol	11-23/24/25-39/23/24/25	7-16-36/37-45	[F][T]
(2-(N-morpholino)ethanesulfonic acid	10-20-36/37	-	[Xn]
NaOH 1M	34	6-37/39-45	[C]
	-	22-24/25	-
poly(ethyleneimine)	-	-	-
poly(diallyldimethylammonium chloride)	-	-	-
Thioglycolic acid	23/24/25-34	25-27-28-45	[T]
Toluene	11-38-48/20-63-65-67	36/37-46-62	[F][Xn]
Thioglycerol	21/22-36/37/38	26-36	[Xn]
Zn(ClO ₄) ₂ ·6H ₂ O	8-34	17-26-27-36/37/39-45	[O][C]

Risk (R-) and safety precaution (S-) phrases used in the classification, packaging, labelling and provision of information on dangerous substances

Risk phrases (R-Phrases)

- R1: Explosive when dry
- R2: Risk of explosion by shock, friction fire or other sources of ignition
- R3: Extreme risk of explosion by shock friction, fire or other sources of ignition
- R4: Forms very sensitive explosive metallic compounds
- R5: Heating may cause an explosion
- R6: Explosive with or without contact with air
- R7: May cause fire
- R8: Contact with combustible material may cause fire
- R9: Explosive when mixed with combustible material
- R10: Flammable
- R11: Highly flammable
- R12 : Extremely flammable
- R13: Extremely flammable liquefied gas
- R14: Reacts violently with water
- R15: Contact with water liberates highly flammable gases
- R16: Explosive when mixed with oxidising substances
- R17: Spontaneously flammable in air
- R18: In use, may form flammable/explosive vapour-air mixture
- R19: May form explosive peroxides
- R20: Harmful by inhalation
- R21: Harmful in contact with skin
- R22: Harmful if swallowed
- R23: Toxic by inhalation
- R24: Toxic in contact with skin
- R25: Toxic if swallowed
- R26: Very toxic by inhalation
- R27: Very toxic in contact with skin
- R28: Very toxic if swallowed
- R29: Contact with water liberates toxic gas
- R30: Can become highly flammable in use
- R31: Contact with acids liberates toxic gas
- R32: Contact with acids liberates very toxic gas
- R33: Danger of cumulative effects
- R34: Causes burns
- R35: Causes severe burns
- R36: Irritating to eyes
- R37: Irritating to respiratory system
- R38: Irritating to skin
- R39: Danger of very serious irreversible effects
- R40: Possible risk of irreversible effects
- R41: Risk of serious damage to eyes
- R42: May cause sensitisation by inhalation
- R43: May cause sensitisation by skin contact
- R44: Risk of explosion if heated under confinement
- R45: May cause cancer

- R46: May cause heritable genetic damage
- R47: May cause birth defects
- R48: Danger of serious damage to health by prolonged exposure
- R49: May cause cancer by inhalation
- R50: Very toxic to aquatic organisms
- R51: Toxic to aquatic organisms
- R52: Harmful to aquatic organisms
- R53: May cause long-term adverse effects in the aquatic environment
- R54: Toxic to flora
- R55: Toxic to fauna
- R56: Toxic to soil organisms
- R57: Toxic to bees
- R58: May cause long-term adverse effects in the environment
- R59: Dangerous to the ozone layer
- R60: May impair fertility
- R61: May cause harm to the unborn child
- R62: Possible risk of impaired fertility
- R63: Possible risk of harm to the unborn child
- R64: May cause harm to breastfed babies

Combination of risks

- R14/15: Reacts violently with water, liberating highly flammable gases
- R15/29: Contact with water liberates toxic, highly flammable gas
- R20/21: Harmful by inhalation and in contact with skin
- R20/21/22: Harmful by inhalation, in contact with skin and if swallowed
- R20/22: Harmful by inhalation and if swallowed
- R21/22: Harmful in contact with skin and if swallowed
- R23/24: Toxic by inhalation and in contact with skin
- R23/24/25: Toxic by inhalation, in contact with skin and if swallowed
- R23/25: Toxic by inhalation and if swallowed
- R24/25: Toxic in contact with skin and if swallowed
- R26/27: Very toxic by inhalation and in contact with skin
- R26/27/28: Very toxic by inhalation, in contact with skin and if swallowed
- R26/28: Very toxic by inhalation and if swallowed
- R27/28: Very toxic in contact with skin and if swallowed
- R36/37: Irritating to eyes and respiratory system
- R36/37/38: Irritating to eyes, respiratory system and skin
- R36/38: Irritating to eyes and skin
- R37/38: Irritating to respiratory system and skin
- R42/43: May cause sensitisation by inhalation and skin contact.
- R48/20: Harmful: danger of serious damage to health by prolonged exposure
- R48/20/21: Harmful: danger of serious damage to health by prolonged exposure through inhalation and in contact with the skin
- R48/20/21/22: Harmful: danger of serious damage to health by prolonged exposure through inhalation, in contact with skin and if swallowed
- R48/20/22: Harmful: danger of serious damage to health by prolonged exposure through inhalation, and if swallowed
- R48/21: Harmful: danger of serious damage to health by prolonged exposure in contact with skin
- R48/21/22: Harmful: danger of serious damage to health by prolonged exposure in contact with skin and if swallowed

R48/22: Harmful: danger of serious damage to health by prolonged exposure if swallowed
R48/23: Toxic: danger of serious damage to health by prolonged exposure through inhalation
R48/23/24: Toxic: danger of serious damage to health by prolonged exposure through inhalation and in contact with skin
R48/23/24/25: Toxic: danger of serious damage to health by prolonged exposure through inhalation, in contact with skin and if swallowed
R48/23/25: Toxic: danger of serious damage to health by prolonged exposure through inhalation and if swallowed
R48/24: Toxic: danger of serious damage to health by prolonged exposure in contact with skin
R48/24/25: Toxic: danger of serious damage to health by prolonged exposure in contact with skin and if swallowed
R48/25: Toxic: danger of serious damage to health by prolonged exposure if swallowed
R50/53: Very toxic to aquatic organisms, may cause long term adverse effects in the aquatic environment
R51/53: Toxic to aquatic organisms, may cause long term adverse effects in the aquatic environment
R52/53: Harmful to aquatic organisms, may cause long-term adverse effects in the aquatic environment

Safety precaution phrases (S-Phrases)

S1: Keep locked up
S2: Keep out of reach of children
S3: Keep in a cool place
S4: Keep away from living quarters
S5: Keep contents under . . . (appropriate liquid to be specified by the manufacturer)
S6: Keep under . . . (inert gas to be specified by the manufacturer)
S7: Keep container tightly closed
S8: Keep container dry
S9: Keep container in a well ventilated place
S12: Do not keep the container sealed
S13: Keep away from food, drink and animal feeding stuffs
S14: Keep away from . . . (incompatible materials to be indicated by the manufacturer)
S15: Keep away from heat
S16: Keep away from sources of ignition-No Smoking
S17: Keep away from combustible material
S18: Handle and open container with care
S20: When using do not eat or drink
S21: When using do not smoke
S22: Do not breathe dust
S23: Do not breathe gas/fumes/vapour/spray (appropriate wording to be specified by manufacturer)
S24: Avoid contact with skin
S25: Avoid contact with eyes
S26: In case of contact with eyes, rinse immediately with plenty of water and seek medical advice
S27: Take off immediately all contaminated clothing

A3. Safety precaution information on the used chemicals

- S28: After contact with skin, wash immediately with plenty of . . (to be specified by the manufacturer)
- S29: Do not empty into drains
- S30: Never add water to this product
- S33: Take precautionary measures against static discharges
- S34: Avoid shock and friction
- S35: This material and its container must be disposed of in a safe way
- S36: Wear suitable protective clothing
- S37: Wear suitable gloves
- S38: In case of insufficient ventilation, wear suitable respiratory equipment
- S39: Wear eye/face protection
- S40: To clean the floor and all objects contaminated by this material use (to be specified by the manufacturer)
- S41: In case of fire and/or explosion do not breath fumes
- S42: During fumigation/spraying wear suitable respiratory equipment (appropriate wording to be specified by the manufacturer)
- S43: In case of fire, use ... (indicate in the space the precise type of fire fighting equipment. If water increases the risk, add "never use water")
- S44: If you feel unwell, seek medical advice (show the label where possible)
- S45: In case of accident or if you feel unwell, seek medical advice immediately (show the label where possible)
- S46: If swallowed, seek medical advice immediately and show the container or label
- S47: Keep at temperature not exceeding ... °C (to be specified by the manufacturer)
- S48: Keep wetted with ... (appropriate material to be specified by the manufacturer)
- S49: Keep only in the original container
- S50: Do not mix with ... (to be specified by the manufacturer)
- S51: Use only in well ventilated areas
- S52: Not recommended for interior use on large surface areas
- S53: Avoid exposure - obtain special instructions before use
- S54: Obtain the consent of pollution control authorities before discharging to waste-water treatment plants
- S55: Treat using the best available techniques before discharge into drains or the aquatic environment
- S56: Do not discharge into drains or the environment, disposwe to an authorised waste collection point
- S57: Use appropriate containment to avoid environmental contamination
- S58: To be disposed of as hazardous waste
- S59: Refer to manufacturer/supplier for information on recovery/recycling
- S60: This material and/or its container must be disposed of as hazardous waste
- S61: Avoid release to the environment. Refer to special instructions / safety data sheet
- S62: If swallowed, do not induce vomiting: seek medical advice immediately and show the containeror label

Combined safety phrases

S1/2: Keep locked up and out of reach of children

S3/9: Keep in a cool, well ventilated place

S3/7/9: Keep container tightly closed in a cool, well ventilated place

S3/14: Keep in a cool place away from ... (incompatible materials to be indicated by the manufacturer)

S3/9/14: Keep in a cool, well ventilated place away from ... (incompatible materials to be indicated by the manufacturer)

S3/9/49: Keep only in the original container in a cool, well ventilated place

S3/9/14/49: Keep only in the original container in a cool, well ventilated place away from (incompatible materials to be indicated by the manufacturer)

S3/9/49: Keep only in the original container in a cool, well ventilated place

S3/14: Keep in a cool place away from...(incompatible materials to be indicated by the manufacturer)

S7/8: Keep container tightly closed and dry

S7/9: Keep container tightly closed and in a well ventilated place

S7/47: Keep container tightly closed and at a temperature not exceeding...°C (to be specified by manufacturer)

S20/21: When using do not eat, drink or smoke

S24/25: Avoid contact with skin and eyes

S29/56: Do not empty into drains, dispose of this material and its container to hazardous or special waste collection point

S36/37: Wear suitable protective clothing and gloves

S36/37/39: Wear suitable protective clothing, gloves and eye/face protection

S36/39: Wear suitable protective clothing, and eye/face protection

S37/39: Wear suitable gloves and eye/face protection

S47/49: Keep only in the original container at temperature not exceeding...°C (to be specified by the manufacturer)